

FINAL REPORT

Advanced Signal Processing & Classification:
UXO Standardized Test Site Data

SERDP Project MR-1505

APRIL 2012

Dean Keiswetter
SAIC

This document has been cleared for public release



Report Documentation Page		Form Approved OMB No. 0704-0188
Public reporting burden for the collection of information is estimated to average 1 hour per response, including the time for reviewing instructions, searching existing data sources, gathering and maintaining the data needed, and completing and reviewing the collection of information. Send comments regarding this burden estimate or any other aspect of this collection of information, including suggestions for reducing this burden, to Washington Headquarters Services, Directorate for Information Operations and Reports, 1215 Jefferson Davis Highway, Suite 1204, Arlington VA 22202-4302. Respondents should be aware that notwithstanding any other provision of law, no person shall be subject to a penalty for failing to comply with a collection of information if it does not display a currently valid OMB control number.		
1. REPORT DATE APR 2012	2. REPORT TYPE N/A	3. DATES COVERED -
4. TITLE AND SUBTITLE Advanced Signal Processing & Classification: UXO Standardized Test Site Data		5a. CONTRACT NUMBER
		5b. GRANT NUMBER
		5c. PROGRAM ELEMENT NUMBER
6. AUTHOR(S)	5d. PROJECT NUMBER	
	5e. TASK NUMBER	
	5f. WORK UNIT NUMBER	
7. PERFORMING ORGANIZATION NAME(S) AND ADDRESS(ES) SAIC		8. PERFORMING ORGANIZATION REPORT NUMBER
9. SPONSORING/MONITORING AGENCY NAME(S) AND ADDRESS(ES)		10. SPONSOR/MONITOR'S ACRONYM(S)
		11. SPONSOR/MONITOR'S REPORT NUMBER(S)
12. DISTRIBUTION/AVAILABILITY STATEMENT Approved for public release, distribution unlimited		
13. SUPPLEMENTARY NOTES The original document contains color images.		
14. ABSTRACT <p>Our objective was to study discrimination capabilities of feature based characterization and classification techniques using standard survey data acquired by others at the UXO Standardized Test Sites in APG and YPG. The fundamental issues investigated included the model used during characterization and the impact that classifier selection has on classification performance. After re-leveling and lagging the EM61 cart data, we inverted anomaly data for each data type using dipole, ellipsoidal, empirical, loop fit, joint frequency-time domain, and singularity expansion models. We then classified the resulting feature vectors with SVM, RVM, GLRT, and KNN statistical classifiers. We evaluated classification performance using two metrics derived from ROC curves; namely, (i) the total area under the curve and (ii) the probability of false alarms at 0.95 probability of detection. We selected five data sets to include in this study based on data quality, type, signal-to-noise, and availability at appropriate intermediate processing stages. The datasets included time-domain EM61 (man-towed single sensor cart and vehicle-towed array), time-domain EM63, frequency-domain GEM-3, and magnetic data. None of the classifiers or sensor/model combinations performed extremely well when the targets of interest (TOI) included 20mm- through 155mm-projectiles. Classification performance measures, defined here using area under the curve, were 0.8 for the best case(s). Additionally, all classifiers or sensor/model combinations produced multiple false negatives. False alarm rates, at a detection performance of 0.95, were as high as 0.95. Simplifying the problem by artificially limiting the UXO by size or by analyzing data acquired in a cued deployment did improve classification performances. Segmenting the UXO by size classes improved classification in direct proportion to the extent that the features of the UXO and clutter classes were separable. The cued data collection and comparison exercise showed improved classification capabilities with regard to deriving meaningful shape parameters when compared to data acquired on dynamic platforms.</p>		
15. SUBJECT TERMS		

16. SECURITY CLASSIFICATION OF:			17. LIMITATION OF ABSTRACT SAR	18. NUMBER OF PAGES 92	19a. NAME OF RESPONSIBLE PERSON
a. REPORT unclassified	b. ABSTRACT unclassified	c. THIS PAGE unclassified			

This report was prepared under contract to the Department of Defense Strategic Environmental Research and Development Program (SERDP). The publication of this report does not indicate endorsement by the Department of Defense, nor should the contents be construed as reflecting the official policy or position of the Department of Defense. Reference herein to any specific commercial product, process, or service by trade name, trademark, manufacturer, or otherwise, does not necessarily constitute or imply its endorsement, recommendation, or favoring by the Department of Defense.

Contents

List of Acronyms	xi
1. Abstract	1
2. Objective	2
3. Background	2
4. Materials and Methods.....	6
4.1 Sensor Descriptions.....	6
4.1.1 MTADS Data Acquisition System.....	6
4.1.1.1. MTADS Magnetometer Array	6
4.1.1.2. MTADS EM61 Array.....	7
4.1.1.3. MTADS GEM-3 Array	8
4.1.2 EM63 man-portable.....	9
4.1.3 EM61 man-portable.....	10
4.1.4 Data Example	11
4.2 Anomalies of Opportunity.....	13
4.3 Data Models	13
4.3.1 Dipole Model.....	13
4.3.2 POB model – GPA version	19
4.3.3 Empirical fit to GEM3.....	20
4.3.4 Ellipsoid Model	23
4.3.5 TD-FD Loop Model	26
4.3.6 Duke’s Singularity Expansion Model	26
4.3.7 Magnetic Model	27
4.4 Statistical Pattern Recognition Toolbox (SPRT) Framework	28
4.4.1 Feature normalization.....	29
4.4.2 Feature selection.....	30
4.4.3 Classifiers	30
4.4.4 Training Labels and Types	31
5. Results and Discussion	34
5.1 Performance Statistics – all UXO and all non-UXO.....	35
5.2 ROC Performance as a function of Classifier	36

5.3	Performance as a function of Data/Model.....	37
5.4	Inverted Features	38
5.5	All UXO versus all non-UXO Results Summary.....	40
5.6	Subgroups based on Size.....	40
5.7	Performance Bounds	43
5.8	Comparison of Dynamic versus Static Data Collection.....	45
5.9	Discussion	52
6.	Conclusions and Implications for Future Research/Implementation.....	52

Figures

Figure 3-1 Composite image of Aberdeen Proving Ground, MD, as configured while the data analyzed in this study was collected.	3
Figure 3-2 Photographs of standardized UXO emplaced at APG and YPG.....	4
Figure 3-3 Photographs of example clutter emplaced at APG and YPG. A significant fraction of the clutter items included in this study was medium to large fragments and possessed thick walls.	5
Figure 4-1 MTADS tow vehicle and magnetometer array	7
Figure 4-2 MTADS EM61 array pulled by the MTADS tow vehicle.	8
Figure 4-3 Close-up of MTADS EM61 array with GPS and IMU.....	8
Figure 4-4 MTADS GEM array mounted on the EM sensor cart. In addition to the three GEM sensors, note the three GPS antennae and the IMU for platform motion measurement.	9
Figure 4-5 Photograph of the EM63 sensor during data acquisition by the demonstrator.	10
Figure 4-6 Photograph of the man-portable EM61 sensor during acquisition at APG.....	11
Figure 4-7 Example data from a small portion of APG open field. The superimposed symbols and text identify anomalies for which ground truth has been released. The grid lines are spaced 25m apart.	12
Figure 4-8 Distribution of anomalies for which ground truth information has been released (red circles) at the time of the study	15
Figure 4-9 Fitted features derived from the NRL EM61 training data, YPG site, fit errors less than 31%.	17
Figure 4-10 Fitted features derived from the TTFW EM61 training data, YPG site, fit errors less than 31%.	18
Figure 4-11 Fitted features derived from the WES EM63 training data, YPG site, fit errors less than 31%.	20
Figure 4-12 Empirical fitted features derived from the NRL GEM-3 training data, YPG site, fit errors less than 31%.....	22
Figure 4-13 Ellipsoidal scale fitted features derived from the NRL GEM-3 training data, YPG site, fit errors less than 31%.....	24
Figure 4-14 Ellipsoidal tau fitted features derived from the NRL GEM-3 training data, YPG site, fit errors less than 31%.	25
Figure 4-15 Actual versus estimated depth and size plots and other relevant features plots; NRL magnetic array data, YPG open field.....	28
Figure 4-16 Classification ROCs for different scenarios of training and test data sets	32
Figure 4-17 Type and number of training labels available for this study. As used here, ‘NS’ indicates non-standard munitions. All other notations are specific subtypes of a particular munition type.	33

Figure 5-1 Schematic showing the forward sequential feature selection process adopted for identifying the best performing set of features for each combination of data type and model....	34
Figure 5-2 Comparison of hypothetical ROC curves possessing specific AUC measures.....	34
Figure 5-3 Performance ROCs as a function of classifiers for specific data types and best performing model.....	36
Figure 5-4 Performance ROCs for specific data types and models as detailed in the key.	37
Figure 5-5 Inverted model features for EM63 data	38
Figure 5-6 Inverted model features for EM61 data	39
Figure 5-7 Inverted model features for magnetic data.....	40
Figure 5-8 Performance ROCs for size based scenarios versus all clutter	41
Figure 5-9 Performance ROCs by data type for Large UXO versus small clutter; KNN classifier	42
Figure 5-10 Performance ROCs by data type for Large UXO versus small and medium sized clutter; KNN classifier	43
Figure 5-11 Performance bounds assuming inverted features duplicate the observed physical dimensions of length and width (assumed to be equal to the diameter for axial symmetric UXO). Left column – inverted polarization features. Ground Truth (GT) dimensions as reported. Right side – ROC generated by submitting the length and width data to a KNN classifier.....	44
Figure 5-12 Photographs of three different collection schemes compared in this section. Top left shows a cued deployment using a fixed sampling scheme. Top right shows the TEMTADS vehicular array. Bottom left shows a man-towed deployment scheme.	45
Figure 5-13 Comparison of dipole fit errors for common anomalies at APG with an EM61 sensor using a template, cart, and vehicular array deployment.....	46
Figure 5-14 Similar errors in reported depth estimates are observed for the three deployment schemes; labeled UXO only.....	47
Figure 5-15 Polarization shape comparison plots (principal axis B1 compared to second/tertiary B2,B3 polarizations)	48
Figure 5-16 Performance ROCs for template, cart, and vehicular array; EM61 sensor, all UXO versus all clutter	49
Figure 5-17 Polarizations segmented by survey modality and target size.....	50
Figure 5-18 Performance ROCs for template, cart, and vehicular array; EM61 sensor, sized based UXO classes versus all clutter	51
Figure 7-1 ROC curves for NRL EM61 array data using the dipole model at YPG for different classifiers and features selection methodologies using features of anomalies with fit errors less than 31% . The targets of interest were all ordnance ranging from 20mm to 155mm.	55
Figure 7-2 ROC curves for NRL EM61 array data using the dipole model at YPG for different classifiers and features selection methodologies using features of anomalies with fit errors less	

than 31% . The targets of interest were small sized ordnance items (20mm, 40mm, M42, BDU-28, BDU-26).	55
Figure 7-3 ROC curves for NRL EM61 array data using the dipole model at YPG for different classifiers and features selection methodologies using features of anomalies with fit errors less than 31% . The targets of interest were medium sized ordnance items (57mm, MK118, 60mm, 81mm, 2.75in).	56
Figure 7-4 ROC curves for NRL EM61 array data using the dipole model at YPG for different classifiers and features selection methodologies using features of anomalies with fit errors less than 31% . The targets of interest were large sized ordnance items (105mm, 155mm).	56
Figure 7-5 ROC curves for TTFW EM61 cart data using the dipole model at YPG for different classifiers and features selection methodologies using features of anomalies with fit errors less than 31% . The targets of interest were all ordnance ranging from 20mm to 155mm.	57
Figure 7-6 ROC curves for TTFW EM61 cart data using the dipole model at YPG for different classifiers and features selection methodologies using features of anomalies with fit errors less than 31% . The targets of interest were small sized ordnance items (20mm, 40mm, M42, BDU-28, BDU-26).	58
Figure 7-7 ROC curves for TTFW EM61 cart data using the dipole model at YPG for different classifiers and features selection methodologies using features of anomalies with fit errors less than 31% . The targets of interest were medium sized ordnance items (57mm, MK118, 60mm, 81mm, 2.75in).	58
Figure 7-8 ROC curves for TTFW EM61 cart data using the dipole model at YPG for different classifiers and features selection methodologies using features of anomalies with fit errors less than 31% . The targets of interest were large sized ordnance items (105mm, 155mm).	59
Figure 7-9 ROC curves for NRL Mag array data at YPG for different classifiers and features selection methodologies using features of anomalies with fit errors less than 31% . The targets of interest were all ordnance ranging from 20mm to 155mm.	60
Figure 7-10 ROC curves for NRL Mag array data at YPG for different classifiers and features selection methodologies using features of anomalies with fit errors less than 31% . The targets of interest were small sized ordnance items (20mm, 40mm, M42, BDU-28, BDU-26).	60
Figure 7-11 ROC curves for NRL Mag array data at YPG for different classifiers and features selection methodologies using features of anomalies with fit errors less than 31% . The targets of interest were medium sized ordnance items (57mm, MK118, 60mm, 81mm, 2.75in).	61
Figure 7-12 ROC curves for NRL Mag array data at YPG for different classifiers and features selection methodologies using features of anomalies with fit errors less than 31% . The targets of interest were large sized ordnance items (105mm, 155mm).	61
Figure 7-13 ROC curves for NRL array data using the cooperative Mag/EM approach at YPG for different classifiers and features selection methodologies using features of anomalies with fit errors less than 31% . The targets of interest were all ordnance ranging from 20mm to 155mm.	62
Figure 7-14 ROC curves for NRL array data using the cooperative Mag/EM approach at YPG for different classifiers and features selection methodologies using features of anomalies with fit	

errors less than 31% . The targets of interest were small sized ordnance items (20mm, 40mm, M42, BDU-28, BDU-26).	63
Figure 7-15 ROC curves for NRL array data using the cooperative Mag/EM approach at YPG for different classifiers and features selection methodologies using features of anomalies with fit errors less than 31% . The targets of interest were medium sized ordnance items (57mm, MK118, 60mm, 81mm, 2.75in).	63
Figure 7-16 ROC curves for NRL array data using the cooperative Mag/EM approach at YPG for different classifiers and features selection methodologies using features of anomalies with fit errors less than 31% . The targets of interest were large sized ordnance items (105mm, 155mm).	64
Figure 7-17 ROC curves for WES EM63 data using the POB model at YPG for different classifiers and features selection methodologies using features of anomalies with fit errors less than 31% . The targets of interest were all ordnance ranging from 20mm to 155mm.	65
Figure 7-18 ROC curves for WES EM63 data using the POB model at YPG for different classifiers and features selection methodologies using features of anomalies with fit errors less than 31% . The targets of interest were small sized ordnance items (20mm, 40mm, M42, BDU-28, BDU-26).	65
Figure 7-19 ROC curves for WES EM63 data using the POB model at YPG for different classifiers and features selection methodologies using features of anomalies with fit errors less than 31% . The targets of interest were medium sized ordnance items (57mm, MK118, 60mm, 81mm, 2.75in).	66
Figure 7-20 ROC curves for WES EM63 using the POB model at YPG for different classifiers and features selection methodologies using features of anomalies with fit errors less than 31% . The targets of interest were large sized ordnance items (105mm, 155mm).	66
Figure 7-21 ROC curves for WES EM63 data using the SEM model at YPG for different classifiers and features selection methodologies using features of anomalies with fit errors less than 31% . The targets of interest were all ordnance ranging from 20mm to 155mm.	67
Figure 7-22 ROC curves for WES EM63 data using the SEM model at YPG for different classifiers and features selection methodologies using features of anomalies with fit errors less than 31% . The targets of interest were small sized ordnance items (20mm, 40mm, M42, BDU-28, BDU-26).	68
Figure 7-23 ROC curves for WES EM63 data using the SEM model at YPG for different classifiers and features selection methodologies using features of anomalies with fit errors less than 31% . The targets of interest were medium sized ordnance items (57mm, MK118, 60mm, 81mm, 2.75in).	68
Figure 7-24 ROC curves for WES EM63 data using the SEM model at YPG for different classifiers and features selection methodologies using features of anomalies with fit errors less than 31% . The targets of interest were large sized ordnance items (105mm, 155mm).	69
Figure 7-25 ROC curves for NRL GEM-3 array data using the ellipsoidal scale model at YPG for different classifiers and features selection methodologies using features of anomalies with fit errors less than 31% . The targets of interest were all ordnance ranging from 20mm to 155mm.	70

Figure 7-26 ROC curves for NRL GEM-3 array data using the ellipsoidal scale model at YPG for different classifiers and features selection methodologies using features of anomalies with fit errors less than 31% . The targets of interest were small sized ordnance items (20mm, 40mm, M42, BDU-28, BDU-26).	70
Figure 7-27 ROC curves for NRL GEM-3 array data using the ellipsoidal scale model at YPG for different classifiers and features selection methodologies using features of anomalies with fit errors less than 31% . The targets of interest were medium sized ordnance items (57mm, MK118, 60mm, 81mm, 2.75in).	71
Figure 7-28 ROC curves for NRL GEM-3 array data using the ellipsoidal scale model at YPG for different classifiers and features selection methodologies using features of anomalies with fit errors less than 31% . The targets of interest were large sized ordnance items (105mm, 155mm).	71
Figure 7-29 ROC curves for NRL GEM-3 array data using the ellipsoidal tau model at YPG for different classifiers and features selection methodologies using features of anomalies with fit errors less than 31% . The targets of interest were all ordnance ranging from 20mm to 155mm.	72
Figure 7-30 ROC curves for NRL GEM-3 array data using the ellipsoidal tau model at YPG for different classifiers and features selection methodologies using features of anomalies with fit errors less than 31% . The targets of interest were small sized ordnance items (20mm, 40mm, M42, BDU-28, BDU-26).	73
Figure 7-31 ROC curves for NRL GEM-3 array data using the ellipsoidal tau model at YPG for different classifiers and features selection methodologies using features of anomalies with fit errors less than 31% . The targets of interest were medium sized ordnance items (57mm, MK118, 60mm, 81mm, 2.75in).	73
Figure 7-32 ROC curves for NRL GEM-3 array data using the ellipsoidal tau model at YPG for different classifiers and features selection methodologies using features of anomalies with fit errors less than 31% . The targets of interest were large sized ordnance items (105mm, 155mm).	74
Figure 7-33 ROC curves for NRL GEM-3 array data using the empirical model at YPG for different classifiers and features selection methodologies using features of anomalies with fit errors less than 31% . The targets of interest were all ordnance ranging from 20mm to 155mm.	75
Figure 7-34 ROC curves for NRL GEM-3 array data using the empirical model at YPG for different classifiers and features selection methodologies using features of anomalies with fit errors less than 31% . The targets of interest were small sized ordnance items (20mm, 40mm, M42, BDU-28, BDU-26).	75
Figure 7-35 ROC curves for NRL GEM-3 array data using the empirical model at YPG for different classifiers and features selection methodologies using features of anomalies with fit errors less than 31% . The targets of interest were medium sized ordnance items (57mm, MK118, 60mm, 81mm, 2.75in).	76
Figure 7-36 ROC curves for NRL GEM-3 array data using the empirical model at YPG for different classifiers and features selection methodologies using features of anomalies with fit	

errors less than 31% . The targets of interest were large sized ordnance items (105mm, 155mm).	76
Figure 7-37 ROC curves for NRL GEM-3 array data using the loop model at YPG for different classifiers and features selection methodologies using features of anomalies with fit errors less than 31% . The targets of interest were all ordnance ranging from 20mm to 155mm.	78
Figure 7-38 ROC curves for NRL GEM-3 array data using the loop model at YPG for different classifiers and features selection methodologies using features of anomalies with fit errors less than 31% . The targets of interest were small sized ordnance items (20mm, 40mm, M42, BDU-28, BDU-26).	78
Figure 7-39 ROC curves for NRL GEM-3 array data using the loop model at YPG for different classifiers and features selection methodologies using features of anomalies with fit errors less than 31% . The targets of interest were medium sized ordnance items (57mm, MK118, 60mm, 81mm, 2.75in).	79
Figure 7-40 ROC curves for NRL GEM-3 array data using the loop model at YPG for different classifiers and features selection methodologies using features of anomalies with fit errors less than 31% . The targets of interest were large sized ordnance items (105mm, 155mm).	79

Tables

Table 4-1 Datasets included in this study	6
Table 4-2 NRL EM61 Gate timing parameters.....	7
Table 4-3 Number of ground-truthed, isolated anomalies that possess fit errors less than 31%..	15
Table 5-1 Performance Measures as a function of Data and Model.....	35
Table 5-2 Performance Measures for EM61, Mag, and EM63 data types	37
Table 5-3 Size based definitions of UXO and clutter	41
Table 5-4 Sample size for various combinations of UXO and clutter.....	41
Table 5-5 Inverted fit statistics	46
Table 7-1 Best set of features for each of the classifiers with different TOI using the NRL EM61 array data at YPG.....	54
Table 7-2 Best set of features for each of the classifiers with different TOI using the TTFW EM61 cart data at YPG.	57
Table 7-3 Best set of features for each of the classifiers with different TOI using the NRL Mag array data at YPG.....	59
Table 7-4 Best set of features for each of the classifiers with different TOI using the NRL EM61 and Mag array data and the cooperative inversion approach at YPG.....	62
Table 7-5 Best set of features for each of the classifiers with different TOI using the WES EM63 data and the POB model at YPG.....	64

Table 7-6 Best set of features for each of the classifiers with different TOI using the WES EM63 data and the SEM model at YPG.	67
Table 7-7 Best set of features for each of the classifiers with different TOI using the NRL GEM-3 array and the ellipsoidal scale model at YPG.	69
Table 7-8 Best set of features for each of the classifiers with different TOI using the NRL GEM-3 array data and the ellipsoidal tau model at YPG.....	72
Table 7-9 Best set of features for each of the classifiers with different TOI using the NRL GEM-3 array data and the empirical model at YPG.	74
Table 7-10 Best set of features for each of the classifiers with different TOI using the NRL GEM-3 array data and the loop model at YPG.....	77

Acknowledgements

This report was supported wholly by the U.S. Department of Defense, through the Strategic Environmental Research and Development Program (SERDP) through Project MM-1505.

List of Acronyms

AEC	Army Environmental Center
ASR	Archives Search Report
APG	Aberdeen Proving Ground
BD	Bhattacharyya Distance
BoR	Body of Rotation
DAQ	Data Acquisition
DGM	Digital Geophysical Mapping
DSB	Defense Science Board
EE/CA	Engineering Evaluation/Cost Analysis
EMI	Electromagnetic Induction
ESTCP	Environmental Security Technology Certification Program
FAR	False Alarm Rate
FD	Frequency domain
FLD	Fisher Linear Discriminant
FSS	Forward Sequential Selection
GLRT	Generalized Likelihood Ratio Test
GPO	Geophysical Prove Out
GPS	Global Positioning System
HE	High Explosive
IDA	Institute for Defense Analyses
IMU	Inertial Measurement Unit
KDE	Kernel Density Estimation
K-NN	K-nearest neighbor
LSQ	Least Squares
M&F	Mag and Flag
MR	Munitions Response
MTADS	Multi-sensor Towed Array Detection System
NRL	Naval Research Laboratory
Pd	Probability of Detection

Pdisc	Probability of Correct Discrimination
Pfa	Probability of False Alarm
POB	Pasion-Oldenburg-Billings
QA	Quality Assurance
QC	Quality Control
ROC	Receiver Operating Characteristic
RTK	Real Time Kinematic
RTS	Robotic Total Station
RVM	Relevance Vector Machine
SEM	Singularity Expansion Model
SERDP	Strategic Environmental Research and Development Program
SNR	Signal to Noise Ratio
SPRT	Statistical Pattern Recognition Toolbox
SVM	Support Vector Machine
TD	Time domain
TtFW	TetraTech Foster Wheeler
TOI	Target(s) of Interest
UTC	Coordinated Universal Time
UXO	Unexploded Ordnance
VB	Variational Bayes
WES	Waterways Experiment Station
YPG	Yuma Proving Ground

1. Abstract

Our objective was to study discrimination capabilities of feature based characterization and classification techniques using standard survey data acquired by others at the UXO Standardized Test Sites in APG and YPG.

The fundamental issues investigated included the *model* used during characterization and the impact that *classifier selection* has on classification performance. After re-leveling and lagging the EM61 cart data, we inverted anomaly data for each data type using dipole, ellipsoidal, empirical, loop fit, joint frequency-time domain, and singularity expansion models. We then classified the resulting feature vectors with SVM, RVM, GLRT, and KNN statistical classifiers.

We evaluated classification performance using two metrics derived from ROC curves; namely, (i) the total area under the curve and (ii) the probability of false alarms at 0.95 probability of detection. We selected five data sets to include in this study based on data quality, type, signal-to-noise, and availability at appropriate intermediate processing stages. The datasets included time-domain EM61 (man-towed single sensor cart and vehicle-towed array), time-domain EM63, frequency-domain GEM-3, and magnetic data.

None of the classifiers or sensor/model combinations performed extremely well when the targets of interest (TOI) included 20mm- through 155mm-projectiles. Classification performance measures, defined here using area under the curve, were 0.8 for the best case(s). Additionally, all classifiers or sensor/model combinations produced multiple false negatives. False alarm rates, at a detection performance of 0.95, were as high as 0.95.

Simplifying the problem by artificially limiting the UXO by size or by analyzing data acquired in a cued deployment did improve classification performances. Segmenting the UXO by size classes improved classification in direct proportion to the extent that the features of the UXO and clutter classes were separable. The cued data collection and comparison exercise showed improved classification capabilities with regard to deriving meaningful shape parameters when compared to data acquired on dynamic platforms.

2. Objective

The objective of this project was to evaluate and improve physics-inspired discrimination performances by systematically scrutinizing the process; namely, the model used during characterization and the impact that classifier selection and training has on the final decision.

3. Background

The UXO Standardized Test Sites in Aberdeen Maryland and Yuma Arizona represent real world scenarios (Figure 3-1). They were established under SERDP, ESTCP, and Army funding to allow users and developers to baseline and document UXO technology performance by defining the range of applicability of specific UXO technologies, by gathering data on sensor and system performance, and by comparing results. Electromagnetic and magnetic data acquired at these sites over multiple years and by multiple firms provided an opportunity to systematically examine the importance of models, classifiers, and training data when trying to discriminate between UXO and clutter using remotely sensed geophysical data.

The UXO Standardized Test Site program was designed to benchmark and validate capabilities of service firms and research groups. Technology demonstrators were free to choose the geophysical sensor, the positioning system, ancillary orientation sensors, deployment method, and analysis method. Approximately two dozen collections of digital geophysical data were collected, within at least a portion of the sites, from 2002 thru 2006. Most of the demonstrators' utilized magnetic or electromagnetic sensors of one kind or another (only one firm demonstrated a Ground Penetrating Radar technology).

The government scored the demonstrator submittals by using various quantitative metrics aimed at deciphering how well they detected subsurface metallic objects and discriminated UXO from non-UXO metallic debris. Performance results released by the Army Environmental Center (AEC) were generally poor. Based on AEC reports, in fact, little to no discernible discrimination capabilities were demonstrated using survey data [1].

This project investigated whether advanced signal processing and quantitative decision processes would improve the discrimination results.



Figure 3-1 Composite image of Aberdeen Proving Ground, MD, as configured while the data analyzed in this study was collected.

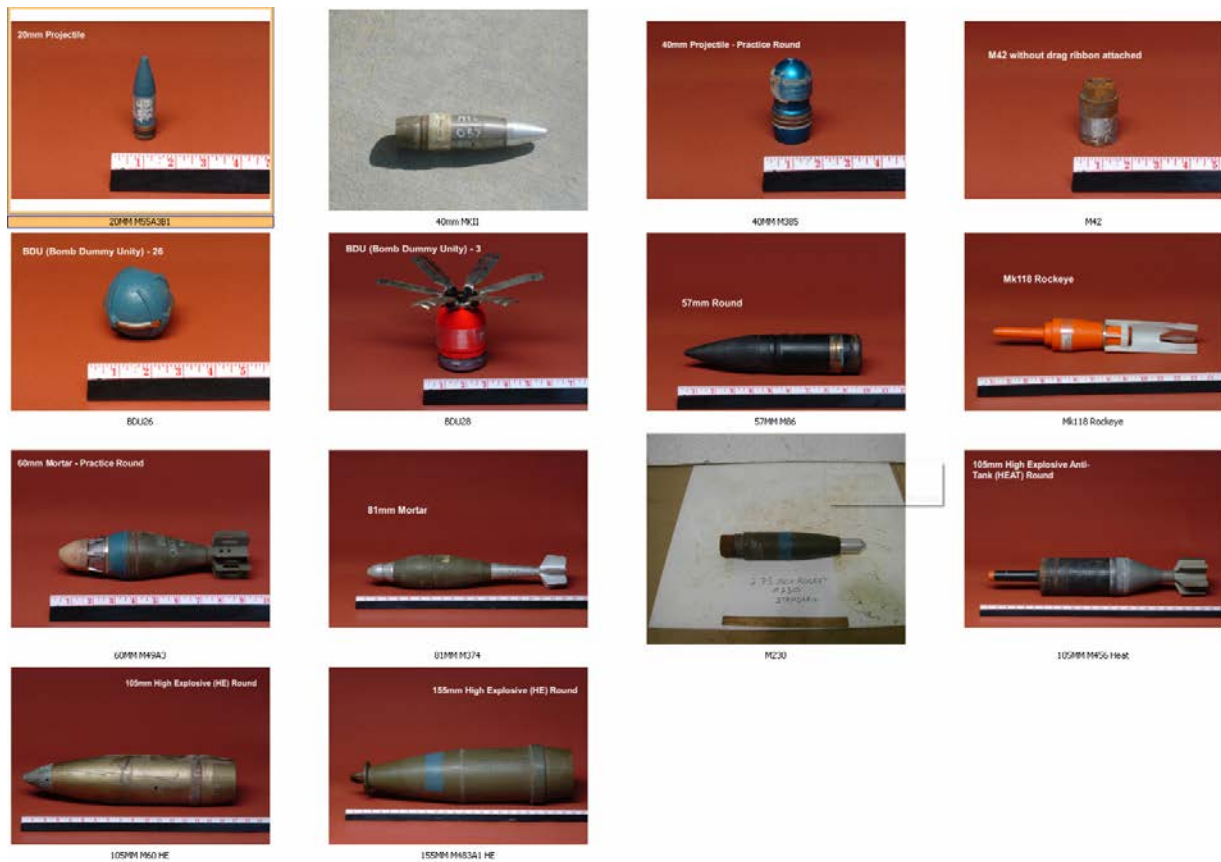


Figure 3-2 Photographs of standardized UXO emplaced at APG and YPG.



Figure 3-3 Photographs of example clutter emplaced at APG and YPG. A significant fraction of the clutter items included in this study was medium to large fragments and possessed thick walls.

4. Materials and Methods

Although there was a large number of data sets available, we down selected the data sets based on data quality (e.g., signal to noise ratio, minimal timing irregularities), data density (<1m lane spacing), data format and structure, and access to unfiltered data. The selected datasets include time-domain (TD) EM61, TD EM63, frequency-domain (FD) GEM-3, and magnetic (Table 4-1).

Table 4-1 Datasets included in this study

	Acquired by	Configuration	Positioning System	Lane Spacing
EM61 MkII	NRL	Towed Array	DGPS	0.5*
	TTFW	Cart	Leica Laser	0.5**
EM63	WES	Cart	DGPS	0.5
GEM-3	NRL	Towed Array	DGPS	0.5
Magnetic	NRL	Towed Array	DGPS	0.25

*two surveys collected along perpendicular transects

** planned 0.5m lane spacing; actual was 0.5 to 1.2m

4.1 Sensor Descriptions

4.1.1 MTADS Data Acquisition System

The multi-sensor towed array detection system (MTADS) was developed over a period of many years by the NRL with funding from SERDP and ESTCP. Common tow vehicles, data acquisition systems, and positioning systems are used for magnetic sensors, EM61 sensors, and GEM-3 sensors. The MTADS hardware utilizes a low-magnetic-signature vehicle that is used to tow the different sensor arrays over large areas (10 - 25 acres / day) to detect buried UXO. Positioning is provided using high performance Real Time Kinematic (RTK) Global Positioning System (GPS) receivers with position accuracies of approximately 5 cm. The positioning technology requires the availability of one or more known first-order survey control points.

4.1.1.1. MTADS Magnetometer Array

The MTADS magnetometer array is a linear array of eight Cs-vapor magnetometer sensors (Figure 4-1). The sensors are sampled at 50 Hz. Given a nominal survey speed of 6 mph, measurements are taken at 6cm intervals down track. The horizontal sensor spacing is 25cm. A single GPS antenna placed directly above the center of the sensor array is used to measure the sensor positions in real-time (5 Hz). All navigation and sensor data are time-stamped with Coordinated Universal Time (UTC) derived from the satellite clocks and recorded by the data acquisition computer (DAQ) in the tow vehicle.

See AEC standardized scoring report #671 for more information regarding this system as deployed at APG [<http://aec.army.mil/usaec/technology/demosites/sr0671.pdf>].



Figure 4-1 MTADS tow vehicle and magnetometer array

4.1.1.2. MTADS EM61 Array

The EM61 MTADS array is an overlapping array of three pulsed-induction sensors with 1x1m coils. The sensors have been modified to make them more compatible with vehicular speeds and to increase their sensitivity to small objects (Table 4-2). Nominal survey speed is three mph and the sensor readings are recorded at 10 Hz. This results in a down-track sampling of ~15 cm and a cross-track interval of 50 cm. In order to obtain sufficient illumination of all three principle axes of the anomaly with the primary field, data is collected in two orthogonal surveys. The EM61 array being pulled by the MTADS tow vehicle is shown in Figure 4-2.

Individual sensors in the EM61 array are located using a three-receiver RTK GPS system. An Inertial Measurement Unit (IMU) is also included on the sensor array to provide complimentary platform orientation information. A close-up view of the sensor platform is shown in Figure 4-3 which shows the three GPS antennae and the IMU (black box under the aft port GPS antenna).

Table 4-2 NRL EM61 Gate timing parameters

	Delay (μ s) 4 Gate Mode	Delay (μ s) Differential Mode
Gate 1	307 (bottom coil)	307 (bottom coil)
Gate 2	508 (bottom coil)	307 (top coil)
Gate 3	738 (bottom coil)	738 (bottom coil)
Gate 4	1000 (bottom coil)	1000 (bottom coil)



Figure 4-2 MTADS EM61 array pulled by the MTADS tow vehicle.



Figure 4-3 Close-up of MTADS EM61 array with GPS and IMU.

4.1.1.3. MTADS GEM-3 Array

The MTADS GEM-3 array consists of three, 96-cm diameter Geophex, Ltd. GEM-3 sensors in a triangular configuration with two sensors across the front of the array and one centered in the rear. The roughly 2-m square array is mounted on a rigid support which is attached to the MTADS EM cart using non-metallic fasteners (Figure 4-4). The GPS / IMU telemetry equipment used for GEMTADS is the same as that used for the EM61 array.

The standard GEM-3 sensor drive electronics have been modified to produce a substantially higher transmit moment for this array. Each individual sensor transmits a composite waveform of one to ten frequencies in the frequency range of 30 to 20,010 Hz with a base period of 1/30 sec. A composite transmitter waveform of nine frequencies log-spaced from 90 to 20010 Hz was used. The array can operate continuously with one sensor actively transmitting while the other two sensors are processing data at any given time. Allowing for a short coil settling time between the transmissions from each sensor, an effective array sampling rate of just over 9 Hz is achieved. Sequential transmitter operation also alleviates the need for the orthogonal survey

mode employed for the EM61 array. Down-track sampling is approximately 15 cm and the cross-track spacing is 50 cm. An interleaved survey pattern is used to decrease the cross-track spacing to 25 cm.

See AEC standardized scoring report #127 for more information regarding this system as deployed at APG [<http://aec.army.mil/usaec/technology/demosites/sr0127.pdf>].



Figure 4-4 MTADS GEM array mounted on the EM sensor cart. In addition to the three GEM sensors, note the three GPS antennae and the IMU for platform motion measurement.

4.1.2 EM63 man-portable

The EM63 is a commercially available sensor produced by Geonics, Ltd., of Mississauga, Ontario, Canada (Figure 4-5). It is a high power, high sensitivity, wide bandwidth full time domain UXO detector. The EM63 consists of a transmitter that generates a pulsed primary magnetic field which induces eddy currents in nearby metallic objects. The time decay of the currents is measured and recorded by the main console at 20 to 30 geometrically spaced time gates covering a time range from 180 microseconds (μ s) to 63 milliseconds (ms).

The EM63 system consists of three major hardware subsystems: (i) EM63 Control Console Sub-System; (ii) Antenna Cart Sub-System; and (iii) GPS Navigation Sub-System. The EM63 Control Console Sub-System consists of receiver and transmitter unit, controlled by an integrated field computer. The Antenna Cart Sub-System consists of the transmitter antenna (the 1x1m bottom coil) and receiver coils. Local positioning and georeferencing was accomplished using a Trimble 5700 RTK GPS system. The Trimble system consists of two receivers that are in radio communication with each other. A roving GPS antenna is mounted in the center of the EM63 coils and 2 meters above the bottom coil. The operator or assistant carries the controller for the roving antenna.

See AEC standardized scoring report #304 for more information regarding this system as deployed at APG [<http://aec.army.mil/usaec/technology/demosites/sr0304.pdf>].



Figure 4-5 Photograph of the EM63 sensor during data acquisition by the demonstrator.

4.1.3 EM61 man-portable

The Geonics EM61 TDEM geophysical sensor, Arc Second Constellation, and Leica Series 1100 Robotic Total Station laser positioning systems were integrated into a man-towed sensing system by TtFW (Figure 4-6). The system is utilized either on nonmagnetic wheels or as a man-portable unit (terrain-dependent) with the lower coil 40 cm above the ground surface. Two coils, 1x1m, are oriented in a horizontal coplanar fashion and separated by a vertical distance of 40 cm. The secondary magnetic field created by metal objects is sampled by the EM61 electronics, which reside in the backpack, at times of 216 μ s, 366 μ s, 660 μ s on the bottom coil and 660 μ s on the top coil after the turn-off of the transmit pulse. Digital data for these four individual time gates are integrated and recorded to a Juniper Allegro field computer at a rate of 12 Hz.

The Arc Second Constellation consists of four laser transmitters and a field computer for logging the position data via wireless modem. Four Trimble Spectra Precision LS920 Laser Transmitters are positioned in a diamond or square geometry over 1/2 to 1 acre depending upon the tree density. The transmitters are leveled, and an automatic routine calculates the relative x-y-z-plane between the transmitters to a tolerance of 1 inch or less. A laser detector receiver is centered over the EM61 coils on a TtFW designed fiberglass doghouse. The detector wand receives the laser pulses from the four transmitters simultaneously, and computes a position based on the known position of the laser transmitters. The georeferenced data are updated at 2 to 3 Hz and sent via wireless modem to the field computer for storage. The Leica Series 1100 RTS consists of a laser-based total station survey instrument (transmitter), prism (receiver), and RCS 100 remote control. The receiver prism is mounted on a TtFW doghouse centered over the EM61 coils, and the RTS automatically tracks the prism at distances of several thousand feet to

an accuracy of approximately 1 inch. Position data for the receiver prism are updated at a rate of 3 to 4 Hz and stored in the robotic total station's on-board computer.

See AEC standardized scoring report #157 for more information regarding this system as deployed at APG [<http://aec.army.mil/usaec/technology/demosites/sr0157.pdf>].



Figure 4-6 Photograph of the man-portable EM61 sensor during acquisition at APG.

4.1.4 Data Example

Example sensor data are presented in Figure 4-7. The EM61 and EM63 data are plotted using a color scale that ranges from 0 to 75mV. The color scale for the GEM data ranges from 0 to 20ppm and for the leveled magnetometry data -25 to 25nT.

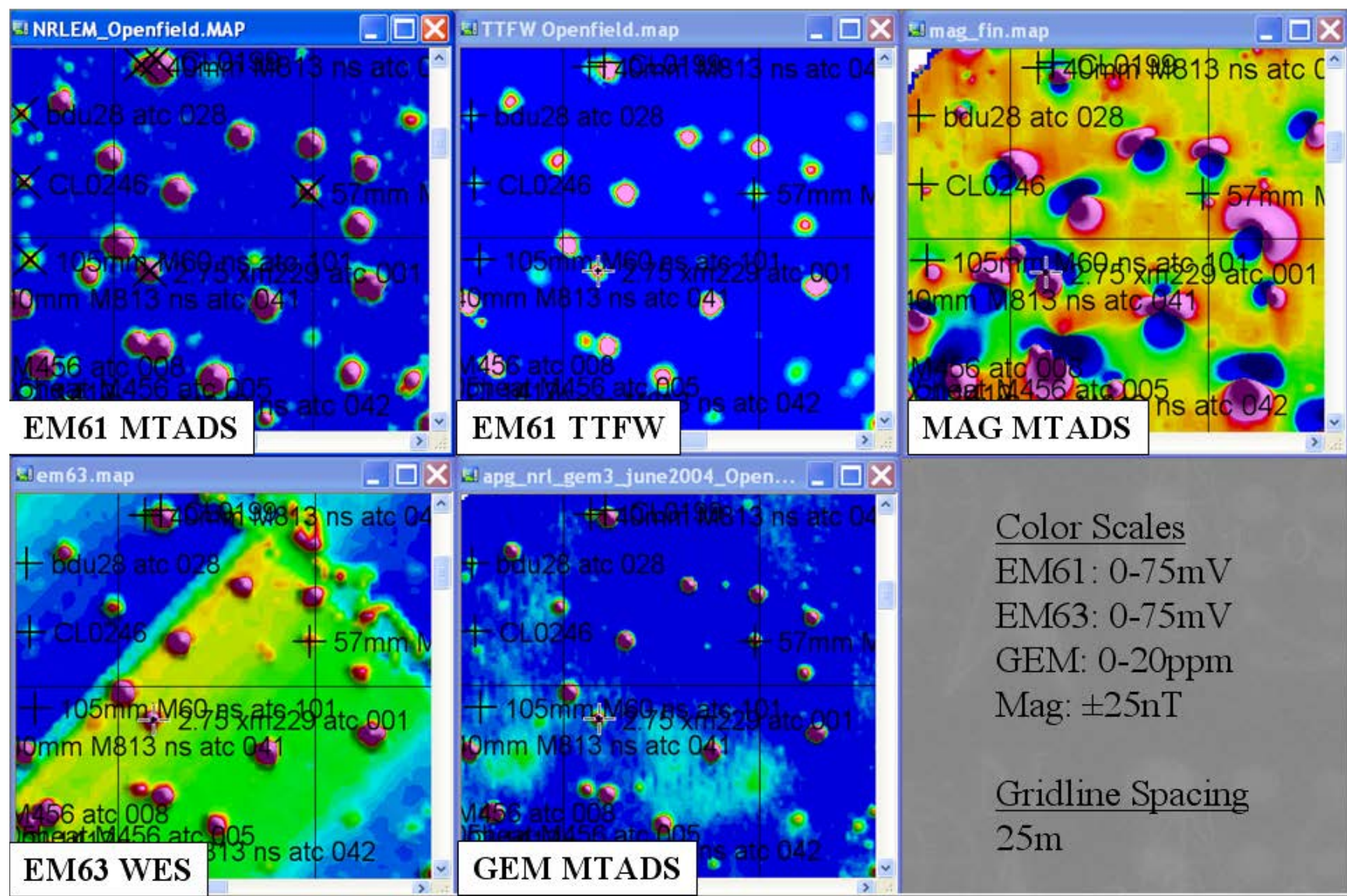


Figure 4-7 Example data from a small portion of APG open field. The superimposed symbols and text identify anomalies for which ground truth has been released. The grid lines are spaced 25m apart.

4.2 Anomalies of Opportunity

Only a subset of the total number of targets emplaced at the test sites were suitable for inclusion in this study. First, in order to compare methods and/or data sets, we required ground truth information. Ground truth information was available for anomalies in the calibration grid, original blind grid, and some of the open field challenge area at the time that this project was active. Not all of the ground truthed targets, however, were suitable for use in this study. The reasons for ground truth release, in fact, included those targets that were ‘least found’, ‘never found’, ‘miscellaneous’, ‘near fence’, and as well as ‘misclassified’. Thus, of the 327 APG open field targets for which ground truth was released, 112 of them were not suitable. At YPG, approximately 50 of the released ground truthed anomalies were not suitable.

To be included in this study, the anomalies also had to be common across the data sets and well characterized by the models. Table 4-3 presents the total number of isolated anomalies that possess correlation coefficients between measured and modeled data of greater than 0.95, which corresponds to fit errors less than 31%, for APG and YPG while Figure 4-8 shows the spatial distribution. We selected a 0.95 correlation coefficient threshold because fits with lower correlations possessed inconsistent polarizations and depth estimates across the models tested.

4.3 Data Models

4.3.1 Dipole Model

Within the dipole model framework, each target is completely characterized by three positional parameters (x_o, y_o, z_o) , three angles (ϕ, θ, ψ) , and three* N_t betas $[\beta_1(t_i), \beta_2(t_i), \beta_3(t_i)]$, where N_t is the number of time gates. The β ’s are eigenvalues of the symmetric effective magnetic polarizability tensor, and represent the response of the target along each of three principal axes.

In order to reduce the number of fit parameters, we made use of the fact that the modeled sensor response is linear in the β ’s. We therefore performed a non-linear Levenberg-Marquardt inversion on the positional and orientation parameters, with an embedded linear determination of the β ’s at each iteration. The algorithm continued until the squared error between measured and modeled data (chi-squared or χ^2) fit between the predicted and measured response at successive iterations changes by less than a set tolerance.

Initial guesses were provided for the six spatial parameters. The three angles were set equal to 45 degrees. The positional parameters x_o and y_o were determined from a signal-weighted mean of the target locations. Previous experience with this method indicated that the final results were most strongly dependent on z_o , as some guesses could lead to local minima. The code therefore was set to loop over several different initial guesses for z_o that covered a reasonable range for the targets. The result with the best χ^2 was chosen as the solution.

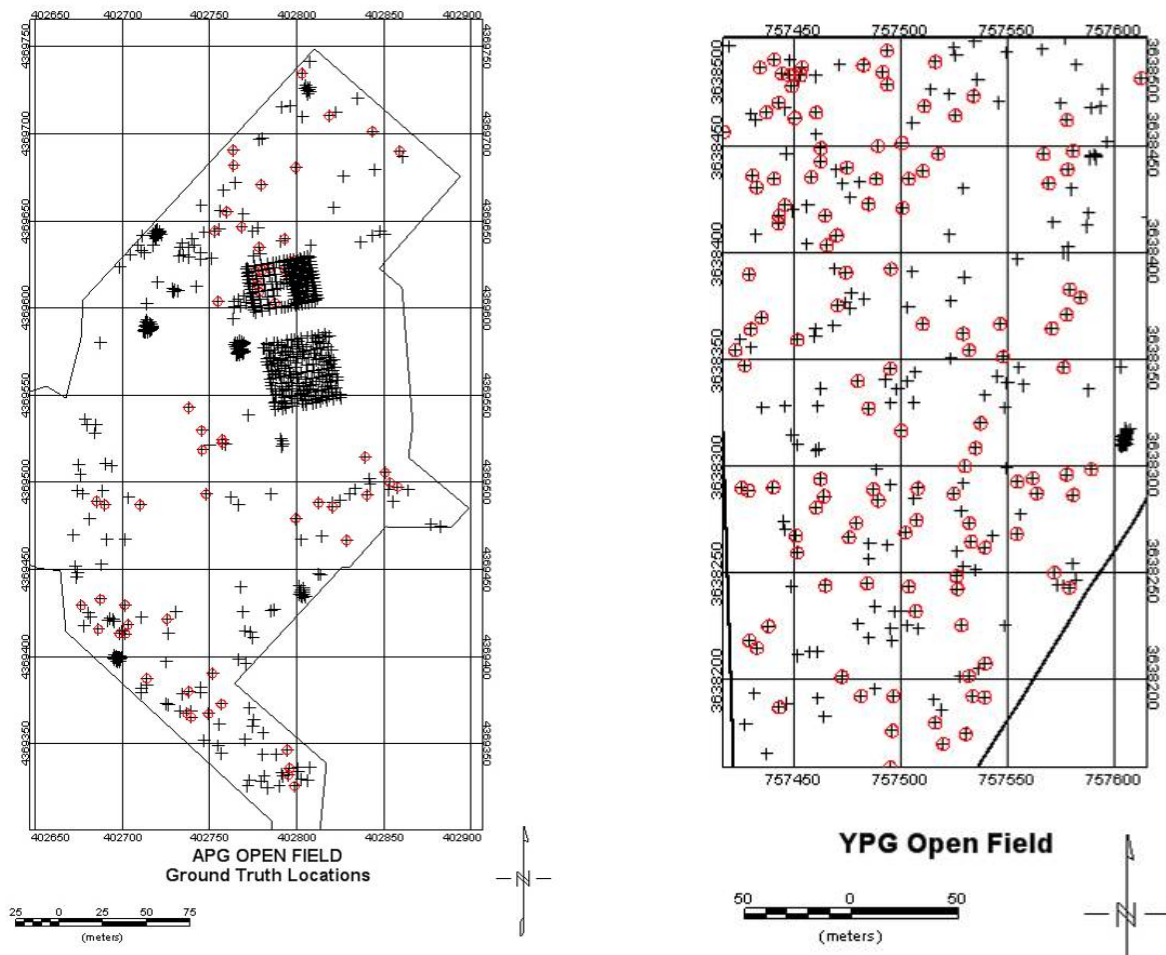


Figure 4-8 Distribution of anomalies for which ground truth information has been released (red circles) at the time of the study

Table 4-3 Number of ground-truthed, isolated anomalies that possess fit errors less than 31%.

	APG UXO	APG NON-UXO	YPG UXO	YPG NON-UXO
CAL	100	0	98	0
BLIND	85	115	74	107
OPEN FIELD	129	197	193	97
TOTAL	314	312	365	204

For the EM63 data, two separate variations on the above algorithm were applied, resulting in four sets of fit results. In the first variation, the code allowed for an offset to be applied to the measured signal, effectively producing a dc leveling of the data. The offset was constant over the anomaly, but different for each time gate. This offset was solved for linearly along with the β 's.

The second variation hinged on how the time gate information was used. In one version, all time gates were solved simultaneously, resulting in a single value for each of the six spatial parameters over all time gates. In the other version, each time gate was solved independently of the others. Here, each time gate has its own values of the 6 polarization parameters.

Figure 4-9 and Figure 4-10 shows fit results for NRLs EM61 training data and TTFW's EM61 training data from the YPG site, respectively. These plots are helpful to visualize how the individual features plot in feature space and to see if certain features are distinct for different groups or types of ordnances. Here, symbols are color coded with red, blue, green and black symbols representing large ordnance (105mm and 155mm), medium ordnance (57mm, MK118, 60mm, 81mm and 2.75in), small ordnance (20mm, 40mm, M42, BDU-28 and BLU-26) and clutter, respectively. The different symbols within each ordnance group represent a particular ordnance type within the group. For example within the large ordnance group the red plus signs, red triangles and red asterisks identify 155mm, 105mm M60 and 105 Heat rounds, respectively. Within the medium ordnance group the blue plus signs, blue asterisks, blue triangles, blue squares, and blue crosses identify 2.75in, 81mm, 60mm, MK118 and 57mm items, respectively. Likewise within the small ordnance group the green plus signs, green asterisks, green triangles, green squares, green crosses, and green diamonds identify BDU-28, BLU-26, M75, M42, 40mm and 20mm items, respectively.

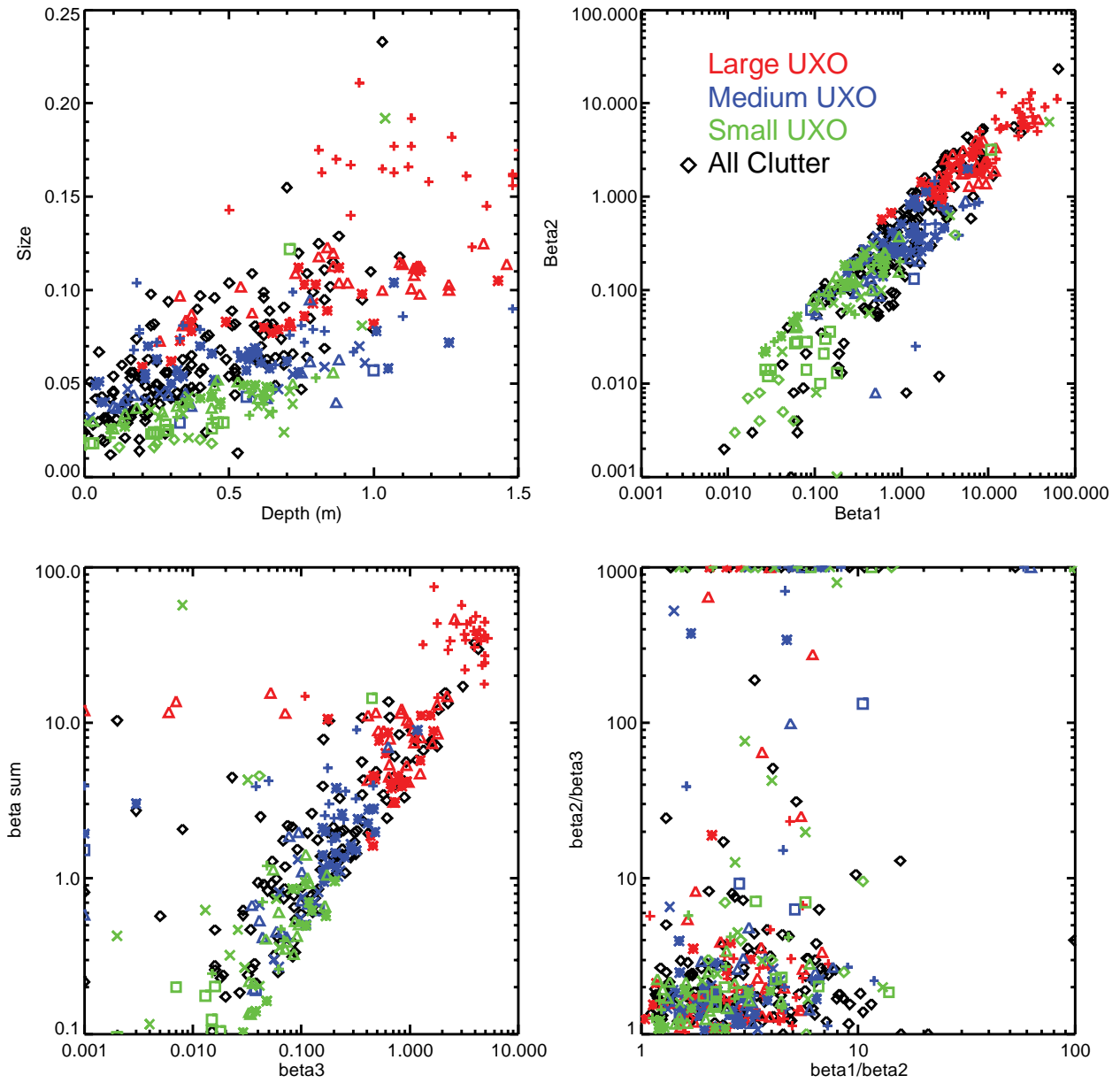


Figure 4-9 Fitted features derived from the NRL EM61 training data, YPG site, fit errors less than 31%.

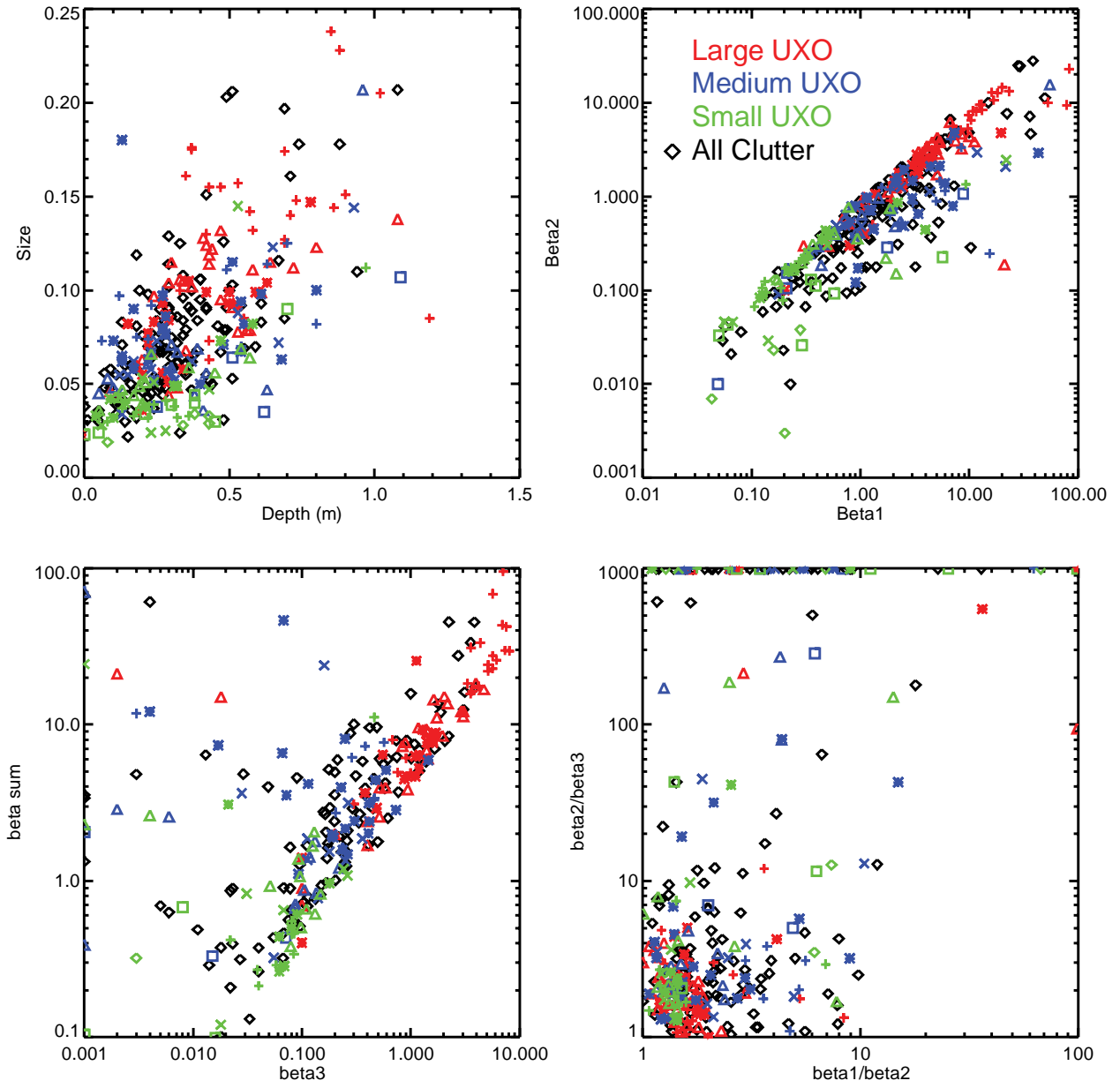


Figure 4-10 Fitted features derived from the TTFW EM61 training data, YPG site, fit errors less than 31%.

4.3.2 Passion-Oldenburg-Billings (POB) model – GPA version

The full POB analysis assumes an axially symmetric (axial and transverse) tensor dipolar target response, and solves for the best fit of 13 parameters; six intrinsic (K_i , B_i , G_i), five extrinsic (x , y , z , azimuth, inclination), and the two ‘time shift’ parameters (A_i). The time dependence is of the form:

$$F(t) = (\text{Geometric Factor}) * K_i (t - A_i)^{-B_i} \exp(-t/G_i)$$

(t in msec, $i = 1, 2$ are the axial and transverse responses.)

The POB algorithm has been incorporated into UX-Analyze under ESTCP project MM-0210 with the modifications described below.

The algorithm has been modified to allow an input target depth if available. If not available the algorithm starts with a zero initial depth estimate, which seems to converge much better to the global best fit minimum than using a depth estimate calculated from the top coil to bottom coil ratio.

The G_i parameters (time constants of late exponential decay) would have diagnostic value (for UXO discrimination), but are difficult to determine in typical EM63 data sets because the late gates are often ‘in the noise’. In fact, the inversion often returns negative G_i time constants, in order to fit the late gate. The ‘time shift’ parameters (A_i) contribute a slight rounding (concave down for negative A_i) in the early log-linear decay which is often observed in field data. However, it is not clear whether this is due to an EM63 timing problem, to unequal amplitude response across the early gates, or to an intrinsic target property. The possible diagnostic value of the A_i is unclear. For these reasons, and to reduce the dimensionality of the modified Nelder-Mead Simplex minimization from 13 to 9 parameters, we have constrained $A_i = \text{zero}$ and the inverse of $G_i = \text{zero}$ in the current POB module.

The POB model was used to characterize WES EM63 data. Figure 4-11 shows fit results for WES’s EM63 training data from the YPG site. As describe above the symbols are color coded with red, blue, green and black symbols representing large ordnance, medium ordnance, small ordnance and clutter, respectively.

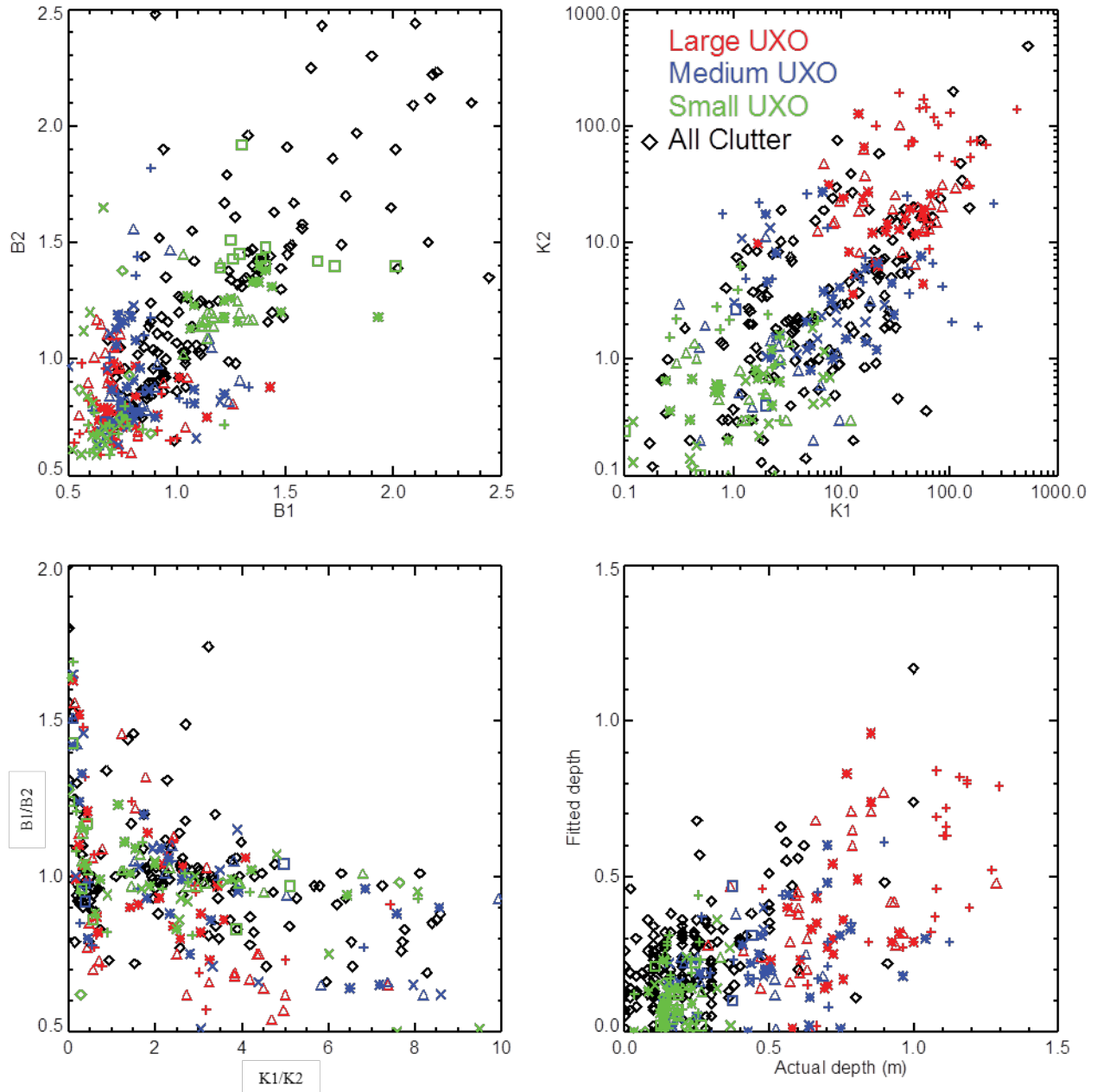


Figure 4-11 Fitted features derived from the WES EM63 training data, YPG site, fit errors less than 31%.

4.3.3 Empirical fit to GEM3

This empirical approach is built upon the dipole approximation. The signal at any spatial point can be represented by a linear combination of 3 β 's. These β 's are the eigenvalues of the symmetric effective magnetic polarizability tensor, and represent the response of the target along each of three principal axes. The β 's are in turn expressed in terms of an empirical five- or six-

parameter model [2]. This model is based on the theoretical responses of spheres and cylinders and has been shown empirically to fit a wide range of objects. The parameters of this model are τ , a time constant; A , an amplitude parameter; and S , f , and ν , shape parameters. In all, there are 18 features reported: 6 each from 3 principal axes. These features represent non-physical fit parameters from a frequency domain response model. Parameters are recovered in a two-stage process: (1) target position and orientation are determined through standard dipole-model inversion; (2) A 6 parameter FD response model is fit separately to observed beta response values, β_j , of each principal axis, which resulted from step (1). The 6 parameter model is:

$$\beta_j = A \left(\frac{f}{g} \frac{g-1}{g+1} + S \right), \quad g = \frac{\alpha^{2C} I_{\nu+1}(\alpha)}{I_{\nu}(\alpha)}, \quad \alpha = \sqrt{i \omega \tau},$$

where fitted parameters S , f , C , and ν are dimensionless, while parameter A has dimension of volume, and parameter τ has dimension of time [2]. The symbol $I_{\nu}(\alpha)$ is the Modified Bessel I function of order ν . All fitted parameters are real scalars. This model was derived from analytic solutions for the conducting loop, for spheres of arbitrary permeability, and for infinite cylinders illuminated transversely, also with arbitrary permeability. It provides exact matches to all of those analytic solutions through parameter adjustment, and also provides good matches to a wide range of irregularly shaped UXO.

Figure 4-12 shows fit results for WES's EM63 training data from the YPG site. As describe above the symbols are color coded with red, blue, green and black symbols representing large ordnance, medium ordnance, small ordnance and clutter, respectively.

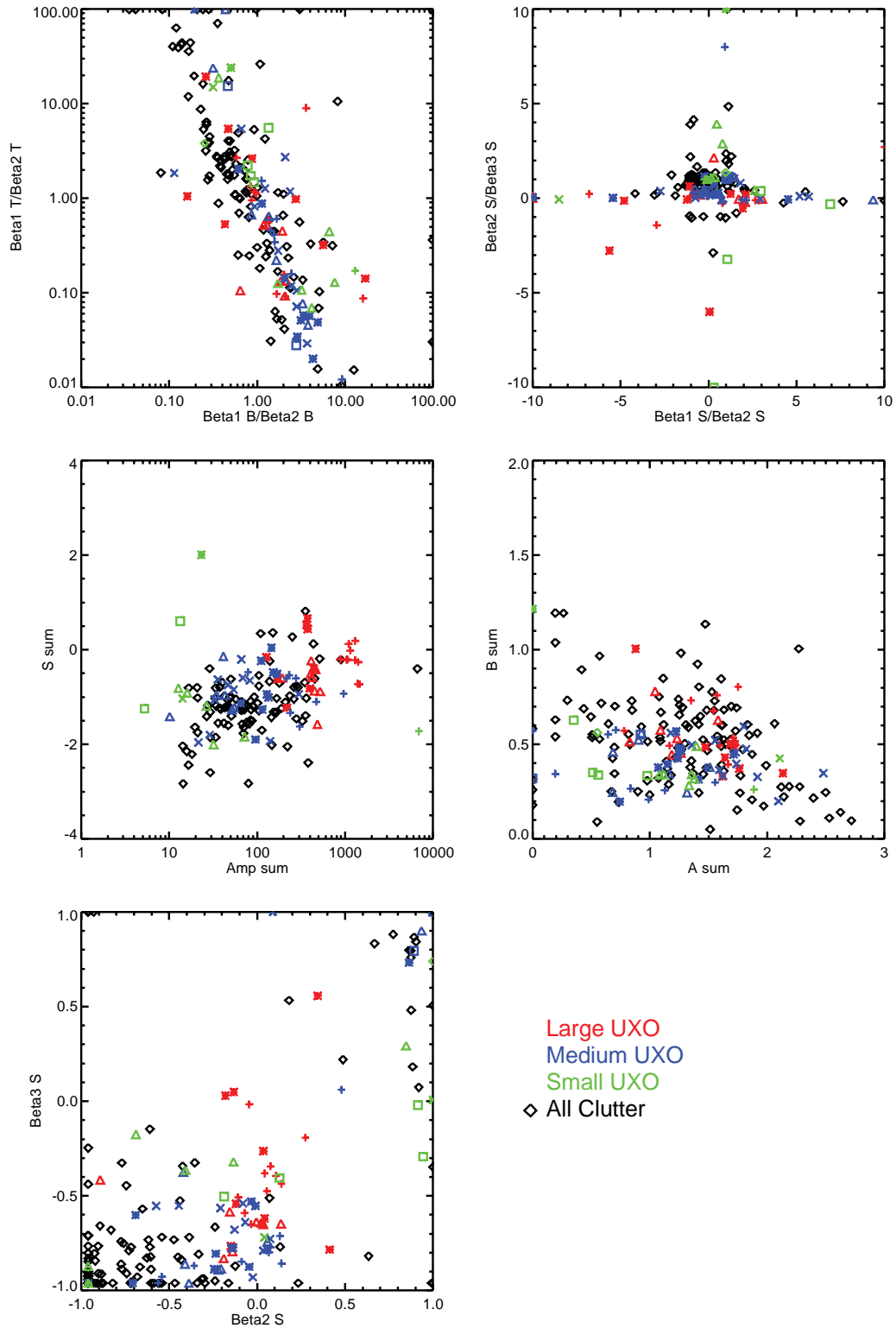


Figure 4-12 Empirical fitted features derived from the NRL GEM-3 training data, YPG site, fit errors less than 31%.

4.3.4 Ellipsoid Model

Similar to the empirical model described in the previous section, the ellipsoid model used to invert the GEM-3 data was also built upon the dipole approximation. As before, the polarizations are first expressed in terms of an empirical 5- or 6-parameter model [2]. The parameters of this model are τ , a time constant; A , an amplitude parameter; and S , f , and v , shape parameters. There are 3 sets of parameters per object, one for each principal axis. Here, in an effort to tie these parameters to actual physical dimensions we modeled the targets as ellipsoids. Assuming that the target is subjected to a uniform transmit field, the demagnetization factors can be expressed analytically in terms of A , b , and c , the semi-principal axes of the ellipsoid. This allows us to express the last four parameters in the empirical model in terms of a , b , c , and μ_r , the relative permeability of the target [3].

The remaining parameter, the τ 's, are handled by two different methods. In the first, the τ 's are simply treated as 3 independent fit parameters. In the second method, we make use of the fact that the τ 's scale as a size squared to tie them into the ellipsoidal semi-principal axes. By utilizing empirical measurements by Ben Barrowes [5], relating the ratio of the time constants to the ratio of ellipsoid sizes, we need add only one new fit parameter, a Scale factor relating a^2 to τ_a .

In summary, both inversion methods require 3 positional parameters (x_o, y_o, z_o), 3 angles (ϕ, θ, ψ), the 3 ellipsoidal semi-principal axes (A, B, C), and the relative permeability of the target (μ_r). The first method then requires 3 τ 's, while the second requires only a scale factor.

Initial guesses were provided for all parameters. The positional parameters x_o and y_o were determined from a signal-weighted mean of the target locations. The other parameters were set to reasonable values. With such a large number of parameters, ensuring that the inversion reaches the global minimum often requires a range of initial guesses for parameter values. In an effort to balance convergence to the global minimum with reasonable run time, we took the following approach. First, we perform multiple loops over the target depth and orientation (plus μ_r for the 3 τ method), but only allow for 5 iterations of the inversion routine. Whichever set of initial guesses leads to the smallest χ^2 fit between the predicted and measured response after these 5 iterations is then used in the full inversion. We found that this approach produced the same result as doing the multiple loops over 100 iterations, but was significantly faster.

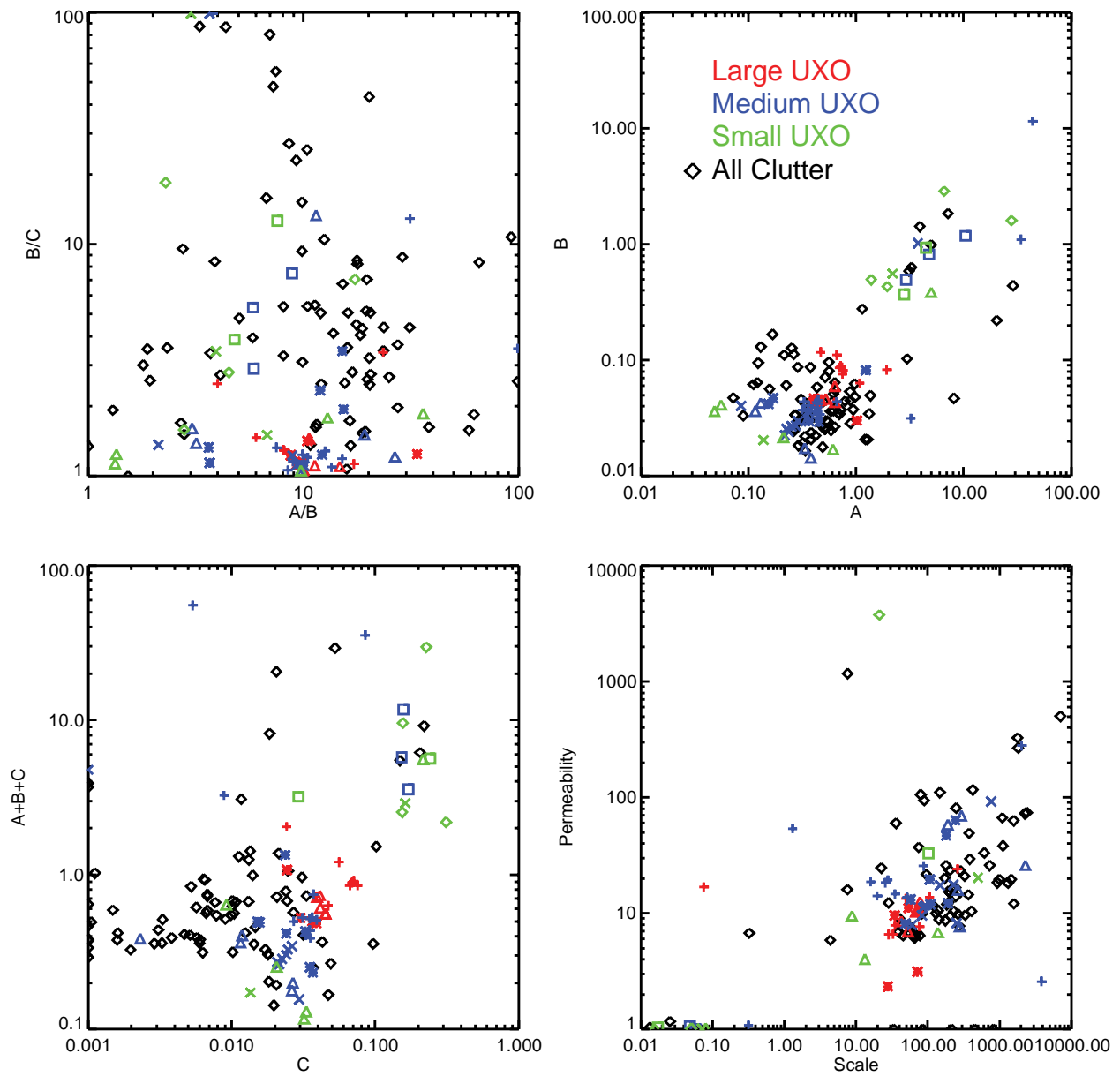


Figure 4-13 Ellipsoidal scale fitted features derived from the NRL GEM-3 training data, YPG site, fit errors less than 31%.

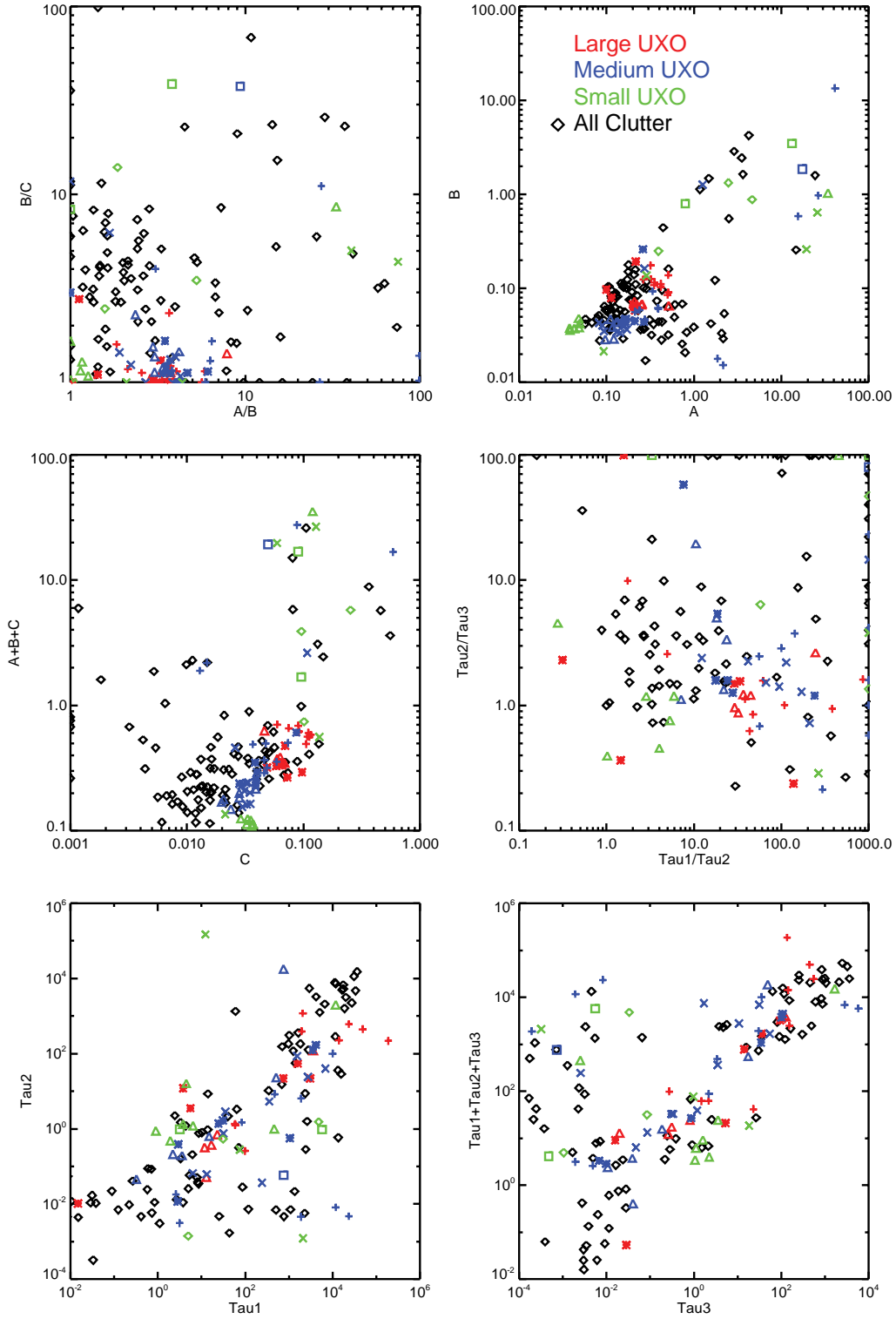


Figure 4-14 Ellipsoidal tau fitted features derived from the NRL GEM-3 training data, YPG site, fit errors less than 31%.

4.3.5 TD-FD Loop Model

Target responses can be expressed as an infinite sum of loop response terms. That applies both for TD and FD. The central idea of this method is to create basis vectors representing signals (both TD and FD) for loops with given fundamental time constants, then find linear combinations of these vectors to best match observed signals. Observed signal include both TD and FD information, and the weights which result from regression represent the contribution in both TD and FD of the associated loop.

During inversion, target XYZ coordinates, and phi,theta,psi euler angles are searched nonlinearly. With each candidate set X,Y,Z,phi,theta,psi typically three basis vectors are found, labeled F,G, and H, corresponding to the signals associated with longitudinal response, and the two transverse responses. The best linear combination of F,G, and H is then found to match observed data on each sensor channel, and the resulting weights are the target betas b1,b2, and b3 for that channel.

In this solver, each candidate X,Y,Z,phi,theta,psi resulted in more than 3 basis vectors. Each loop creates a separate basis vector for each principal axis, so for nl loops, there would be nl * 3 basis vectors offered to the regression routine to match data. In addition, each of these basis vectors contains all points and all channels, so channels are not solved independently. This expands the size of the regression step, but it may be solved linearly with singular value decomposition, keeping solve times fast.

When the number of loops, nl, is high, starting around nl >=10, a problem develops with linear solution. The regression step tends to select large positive & negative weights on similar basis vectors, which almost cancel. This can cause undesired effects such as negative TD estimates at times where no data is present to constrain the model. A different kind of regression can be performed, NNLS(), a least-squares minimization algorithm developed by Lawson and Hanson [6] which restricts weights to be non-negative, but this greatly slows computation. Instead, we rely on keeping nl down to 6 or less.

4.3.6 Duke's Singularity Expansion Model

The Duke Singularity Expansion Model (SEM) for a Body of Rotation (BoM) was based on the idea that the UXO or clutter object can be represented as a single equivalent dipole. The model assumes that the target object is symmetric in a single plane (such as a cylinder). The model describes the dipole moment magnetization tensor as a single pole model in the frequency domain. [7]

$$M(\omega) = zz \left[m_z(0) + \frac{\omega m_z}{\omega - j\omega_z} \right] + (xx + yy) \left[m_p(0) + \frac{\omega m_p}{\omega - j\omega_p} \right].$$

The time-domain magnetization tensor is given by

$$M(t) = zz \left[\frac{d}{dt} u(t) m_z \exp(-\omega_z t) \right] + (xx + yy) \left[\frac{d}{dt} u(t) m_p \exp(-\omega_p t) \right].$$

The scattered magnetic field is given by,

$$H^{scat}(w) = -\frac{1}{4\pi} \nabla \times \left[M(w) \cdot H^{inc}(w) \times \nabla \frac{1}{r} \right], \text{ where}$$

r is the distance from the object to the sensor and the magnetization tensor coordinate system must be aligned with the coordinate system of the sensor.

The model parameters are found by computing the least squares (LSQ) solution between the data and the model, given a particular set of model parameters. The model parameters are found by randomly initializing a set of parameters and then applying a gradient descent algorithm to converge to a locally best-fit (minimum error) solution. The non-linear solution space creates the possibility for many locally minimum error solutions that may not be globally the best-fit to the data. To overcome this problem, the input parameter space is randomly sampled hundreds of thousands of times to find a set of good starting points for the gradient descent algorithm. Since a good initial starting point is the key to finding the best overall solution, it is important to sample the parameter space as densely as possible. The suitability of the initialization is determined by finding the error between the model and the data. This process is typically fast compared to finding the complete gradient descent solution. Once the best initial starting points are found, the full gradient descent solution can be computed for only the best N initial parameters.

4.3.7 Magnetic Model

The theoretical model used is a magnetic dipole. The magnetic field anomaly due to a ferrous object can be expanded in a multi-pole expansion with the leading term representing the dipole contribution. The higher order terms fall off more sharply with distance so if the object is compact and sufficiently far from the sensor the dipole term will dominate.

Target location, depth, and magnetic dipole moment (which is related to size) can be estimated from magnetometer survey data. Figure 4-15 presents estimated versus actual depth and size measures as well as plots of some relevant features.

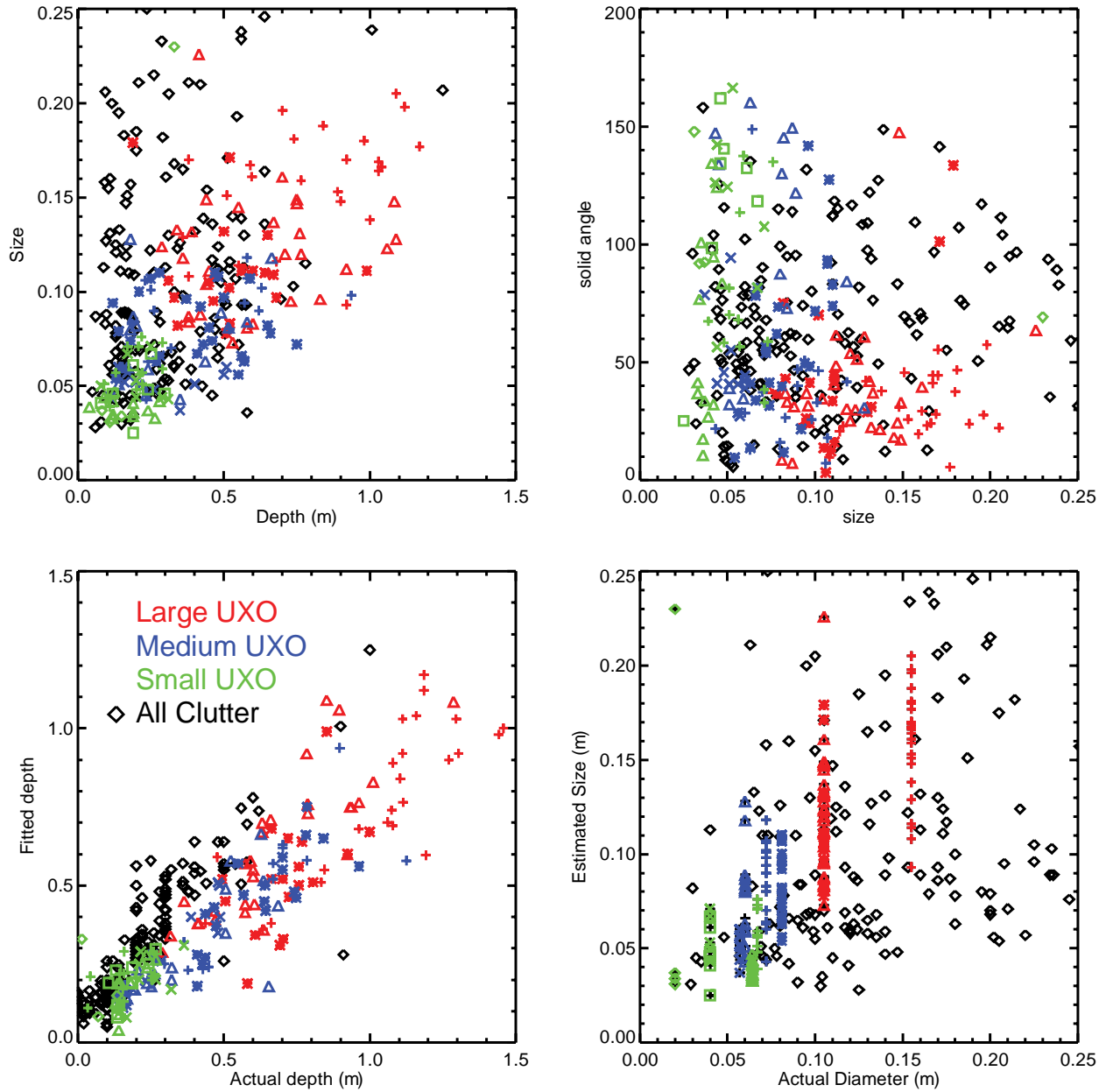


Figure 4-15 Actual versus estimated depth and size plots and other relevant features plots; NRL magnetic array data, YPG open field

4.4 Statistical Pattern Recognition Toolbox (SPRT) Framework

The SPRT provides a cohesive suite of interrelated functions that aid in the development, cross-validation, testing, and final selection of state of the art statistical pattern classifiers. It provided seamless integration of one-off training, k-folds cross-validation, feature generation, feature selection, classifier training, classifier scoring, and classifier/decision boundary display for

general M-ary and binary classification problems. The SPRT is sometimes referred to as the DPRT.

A variety of methods for classification, cross validation, scoring and performance metrics have been implemented in the SPRT, as have several basic programmatic and usability functions (data handling, data display, training, etc.) Classifiers that have been included include a traditional K-nearest-neighbor and a Duke modification to this approach, a Fisher Linear Discriminant (specifically for the SIG effort), a GLRT, a matched subspace detector, Parzen Window density estimation, kernel matching pursuits, a relevance vector machine, a support vector machine (specifically for the SIG effort), and fuzzy k-means. In addition, under the SIG effort, specific data classes that support UXO data and UXO data formats have been developed and included. Feature generation includes principal component analysis and independent component analysis, and Features selection includes Sequential Forward, Sequential Backward, N Forward/K Backward, Branch and Bound, Beam Search (under SERDP/Duke support), a novel Viterbi-based Parallel-Sequential (PARSE) search (under SERDP/Duke support), and an exhaustive search (specifically for the SIG effort). Scoring metrics include area under the ROC, Pd at a given Pf, Pf at a given Pd, and Percent Correct. Many distance metrics are also included for Wrapper-based feature selection methodologies. Cross-validation techniques include automatic k-folds cross validation over data sets and N-K folds averages over N iterations of K-folds. The SPRT provides a bridge between theoretical classifier development and real-life design issues.

The SPRT was used to classify and analyze ground truthed data acquired at YPG. Polygons were developed by hand, and then the data in the polygons was passed off to the feature extraction algorithms. The feature normalization, selection and classification processes are described below.

4.4.1 Feature normalization

Each feature was normalized independently. The feature normalization consisted of three steps. The feature values were first log-scaled (to prevent taking the log of negative values, the feature values were shifted to have a minimum value of 1 prior to taking the log). The feature values were normalized by the standard deviation calculated over the interquartile values (25 percentile to 75 percentile). We subtract the median value as the final step. Using the standard deviation of the interquartile range, rather than the standard deviation of all values, and subtracting off the median rather than the mean, makes the normalization more robust in the presence of outliers (i.e. outliers don't skew the normalized features).

Some of the feature values that were calculated as ratios of two model parameters can take values of infinity, which will cause problems during classifier training. As part of the feature normalization, any feature values equaling positive or negative infinity were remapped to a value equaling 100 times the maximum non-infinite absolute value. For example, with this remapping rule the sorted feature values $[-\infty -8 -3 0 2 3 \infty]$ would be remapped to $[-800 -8 -3 0 2 3 800]$ since the maximum non-infinite absolute value is eight.

4.4.2 Feature selection

Feature selection was implemented using wrapper techniques, measuring classification performance on a set of training data with various sets of features to find the best-performing feature set. The feature selection technique was performed using four classifiers described below. A forward sequential feature selection routine was used to find a rank-ordered list of the 20 best features for models having more than 20 features; for models with fewer than 20 features it was possible to perform an exhaustive feature search for the best feature set containing between 1 and 5 features. The wrapper techniques used k-folds cross-validation with $k = 5$. The fitness metric for each feature set or feature, used to determine the best feature set in the exhaustive search or which feature to add next in the forward sequential search, was the area under the ROC curve. If two feature sets / features have the same area under the ROC curve, the probability of false alarm at a probability of detection equaling 90% was used as a tie-breaker. The number of features was selected to maximize the fitness metric (area under the ROC curve) on the training data.

4.4.3 Classifiers

K-NN: The k-nearest neighbor (K-NN) classification rule uses the k neighbors of an unlabeled test point to estimate its label. The posterior probability of the class H given the unlabeled test point x, $p(H|x)$, is approximated by the proportion of the k neighbors in the labeled training data that are from class H. Thus, K-NN provides a simple and intuitive classification rule where new data points are labeled according to a majority-vote of the nearest neighbors. K-NN has been shown to have attractive asymptotic properties when the amount of available training data and the number of neighbors k are both large.

GLRT: The generalized likelihood ratio test is grounded in Bayesian decision theory. The likelihood ratio test $\lambda(x)$ is defined as the ratio of two conditional probabilities: the probability of the features given H_1 $p(x|H_1)$ and the probability of the features given H_0 $p(x|H_0)$, where H_1 and H_0 correspond to the UXO and clutter classes, respectively. Given probability distributions of the feature values for the classes of UXO and clutter, the likelihood ratio test can be calculated for any new data point by taking the ratio of the likelihoods of the features of the new data point under both H_1 and H_0 . However, one issue arising with the likelihood ratio test is that the probability distributions $p(x|H_1)$ and $p(x|H_0)$ are rarely known. Thus, one solution is to assume the conditional probability distributions follow a parametric form with parameters estimated using the training data. The GLRT is calculated using the conditional probabilities that are dependent on the estimated parameters [8]. In our implementation it is assumed that the UXO features have a Gaussian distribution. The clutter features were modeled using an improper uniform distribution that does not have estimated parameters; therefore, we are not training our clutter class (which can be very diverse and difficult to estimate).

SVM and RVM: The support vector machine (SVM) and relevance vector machine (RVM) are generalized linear classifiers. In both the SVM and RVM, the use of a kernel to represent the input data introduces nonlinearity and can transform the data into a higher dimensional space

where it may be separable by a hyperplane. The differences between the SVM and RVM arise in the frameworks for optimization and training. The RVM finds relevance vectors that typically are located near the “centroids” of the decision boundary contours, whereas the SVM finds the support vectors that define the decision boundary. The RVM also does not utilize a margin between the classes, which is directly optimized in the training of the SVM. The SVM finds a decision boundary with the constraint of maximizing the margin, whereas the RVM does not consider a boundary margin in any sense. Instead, the RVM is a Bayesian kernel machine that applies a Bayesian framework to define the weights and relevance vectors through iterative calculation of the posterior weight distributions. A characteristic common to both the RVM and SVM is sparse representation of the decision space using a small subset of the training data. Rather than keeping track of all of the training data, the RVM and SVM techniques only require a limited subset of training vectors to discriminate between classes. The RVM tends to select fewer relevance vectors than the number of support vectors found by the SVM. Therefore, the training data is represented by an even more compact set of vectors which can further reduce the risk of overtraining.

4.4.4 Training Labels and Types

We trained on data from both APG and YPG in order to increase number and type of labeled data. Prior to doing so, we compared classification results of APG and YPG separately (Figure 4-16). We used a common definition of misfit (linear Pearson correlation coefficient) across models for different data types and included only those targets whose mean coherence was greater than 0.89, which correlates to a dipole fit error of approximately 31%. The table at the right hand side of the figure shows the ordnance type distribution of those targets available for training. All told, we had approximately 180 training labels for a wide variety of ordnance types (Figure 4-17).

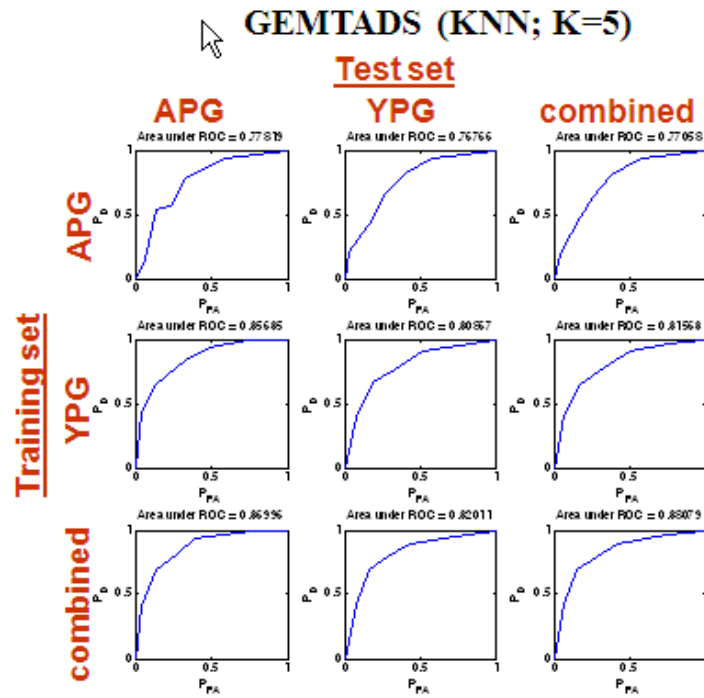


Figure 4-16 Classification ROCs for different scenarios of training and test data sets

TYPE	Number
105mm M456 HEAT	11
105mm M60	14
105mm NS	4
155mm M483A1	11
155mm NS	3
2.75 M230	9
2.75 NS	2
20mm M55	4
40mm M385	1
40mm MK2	8
57mm M86	11
57mm NS	6
60mm M49A3	8
60mm NS	7
81mm M374	7
81mm NS	14
BDU-28	12
BDU-28 NS	7
BLU-26	11
BLU-26 NS	3
M42	8
M42 NS	1
M75	5
M75 NS	11
MK118	2

Figure 4-17 Type and number of training labels available for this study. As used here, ‘NS’ indicates non-standard munitions. All other notations are specific subtypes of a particular munition type.

5. Results and Discussion

To compare classification performances, we first performed a forward sequential feature selection to identify which features produced the best performance for each combination of data type and model (Figure 5-1). We started with features that are intrinsic to the target (i.e., principal axis polarizability, moments, characteristic frequencies, etc.), then generated candidate subsets by adding a single feature to the set of previously-selected features, and finally evaluated subsets using a KNN classifier. Performance measures were defined to be (i) the area under (AUC) the ROC curve and (ii) the probability of false alarm (PFA) at a probability of detection (Pd) of 0.95. Example ROC curves for specific, but arbitrary AUC measures, are shown Figure 5-2.

The full results of the feature selection and performance evaluation are presented in detail in the Appendix. In the following sections, we high light and discuss the most salient results.

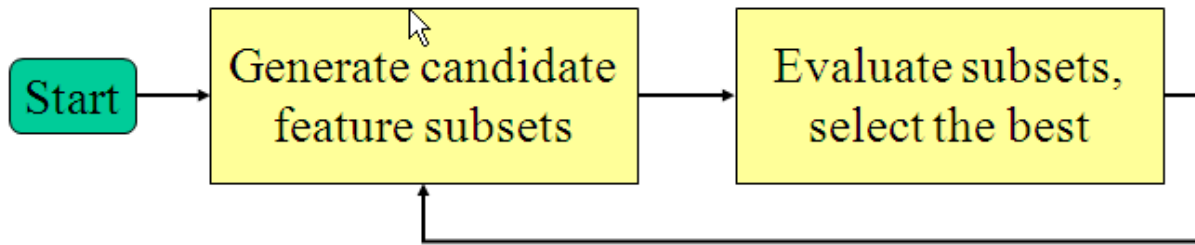


Figure 5-1 Schematic showing the forward sequential feature selection process adopted for identifying the best performing set of features for each combination of data type and model.

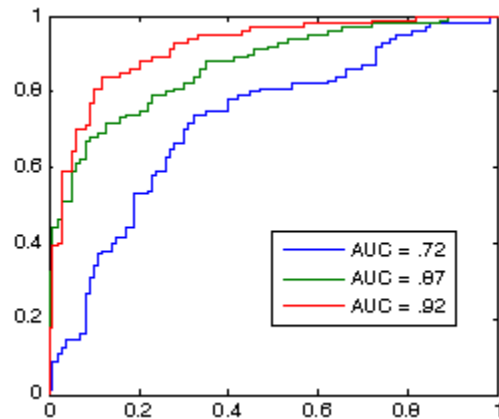


Figure 5-2 Comparison of hypothetical ROC curves possessing specific AUC measures

5.1 Performance Statistics – all UXO and all non-UXO

Table 5-1 presents summary measures for the best performance obtained for each data type and model combination included in the study.

Table 5-1 Performance Measures as a function of Data and Model

Data/Model	AUC	PFA @ PD = 0.95
EM61 Array (UXA)	0.666	0.955
EM61 Array (latest solver w/ Mag)	0.766	0.804
EM61 Cart	0.630	0.938
GEMTADS (best)	0.818	0.723
Magnetic (UXA)	0.677	0.893
EM63 (POB)	0.789	0.625
EM63 (SEM)	0.670	0.964
TDFD	0.737	0.839

5.2 ROC Performance as a function of Classifier

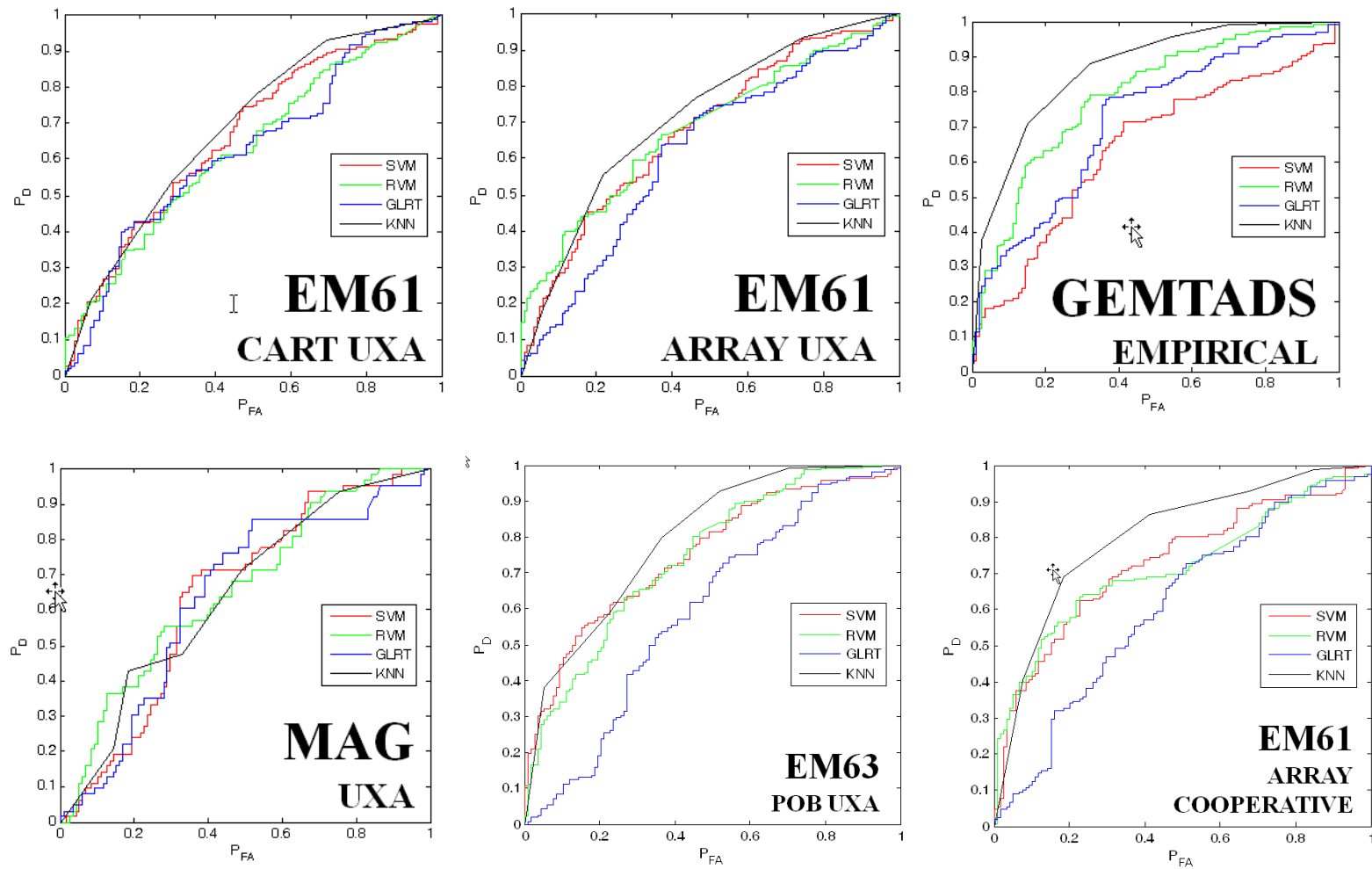


Figure 5-3 Performance ROCs as a function of classifiers for specific data types and best performing model

5.3 Performance as a function of Data/Model

Performance ROCs for various combinations of data type and model are graphically superimposed in Figure 5-4.

We show in Table 5-2 the best performances observed for each data type (EM61, Mag, and EM63). This analysis utilized a KNN classifier for all data types.

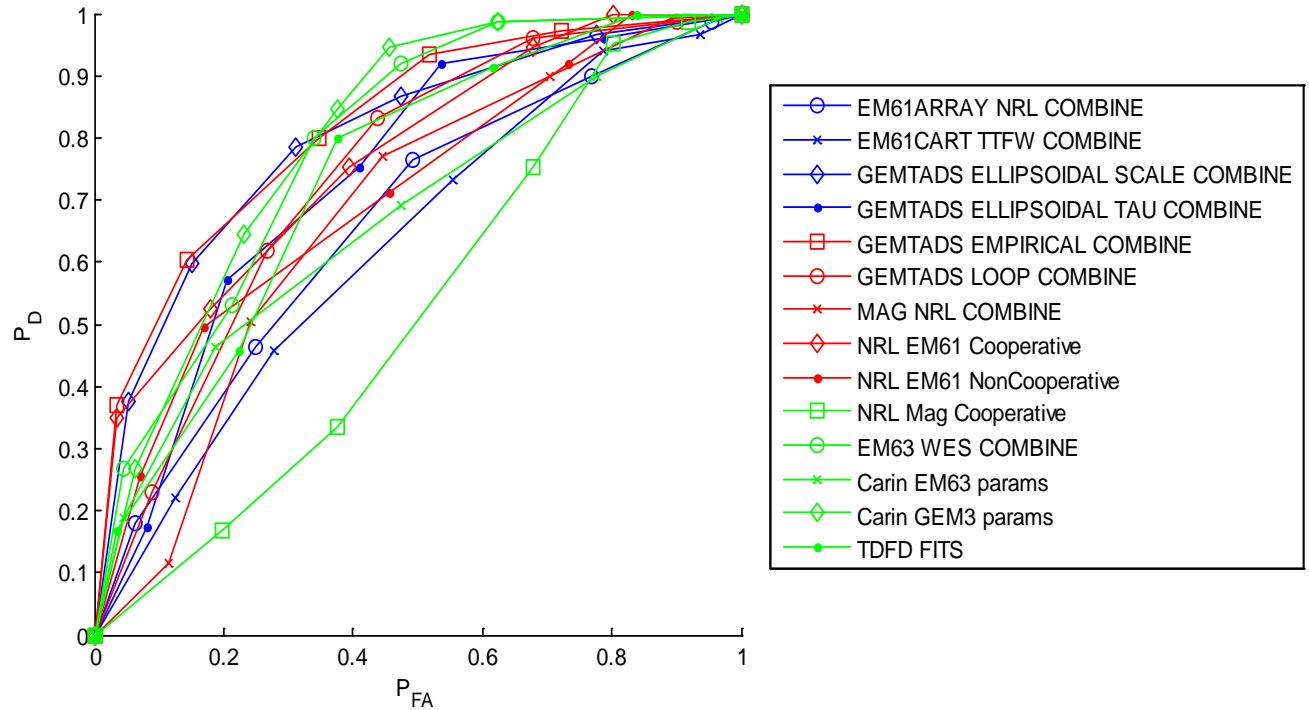


Figure 5-4 Performance ROCs for specific data types and models as detailed in the key.

Table 5-2 Performance Measures for EM61, Mag, and EM63 data types

	AUC	PFA @ PD=0.95
EM61	0.766	0.804
MAG	0.677	0.893
EM63	0.789	0.625

5.4 Inverted Features

In this section, we graphically present the inverted features to provide a feel for the dispersion present in the recovered features. In these figures, the UXO is color coded by size class, where 'Large UXO' includes 105mm and 155mm, 'Medium UXO' includes 57mm, 60mm, 81mm, and 2.75in rockets, and 'Small UXO' includes 20mm, 40mm, M42, M75, MK118, BLU-26, and BLU-28.

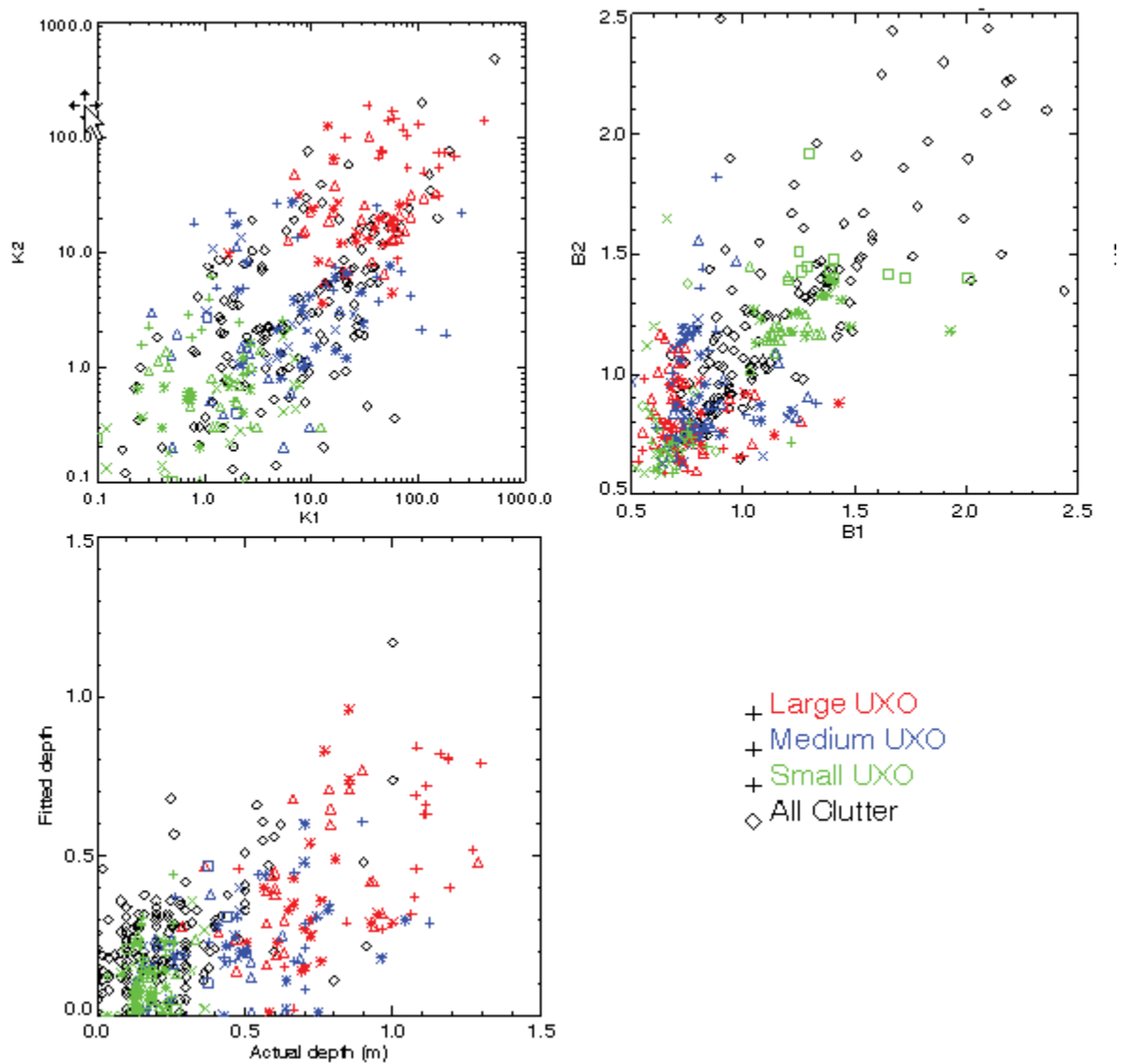


Figure 5-5 Inverted model features for EM63 data

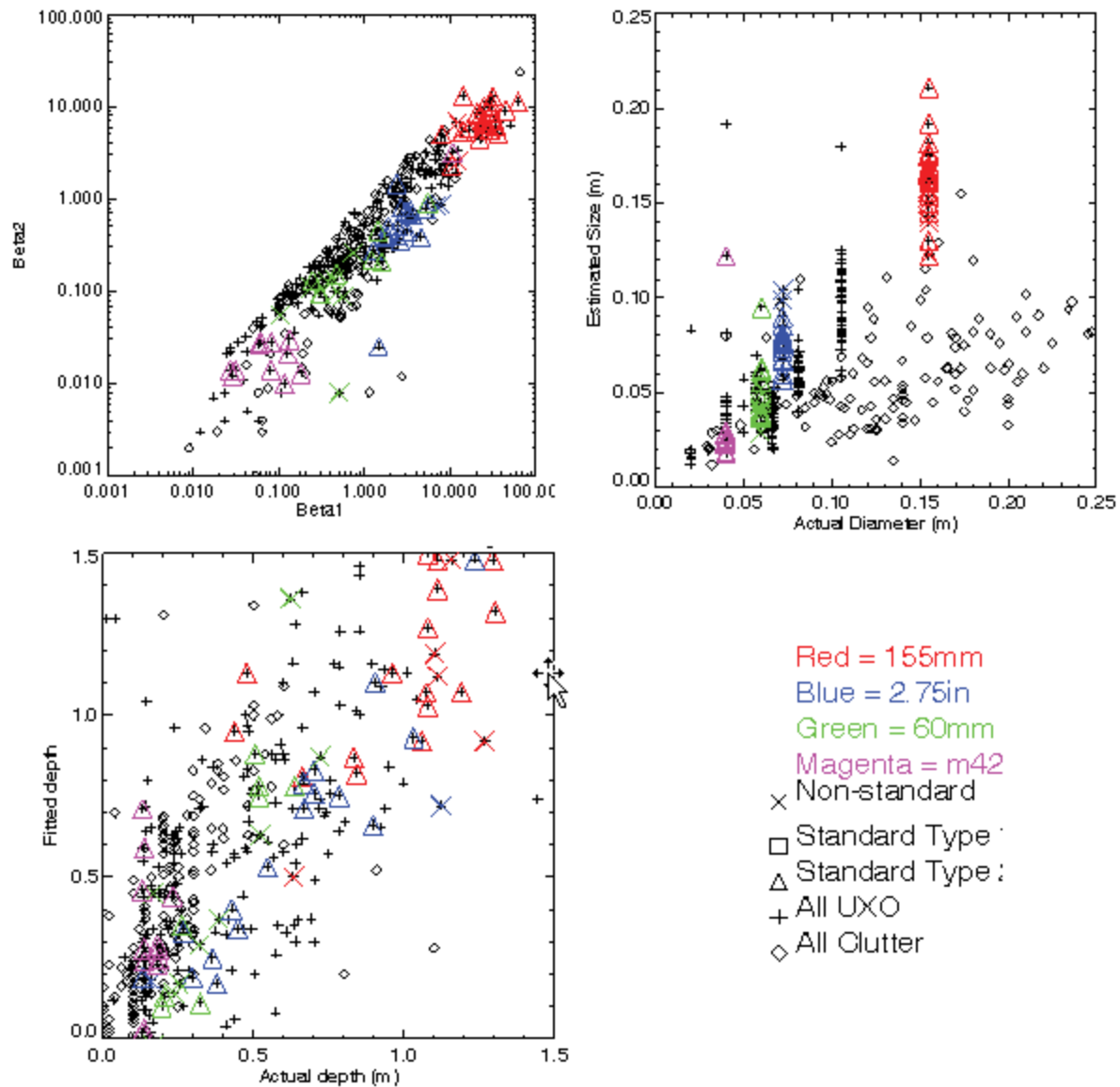


Figure 5-6 Inverted model features for EM61 data

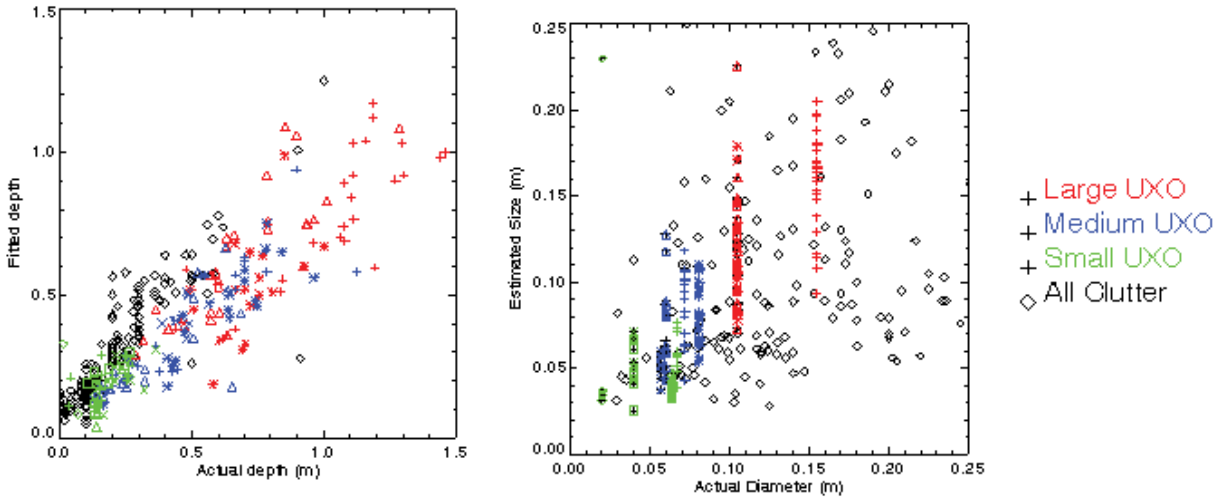


Figure 5-7 Inverted model features for magnetic data

5.5 All UXO versus all non-UXO Results Summary

The analysis up to this point has included all types of UXO present at the standardized test sites and all clutter. Although differences in performances are observed for various combinations of data type, model, and classifier, none of the combinations produces stellar classification performance.

The following general statements summarize classification performances when considering all UXO and all non-UXO:

- KNN classifier showing marginally better performance
- Broadband EMI sensors (EM63 and GEM) performed slightly better than EM61
- Marginal discrimination capabilities are observed if our objective is to separate all UXO from all non-UXO

Poor size- and/or shape-based discrimination results are not surprising for these data, however, given that we observe:

- The nominal dipole fit error is 20-30%
- UXO size ranges from small (20mm) to large (155mm & 500lb bomb)
- Emplaced clutter is primarily medium to large, & thick-walled

5.6 Subgroups based on Size

In this section, we subdivide the UXO and clutter into size classes, as defined in Table 5-3, to see what effects this has on the observed classification performance measures. It is reasonable to consider size-based classes because limited use ranges may not possess the wide range of UXO types and clutter that was emplaced at the standardized test sites. Sample sizes for each class are shown in Table 5-4.

Table 5-3 Size based definitions of UXO and clutter

<i>Class Label</i>	<i>Ordnance Type within Class</i>
Small UXO	20mm, 40mm, M42, M75 , MK118, BLU-26 and BDU-28
Medium UXO	57mm, 60mm, 81mm and 2.75in
Large UXO:	105mm and 155mm
Small clutter	weight < 1000 g (~less than 57mm)
Medium clutter	1000 g < weight < 8000 g (~57mm to 105mm)
Large clutter	weight > 8000 g (~105mm and up)

Table 5-4 Sample size for various combinations of UXO and clutter

TOI	Non-TOI	Number of UXO	Number of non-UXO
All	All	149	112
Large	Small	39	62
Large	Small + Medium	39	103

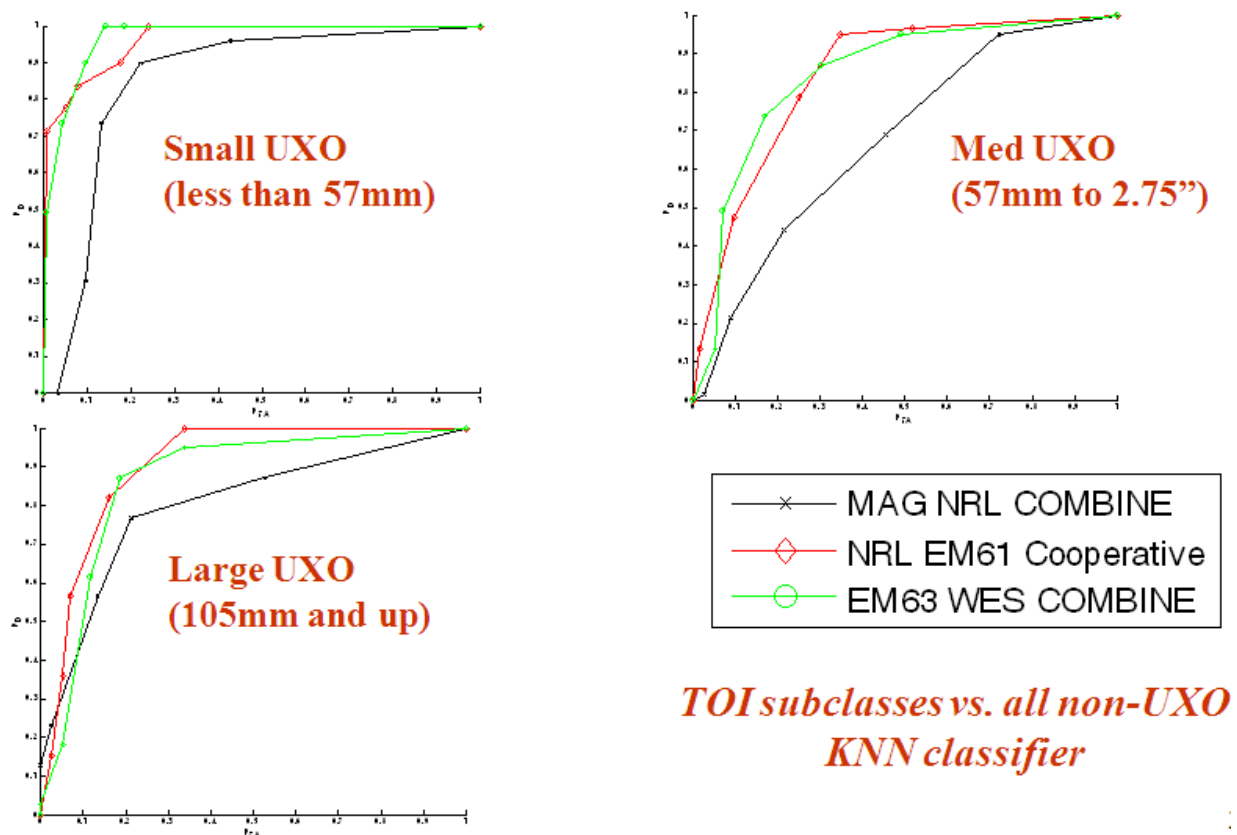


Figure 5-8 Performance ROCs for size based scenarios versus all clutter

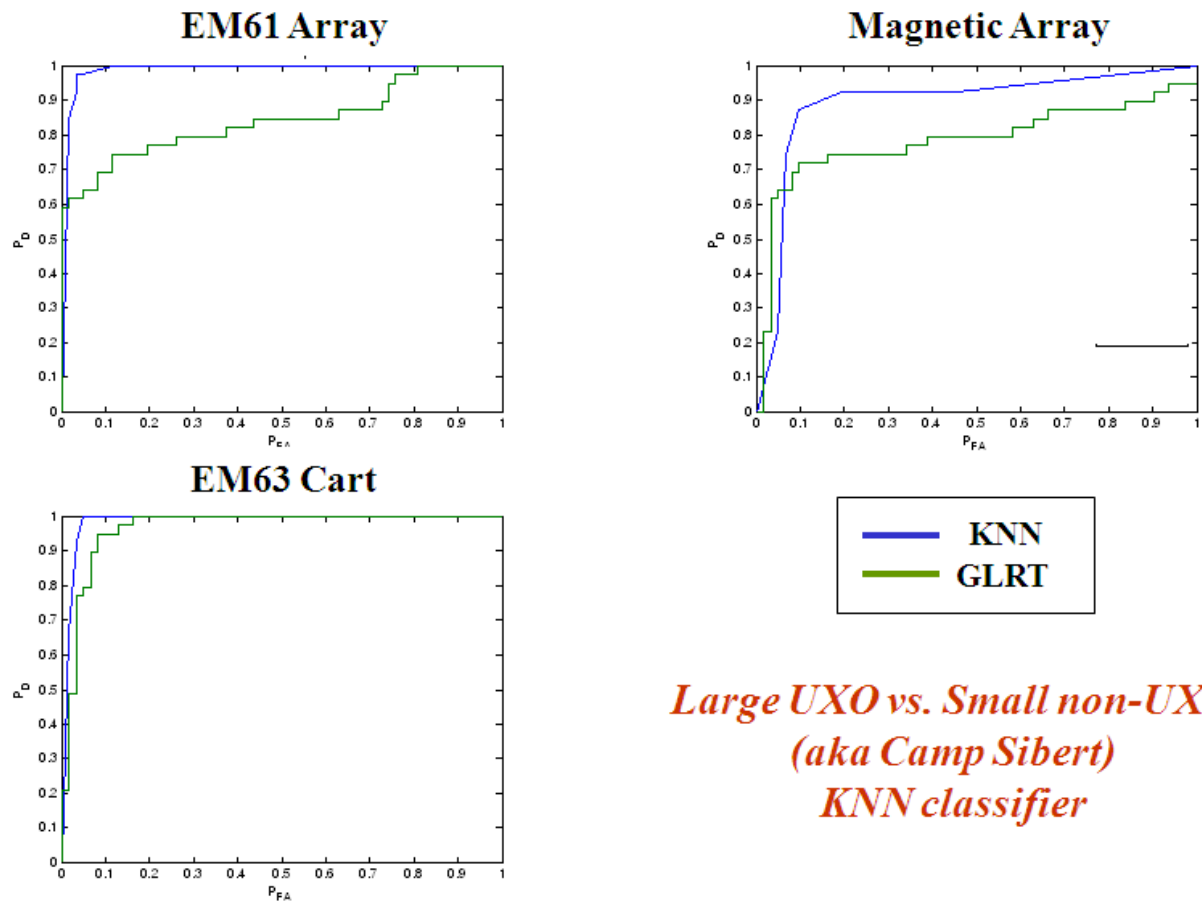


Figure 5-9 Performance ROCs by data type for Large UXO versus small clutter; KNN classifier

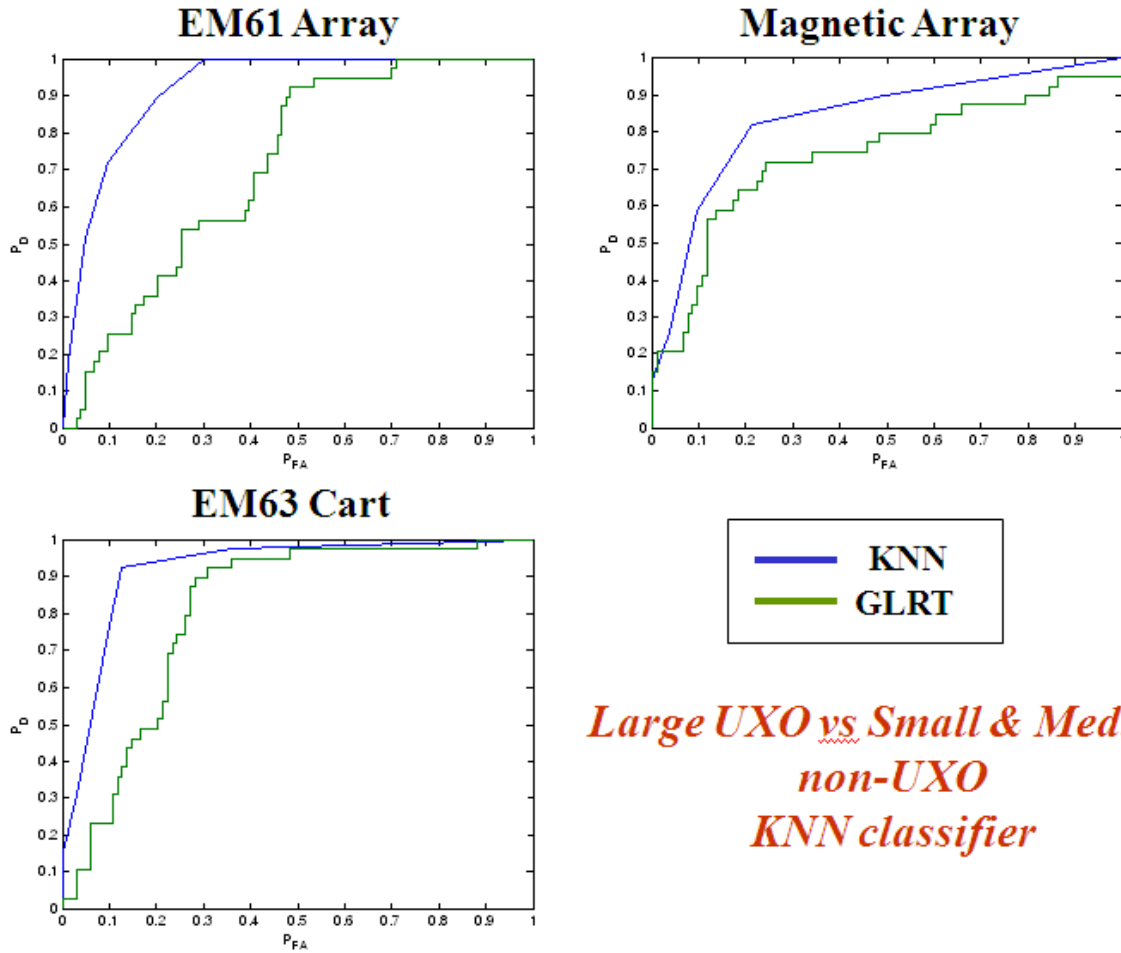


Figure 5-10 Performance ROCs by data type for Large UXO versus small and medium sized clutter; KNN classifier

5.7 Performance Bounds

For discussion purposes, we show in Figure 5-11, the classification performance if the length and width of UXO and clutter, as measured by a tape measure, are submitted to a classifier.

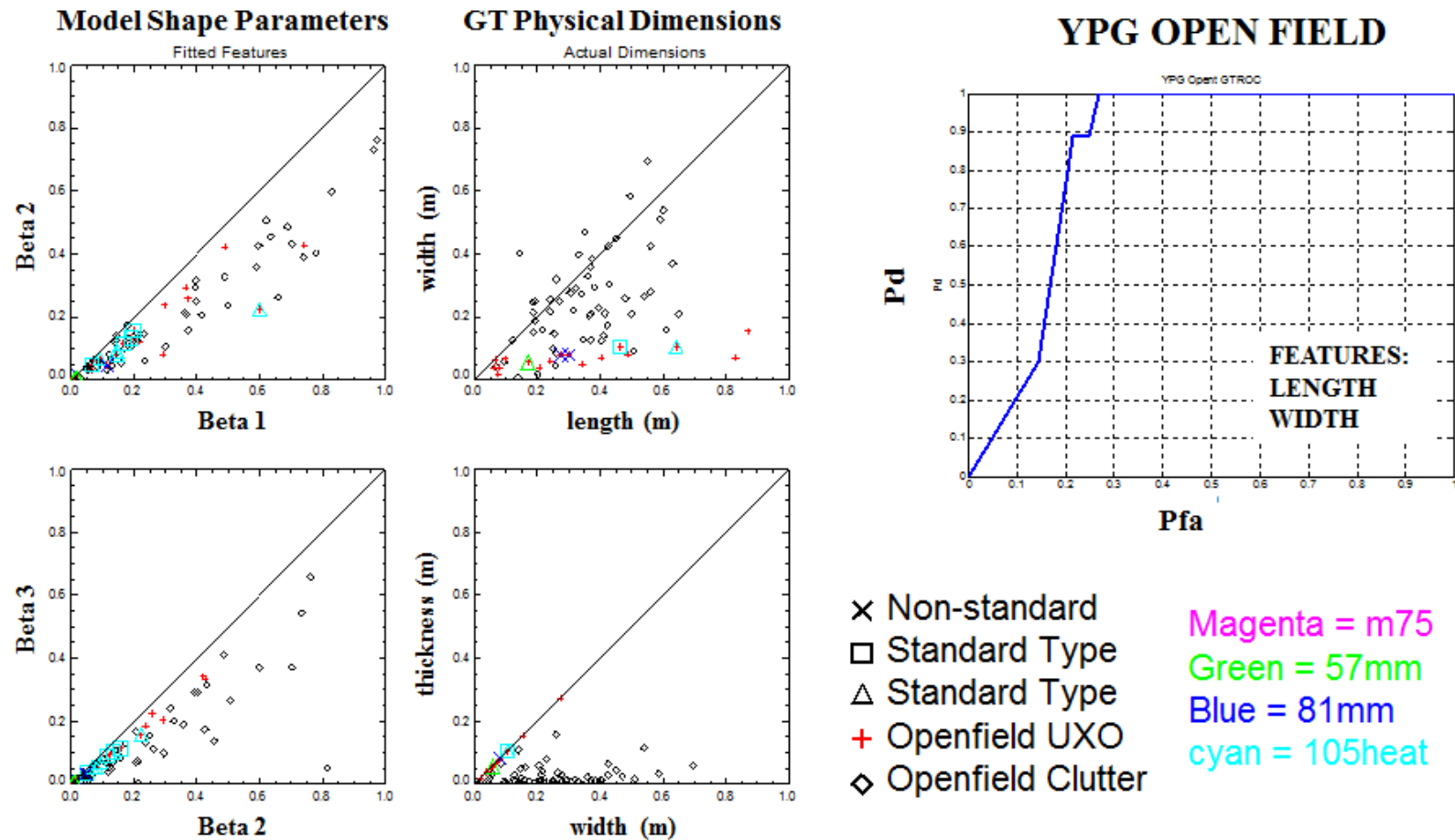


Figure 5-11 Performance bounds assuming inverted features duplicate the observed physical dimensions of length and width (assumed to be equal to the diameter for axial symmetric UXO). Left column – inverted polarization features. Ground Truth (GT) dimensions as reported. Right side – ROC generated by submitting the length and width data to a KNN classifier.

5.8 Comparison of Dynamic versus Static Data Collection

In this section, we present a comparison between data collected in cued mode at APG with reconnaissance data collected in dynamic modes. The cued data collection was acquired, in support of this effort, to provide an opportunity for removing data problems associated with imprecise spatial registrations.

For cued data collection, we acquired EM61 data using a mobile template as shown in Figure 5-12. We used an EM61 coil set of 0.5x1m coils. Data were collected on a 7x5 point rectangle (25cm x 50cm), covering an area of 1.25 x 2.0m. The bottom coil was 20cm above the ground.



Figure 5-12 Photographs of three different collection schemes compared in this section. Top left shows a cued deployment using a fixed sampling scheme. Top right shows the TEMTADS vehicular array. Bottom left shows a man-towed deployment scheme.

Figure 5-13 plots the recovered dipole fit errors versus SNR for common anomalies but different collection schemes. It is evident from this figure, and from Table 5-5, that the template (cued) data possess smaller fit errors than dynamic survey data and that fit error is inversely related to SNR.

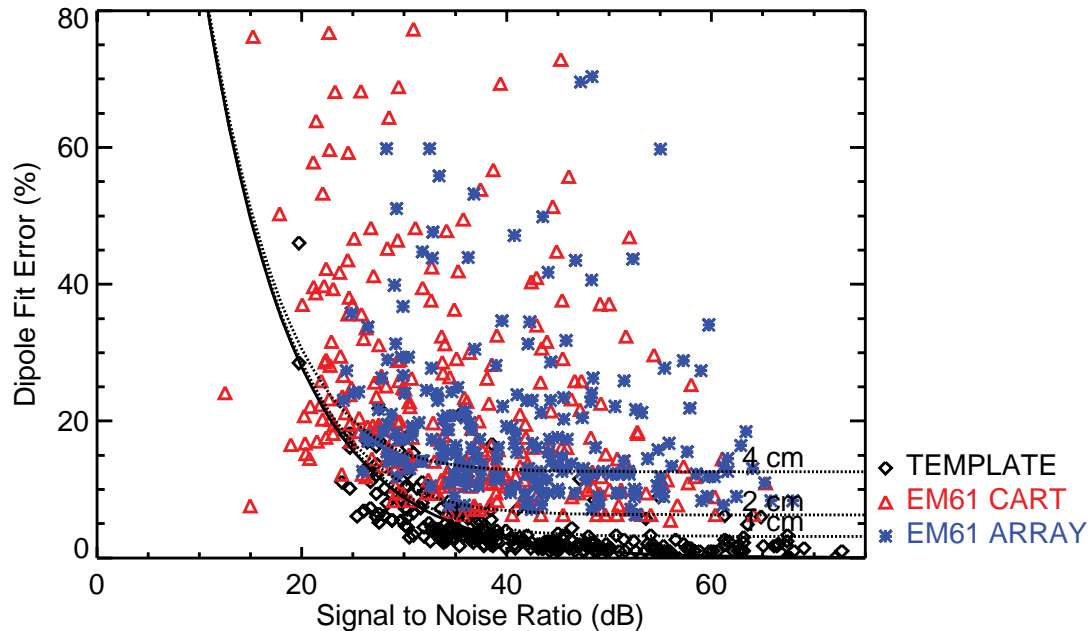


Figure 5-13 Comparison of dipole fit errors for common anomalies at APG with an EM61 sensor using a template, cart, and vehicular array deployment.

Table 5-5 Inverted fit statistics

	<i>SNR Mean</i>	<i>SNR Standard Deviation</i>	<i>Dipole Fit Error (Mean)</i>	<i>Dipole Fit Error Standard Deviation</i>
Template (stationary)	42.9	12.3	4.7	5.1
TTFW (dynamic)	35.7	10.8	24.1	17.2
NRL (dynamic)	41.6	10.7	19.4	11.9

Figure 5-14 and Figure 5-15 show measures of fitted results for the three collection schemes. As observed in these figures, the reported depth errors are somewhat similar for all three data sets. The dispersion in secondary and tertiary polarizability, however, is noticeable. Data acquired using the template possessed the smallest scatter while the EM61 cart (person portable) showed the most scatter.

Classification performance for all UXO versus all clutter for each data type is displayed in Figure 5-16. Not surprising, template performed the best, although it is not considered stellar, and the EM61 cart performed the poorest.

Figure 5-17 and Figure 5-18 presents features and classification performances for size based scenarios. As evident in these figures, sized based classification can be successful if the target population present at the site is favorable.

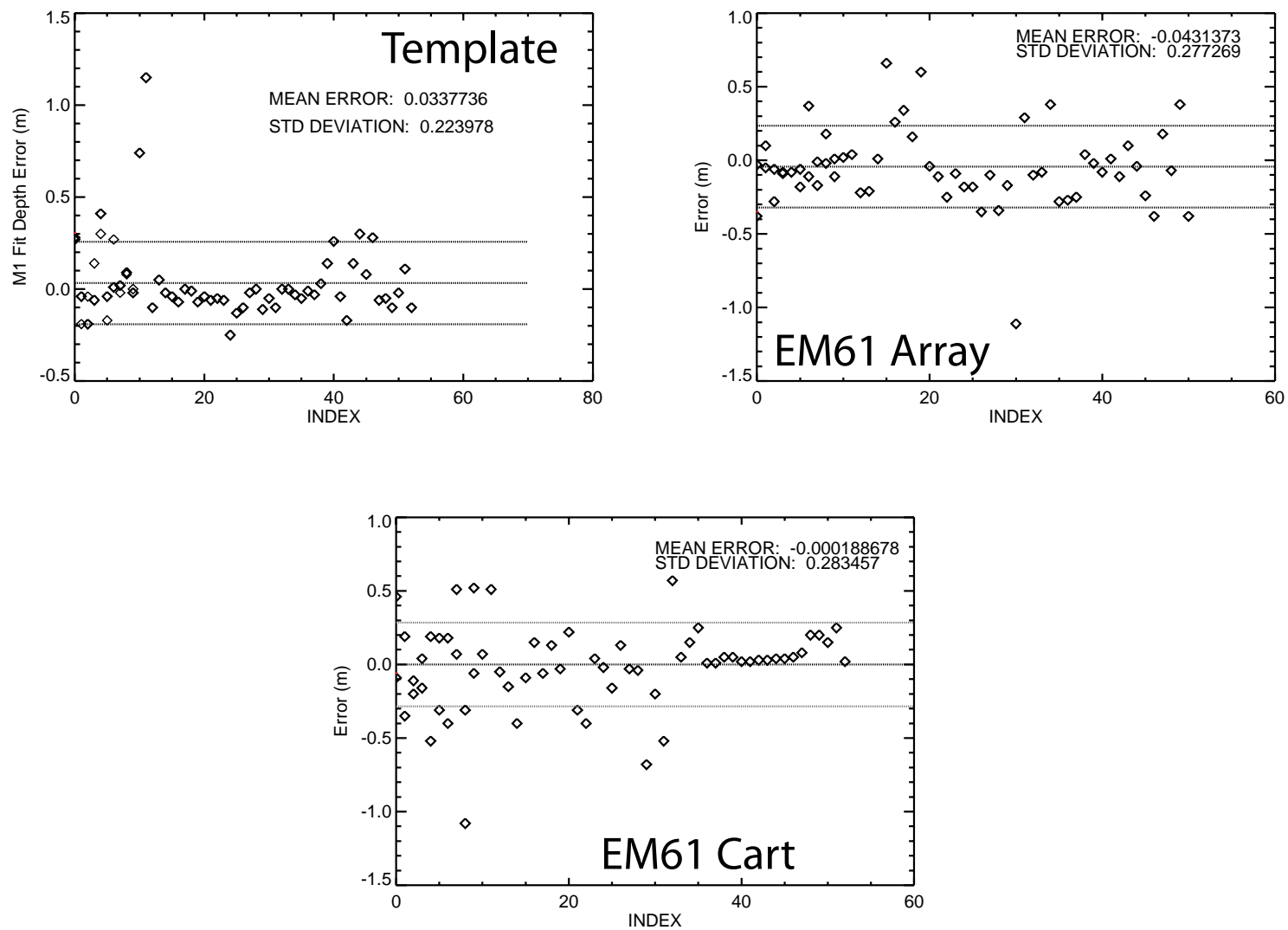


Figure 5-14 Similar errors in reported depth estimates are observed for the three deployment schemes; labeled UXO only.

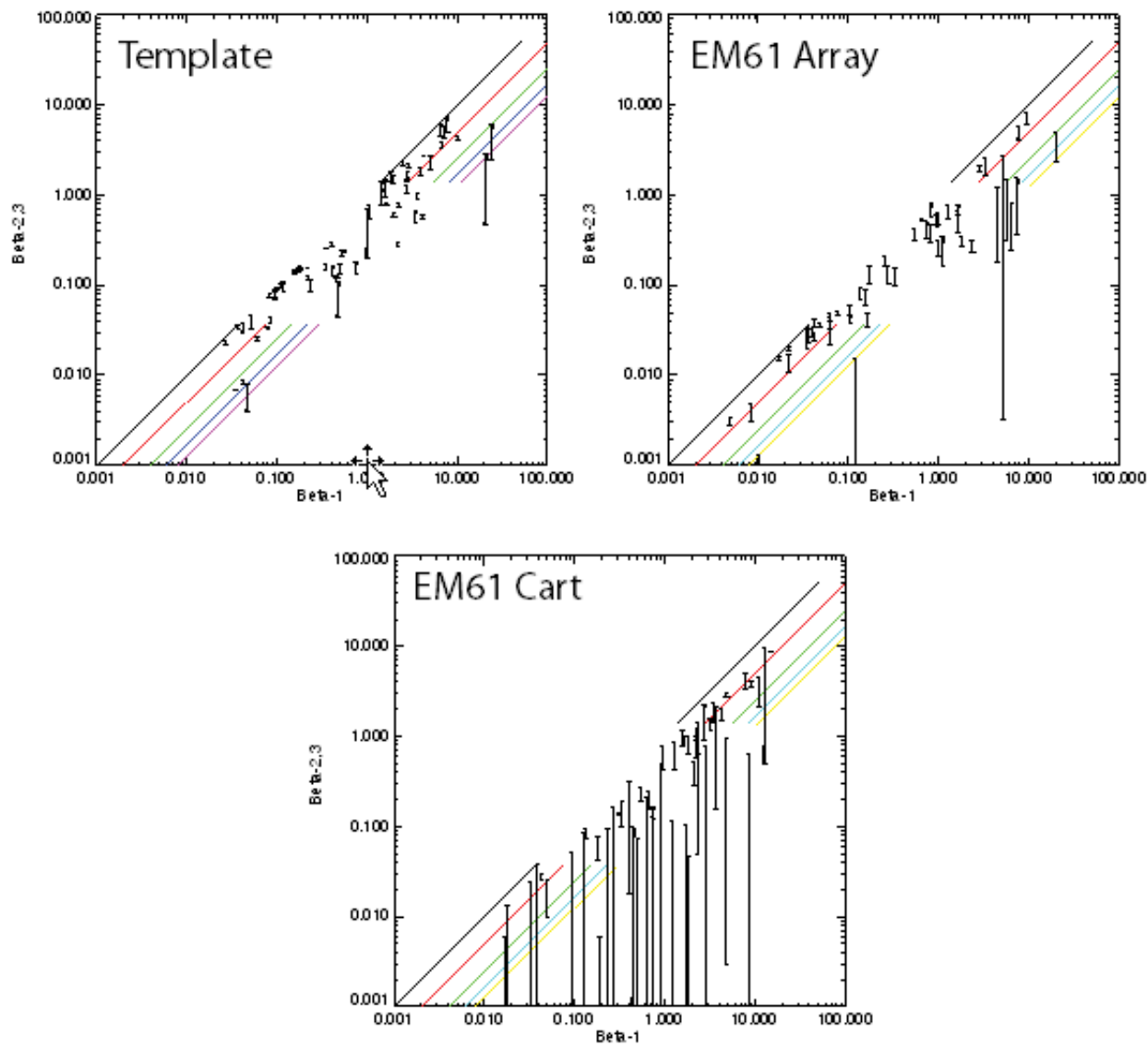
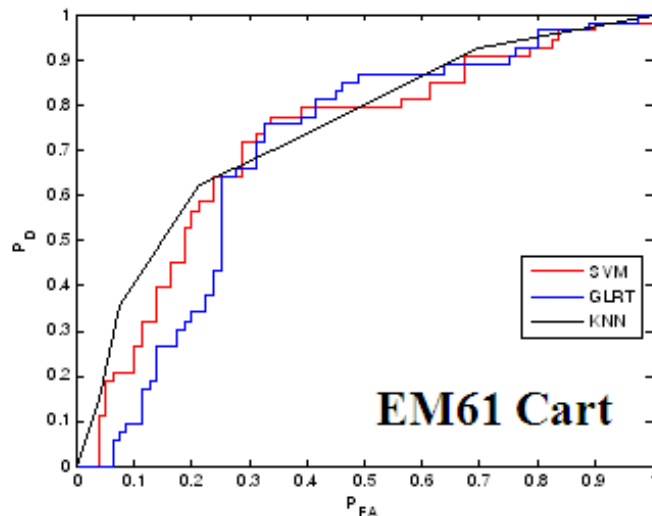
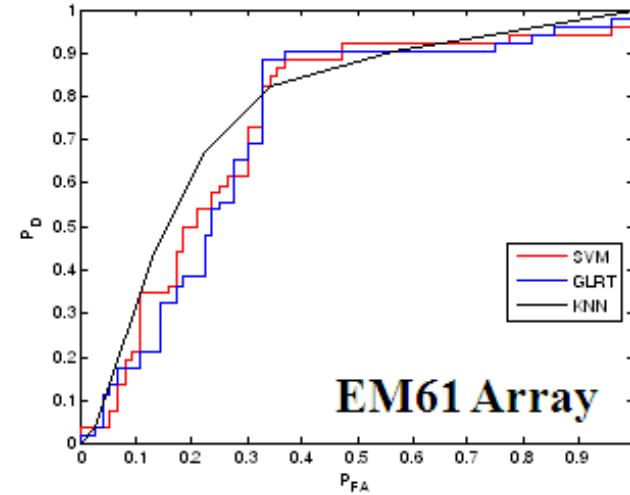
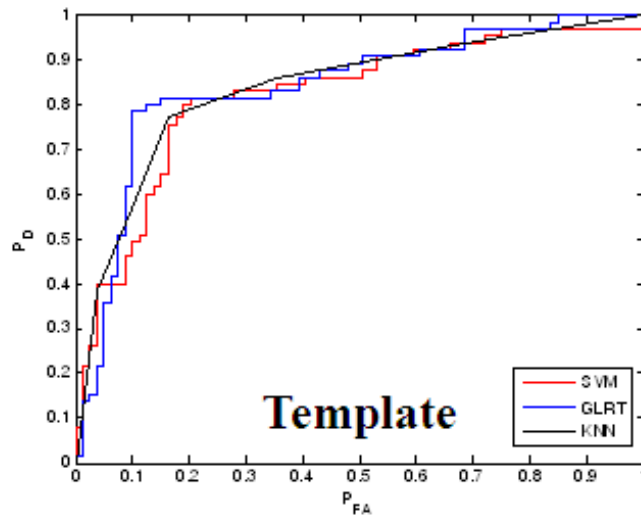


Figure 5-15 Polarization shape comparison plots (principal axis B1 compared to second/tertiary B2,B3 polarizations)



Intrinsic Features Only

Selected to provide optimal AUC
by sensor data and by classifier

All UXO vs. non-UXO
Cued collection
APG Only

Figure 5-16 Performance ROCs for template, cart, and vehicular array; EM61sensor, all UXO versus all clutter

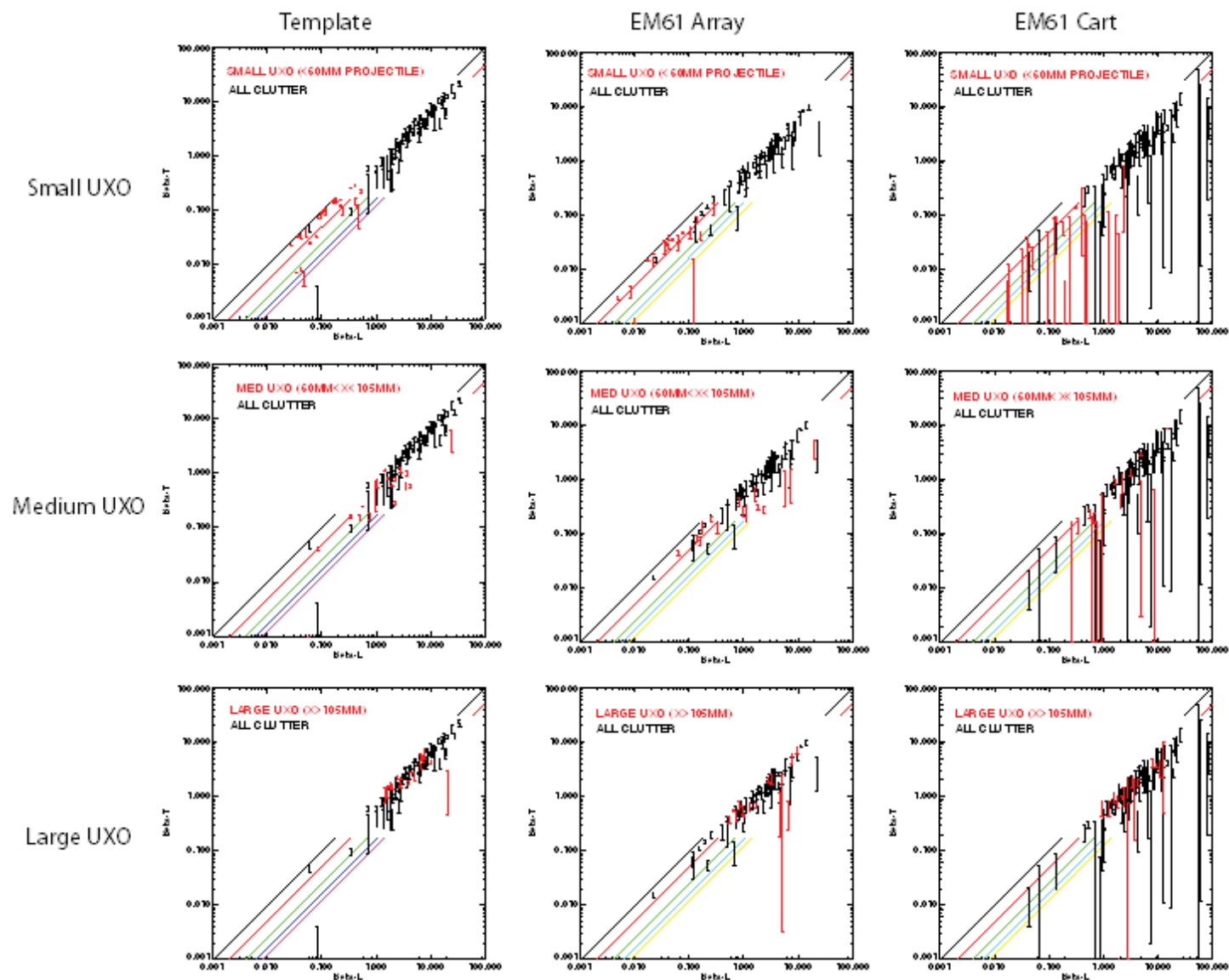
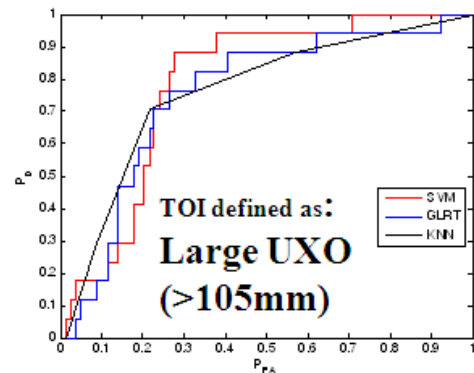
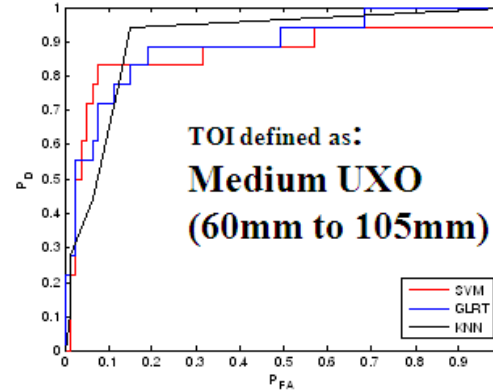
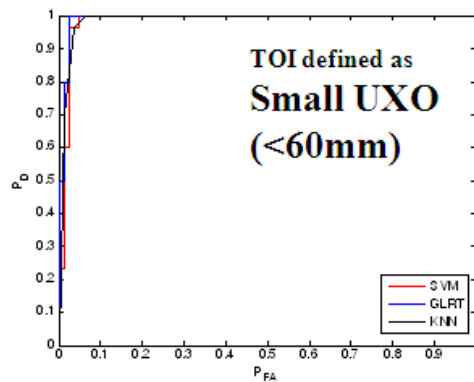


Figure 5-17 Polarizations segmented by survey modality and target size



Intrinsic Features Only
Selected to provide optimal AUC
by sensor data and by classifier

*Variable sized-based TOI classes
vs. all non-UXO*

Template EM61 Data Only, APG

Figure 5-18 Performance ROCs for template, cart, and vehicular array; EM61sensor, sized based UXO classes versus all clutter

5.9 Discussion

Our objective was to study discrimination capabilities of feature based characterization and classification techniques using data of opportunity acquired by others at the UXO Standardized Test Sites in APG and YPG. The fundamental issues investigated included the *model* used during characterization and the impact that *classifier selection* has on classification performance. After re-leveling and lagging the EM61 cart data, we inverted anomaly data for each data type using dipole, ellipsoidal, empirical, loop fit, joint frequency-time domain, and singularity expansion models. We then classified the resulting feature vectors with SVM, RVM, GLRT, and KNN statistical classifiers. We evaluated classification performance using two metrics derived from ROC curves; namely, (i) the total area under the curve and (ii) the probability of false alarms at 0.95 probability of detection.

We selected five data sets to include in this study based on data quality, type, signal-to-noise, and availability at appropriate intermediate processing stages. The datasets included time-domain EM61 (man-towed single sensor cart and vehicle-towed array), time-domain EM63, frequency-domain GEM-3, and magnetic data.

None of the classifiers or sensor/model combinations performed well when the TOI included 20mm through 155mm because the scatter of the features covered much of the feature space and thus overlapped with the features for clutter items. When the TOI were narrowed based on size (small, medium and large) the performance improved significantly.

A related cued data collection and comparison exercise showed an improved capability with regard to deriving meaningful shape parameters when compared to data acquired on dynamic platforms.

6. Conclusions and Implications for Future Research/Implementation

Our efforts to discriminate UXO from clutter using shape based information derived by inverting dynamic EM61, EM63, GEM, or magnetic data acquired at APG and YPG on dynamic platforms resulted in moderate to poor classification performances for all combinations.

Classifying based on inverted size, however, should be relatively successful and may prove useful at limited-use sites that contain a small range of ordnance types. The degree of success will depend entirely on the inherent size differences between the UXO and clutter at a given site.

The implication for future research is that new sensor technologies are required to realize acceptable classification performances. Given that there are multiple advanced sensors currently in development that are designed to maximize discrimination capabilities and mitigate limitations associated with single monostatic transmit-receive EMI systems, we recommend focusing future analyses efforts on their data.

Literature Cited

- [1] <http://aec.army.mil/usaec/technology/uxo03f.html>.
- [2] Miller, J., Bell, T., Soukup, J., and Keiswetter, D., *Simple phenomenological models for wideband frequency-domain electromagnetic induction*, IEEE Transactions on Geoscience and Remote Sensing, Vol., 39, No. 6., June 2001.
- [3] Barrow, B., Khadr, N., Miller, J., and Nelson, H., *An empirically based ellipsoidal model for multiple frequency EMI signatures from UXO*, SAGEEP, 2005.
- [4] Miller, J., *Quantification of UXO variability for Target Discrimination*, Strategic Environmental Research and Development Program, UX-1313, August 2006.
- [5] Barrowes, B., O'Neill, K., Grzegorzczuk, T., Chen, X., Kong, J., 2004, *Broadband analytical magnetoquasistatic electromagnetic induction solution for a conducting and permeable spheroid*, IEEE Transactions on Geoscience and Remote Sensing, v. 42, no. 11, November 2004.
- [6] Lawson, C. L., Hanson, R. J., *Solving Least Square Problems*, Prentice Hall, Englewood Cliffs, NJ. 1974.
- [7] Zhang Y, Collins L, Yu H, Baum C, Carin L, 2003, *Sensing of unexploded ordnance with magnetometer and induction data: theory and signal processing*. IEEE Trans. Geoscience Remote Sensing v. 41: 1005–1015.
- [8] McDonough R. N., Whalen A. D., *Detection of Signals in Noise*, Elsevier Science and Technology Books, April 1995.
- [9] Beal M, *Variational Algorithms for Approximate Bayesian Inference. PhD thesis*, Gatsby Computational Neuroscience Unit, University College London, 2003.

Appendix

K-folds training and testing with $k = 25$ was performed to generate the classification results for comparing performance across model sets and classifiers. Each classifier used the feature set that maximized the area under the ROC curve in the feature selection stage and compared the results to using all the features. The final feature sets for each of the classifiers for the various sensor/model combination and targets of interest (TOI) are listed in Table 6-1 to Table 6-10.

ROC curves are shown in Figure 6-1 to Figure 6-40 for various sensor/model combinations at YPG. For each sensor/model combination a ROC curve is presented for each classifier assuming four different TOI; i) all ordnance (20mm to 155mm), ii) small ordnance (20mm, 40mm, M42, BDU-28, BDU-26), iii) medium ordnance (57mm, MK118, 60mm, 81mm, 2.75in) and iv) large ordnance (105mm and 155mm).

Table 6-1 Best set of features for each of the classifiers with different TOI using the NRL EM61 array data at YPG.

Classifier	TOI All Ordnance Features	TOI Small Ordnance Features	TOI Medium Ordnance Features	TOI Large Ordnance Features
GLRT	Beta1/Beta2	Beta2, Beta3, Beta1/Beta2	Beta2, Beta1/Beta2	Beta2, Beta1/Beta2, Beta2/Beta3, Beta sum
SVM	Beta sum	Beta2, Beta3, Beta1/Beta2	Beta1, Beta1/Beta2, Beta sum	Beta2, Beta1/Beta2, Beta sum
RVM	Beta1, Beta2, Beta1/Beta2, Beta2/Beta3, Beta sum	Beta1, Beta3, Beta1/Beta2, Beta2/Beta3, Beta sum	Beta1, Beta2, Beta1/Beta2	Beta2, Beta3, Beta sum
KNN	Beta1/Beta2, Beta sum	Beta2, Beta1/Beta2, Beta2/Beta3	Beta1, Beta2, Beta1/Beta2, Beta sum	Beta1, Beta3, Beta sum
All features	Beta1, Beta2, Beta3, Beta1/Beta2, Beta2/Beta3, Beta sum			

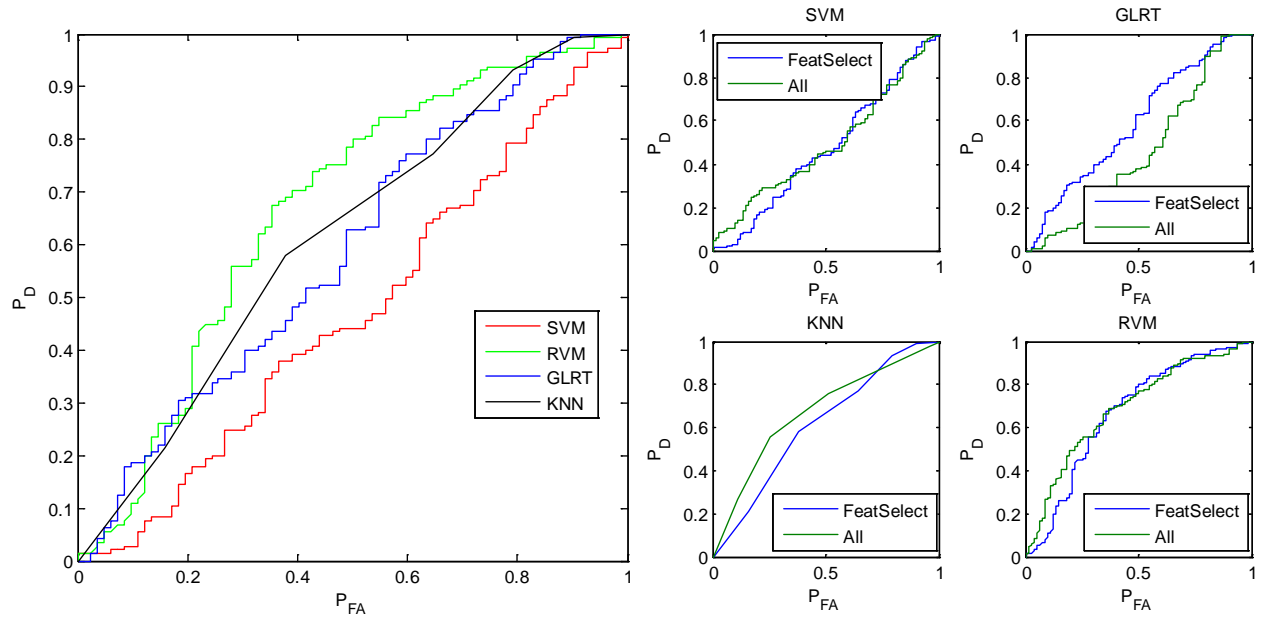


Figure 6-1 ROC curves for NRL EM61 array data using the dipole model at YPG for different classifiers and features selection methodologies using features of anomalies with fit errors less than 31% . The targets of interest were all ordnance ranging from 20mm to 155mm.

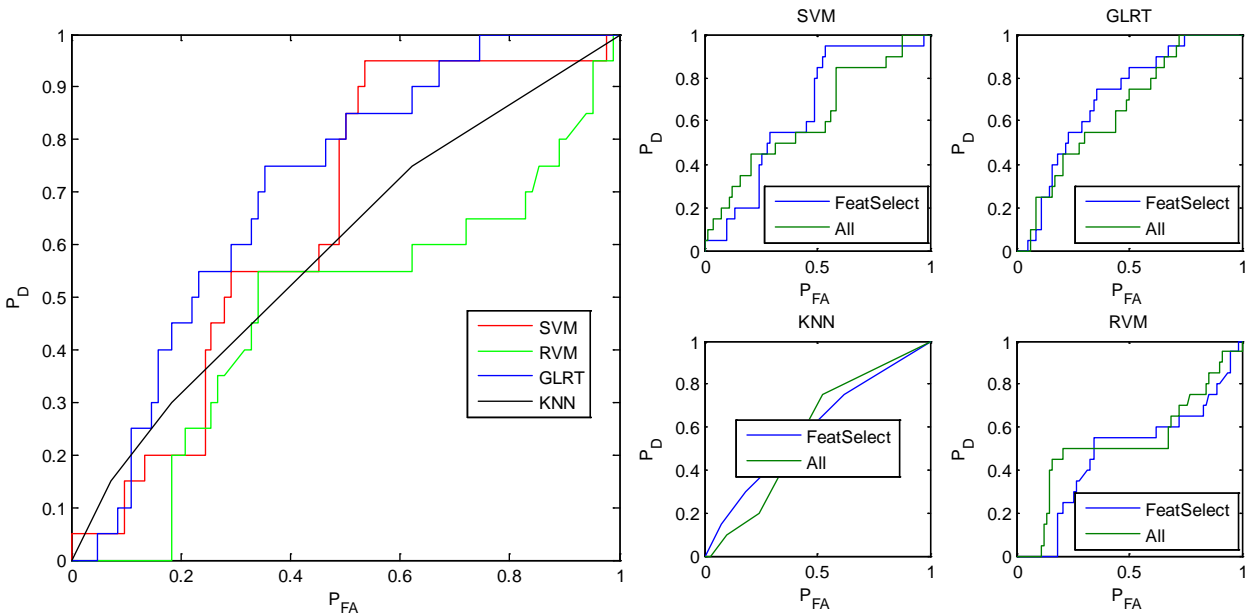


Figure 6-2 ROC curves for NRL EM61 array data using the dipole model at YPG for different classifiers and features selection methodologies using features of anomalies with fit errors less than 31% . The targets of interest were small sized ordnance items (20mm, 40mm, M42, BDU-28, BDU-26).

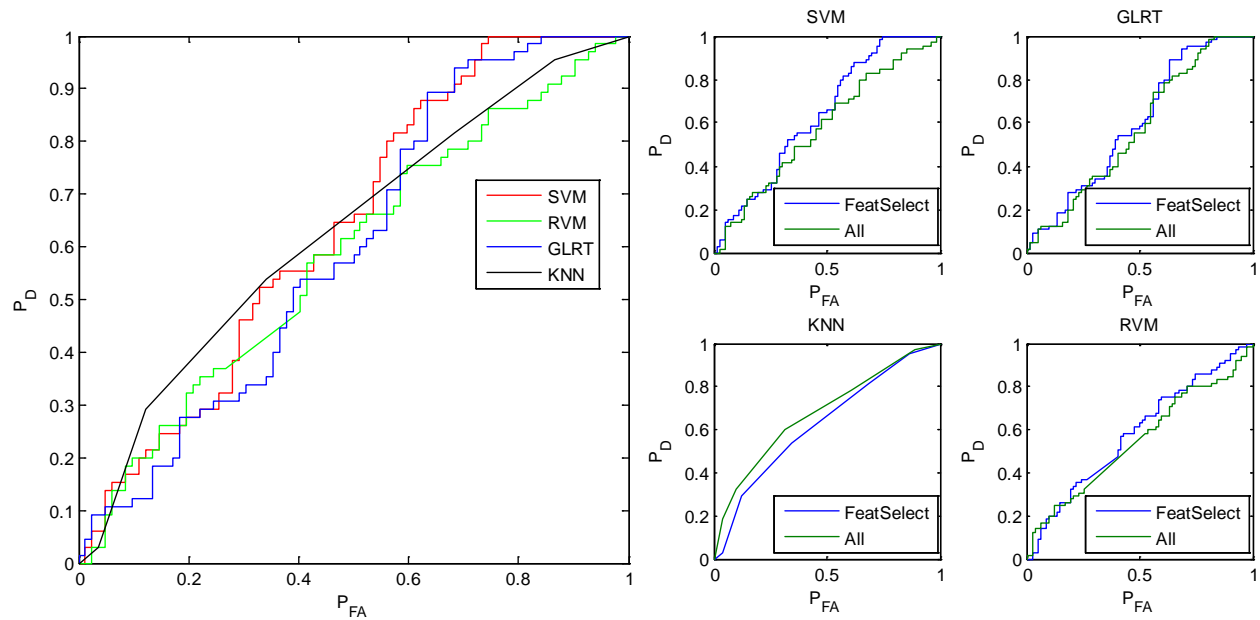


Figure 6-3 ROC curves for NRL EM61 array data using the dipole model at YPG for different classifiers and features selection methodologies using features of anomalies with fit errors less than 31% . The targets of interest were medium sized ordnance items (57mm, MK118, 60mm, 81mm, 2.75in).

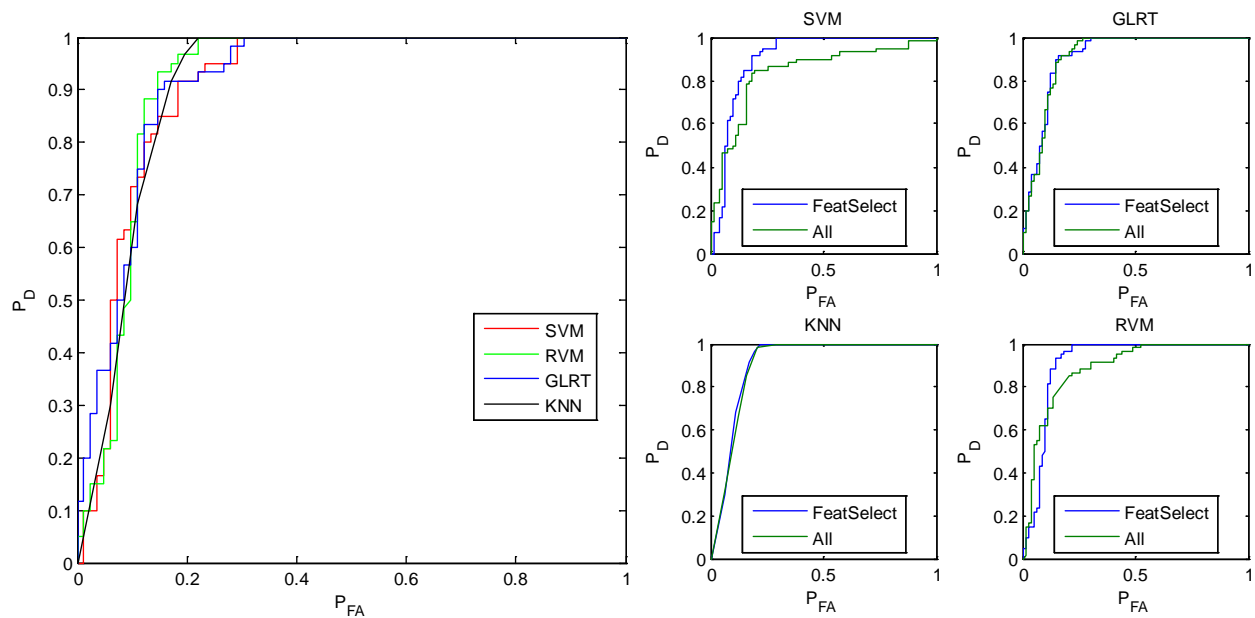


Figure 6-4 ROC curves for NRL EM61 array data using the dipole model at YPG for different classifiers and features selection methodologies using features of anomalies with fit errors less than 31% . The targets of interest were large sized ordnance items (105mm, 155mm).

Table 6-2 Best set of features for each of the classifiers with different TOI using the TTFW EM61 cart data at YPG.

Classifier	TOI All Features	TOI Small Ordnance Features	TOI Medium Ordnance Features	TOI Large Ordnance Features
GLRT	Beta3, Beta1/Beta2, Beta2/Beta3, Beta sum	Beta1, Beta1/Beta2, Beta2/Beta3, Beta sum	Beta2, Beta3, Beta1/Beta2, Beta2/Beta3, Beta sum	Beta2, Beta3, Beta1/Beta2, Beta2/Beta3, Beta sum
SVM	Beta2/Beta3, Beta sum	Beta2, Beta2/Beta3	Beta1, Beta1/Beta2	Beta3, Beta1/Beta2, Beta2/Beta3
RVM	Beta1, Beta2, Beta3, Beta1/Beta2, Beta sum	Beta1, Beta2, Beta3, Beta1/Beta2	Beta2, Beta3, Beta1/Beta2, Beta sum	Beta3, Beta1/Beta2
KNN	Beta1, Beta3, Beta1/Beta2, Beta sum	Beta1, Beta1/Beta2	Beta1, Beta1/Beta2, Beta2/Beta3	Beta2, Beta3, Beta sum
All features	Beta1, Beta2, Beta3, Beta1/Beta2, Beta2/Beta3, Beta sum			

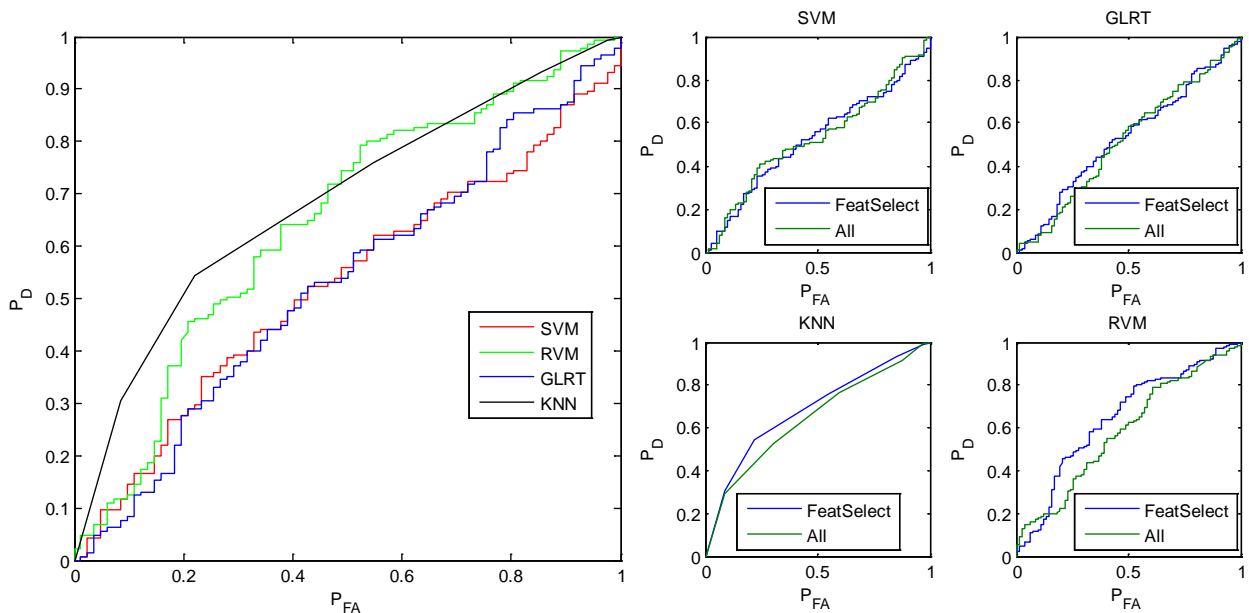


Figure 6-5 ROC curves for TTFW EM61 cart data using the dipole model at YPG for different classifiers and features selection methodologies using features of anomalies with fit errors less than 31% . The targets of interest were all ordnance ranging from 20mm to 155mm.

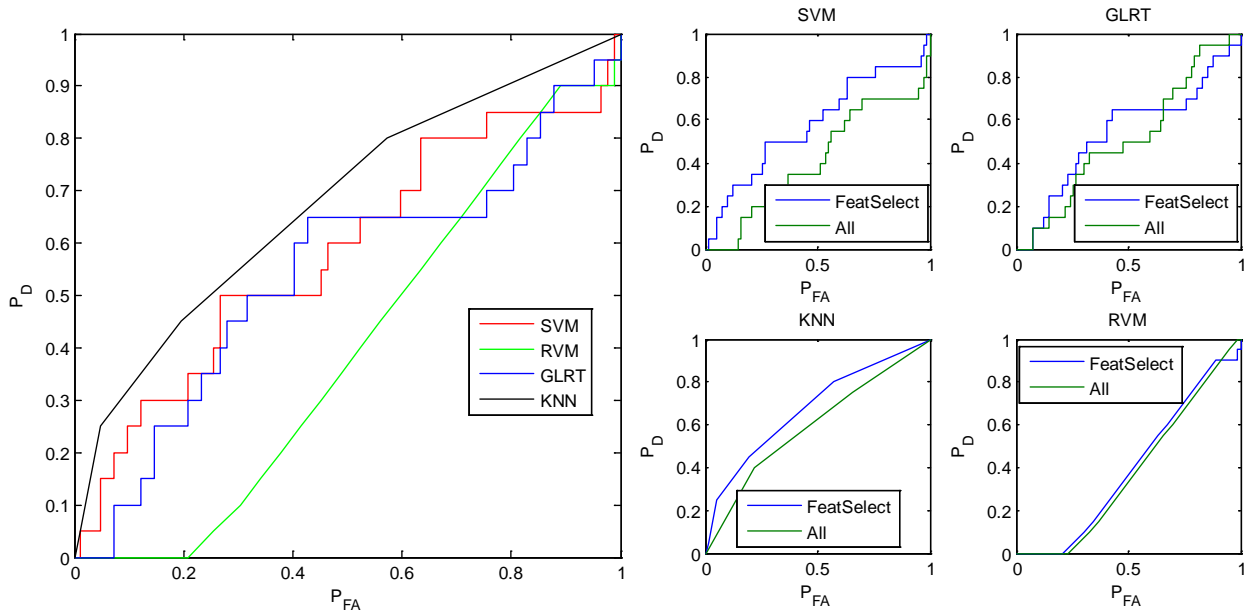


Figure 6-6 ROC curves for TTFW EM61 cart data using the dipole model at YPG for different classifiers and features selection methodologies using features of anomalies with fit errors less than 31% . The targets of interest were small sized ordnance items (20mm, 40mm, M42, BDU-28, BDU-26).

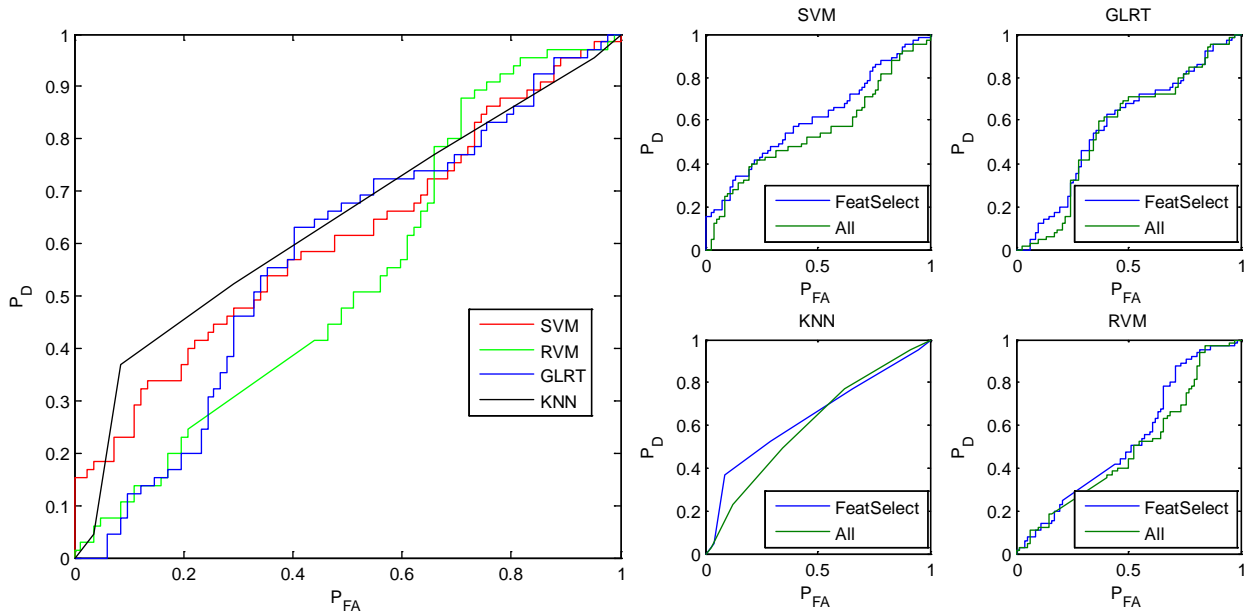


Figure 6-7 ROC curves for TTFW EM61 cart data using the dipole model at YPG for different classifiers and features selection methodologies using features of anomalies with fit errors less than 31% . The targets of interest were medium sized ordnance items (57mm, MK118, 60mm, 81mm, 2.75in).

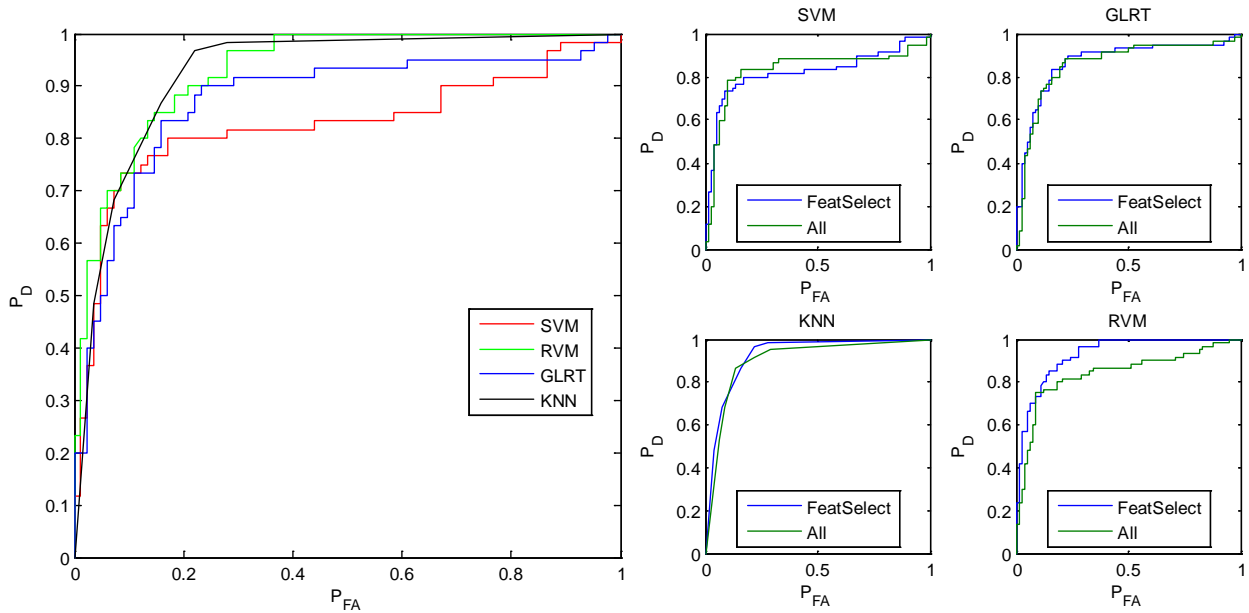


Figure 6-8 ROC curves for TTFW EM61 cart data using the dipole model at YPG for different classifiers and features selection methodologies using features of anomalies with fit errors less than 31% . The targets of interest were large sized ordnance items (105mm, 155mm).

Table 6-3 Best set of features for each of the classifiers with different TOI using the NRL Mag array data at YPG.

Classifier	TOI All Features	Ordnance	TOI Small Features	Ordnance	TOI Medium Features	Ordnance	TOI Large Features	Ordnance
GLRT	Magnetic moment		Magnetic moment		Magnetic moment		Solid angle, Magnetic moment	
SVM	Solid angle, Magnetic moment		Solid angle, Magnetic moment		Magnetic moment		Solid angle, Magnetic moment	
RVM	Solid angle, Magnetic moment		Solid angle, Magnetic moment		Solid angle, Magnetic moment		Solid angle, Magnetic moment	
KNN	Solid angle, Magnetic moment		Solid angle, Magnetic moment		Solid angle, Magnetic moment		Solid angle, Magnetic moment	
All features	Magnetic moment, Solid angle							

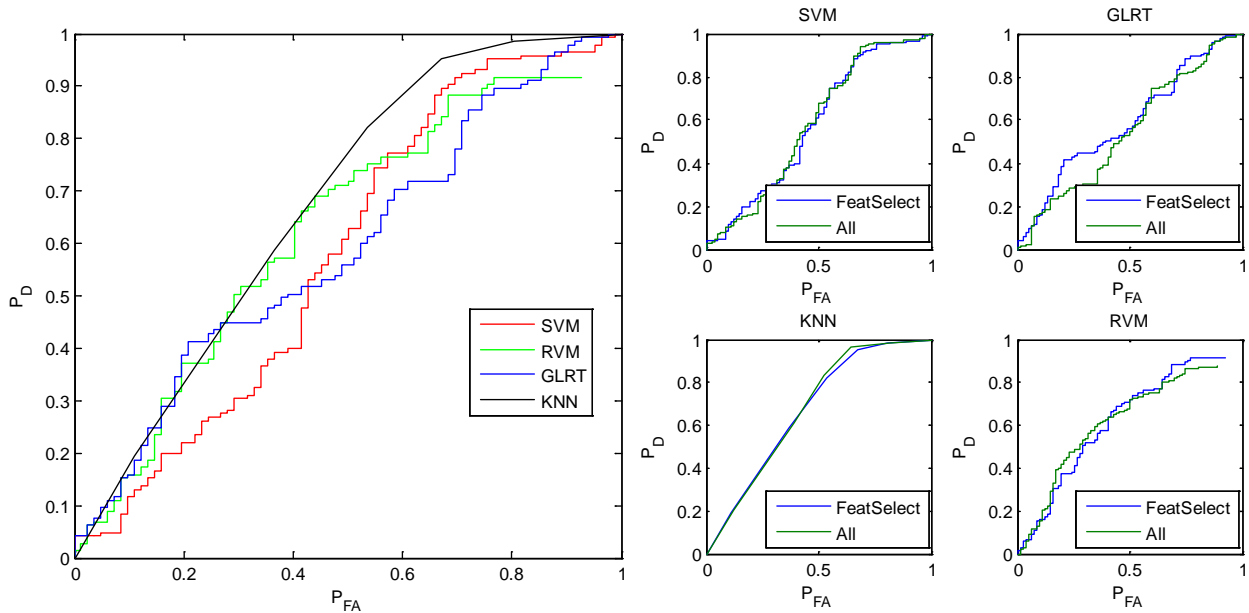


Figure 6-9 ROC curves for NRL Mag array data at YPG for different classifiers and features selection methodologies using features of anomalies with fit errors less than 31% . The targets of interest were all ordnance ranging from 20mm to 155mm.

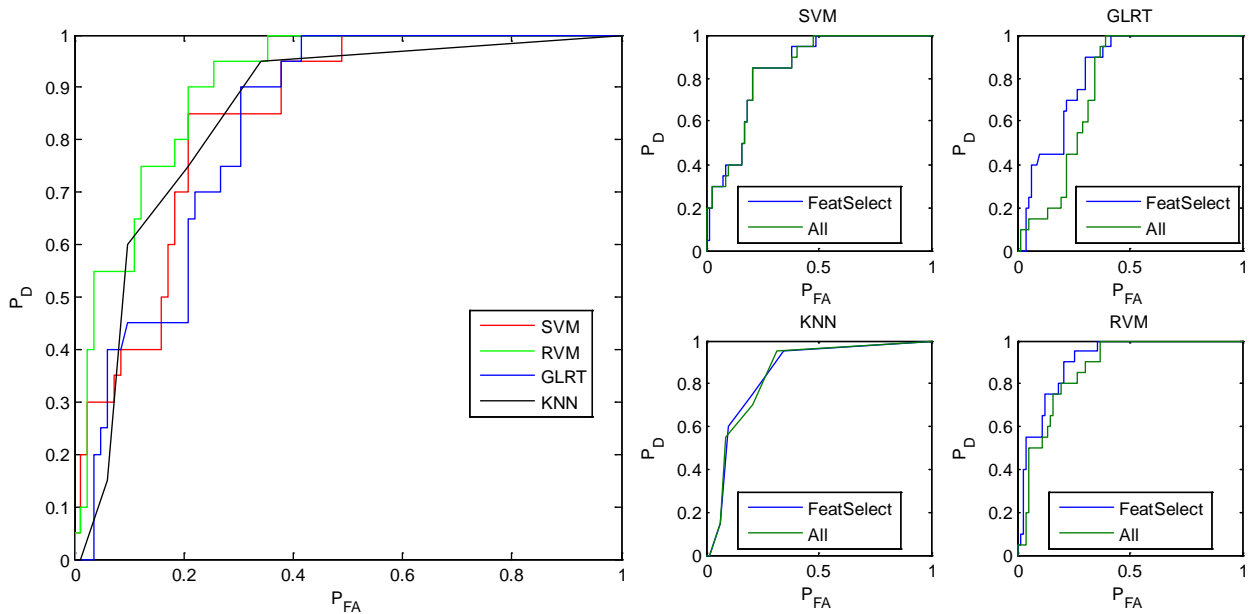


Figure 6-10 ROC curves for NRL Mag array data at YPG for different classifiers and features selection methodologies using features of anomalies with fit errors less than 31% . The targets of interest were small sized ordnance items (20mm, 40mm, M42, BDU-28, BDU-26).

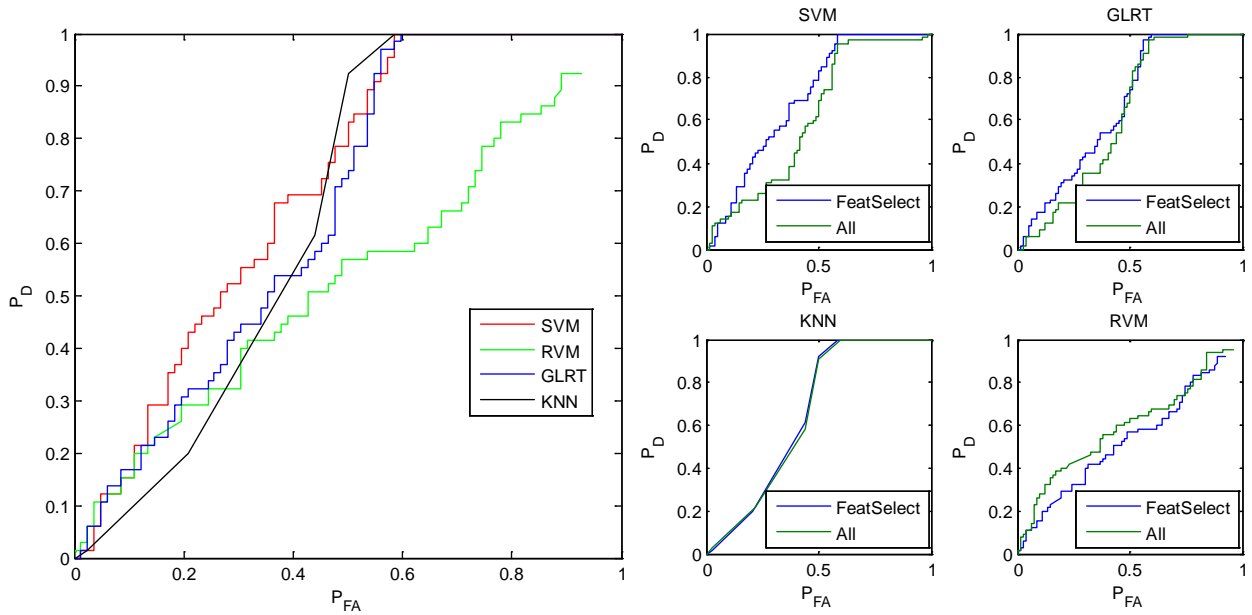


Figure 6-11 ROC curves for NRL Mag array data at YPG for different classifiers and features selection methodologies using features of anomalies with fit errors less than 31% . The targets of interest were medium sized ordnance items (57mm, MK118, 60mm, 81mm, 2.75in).

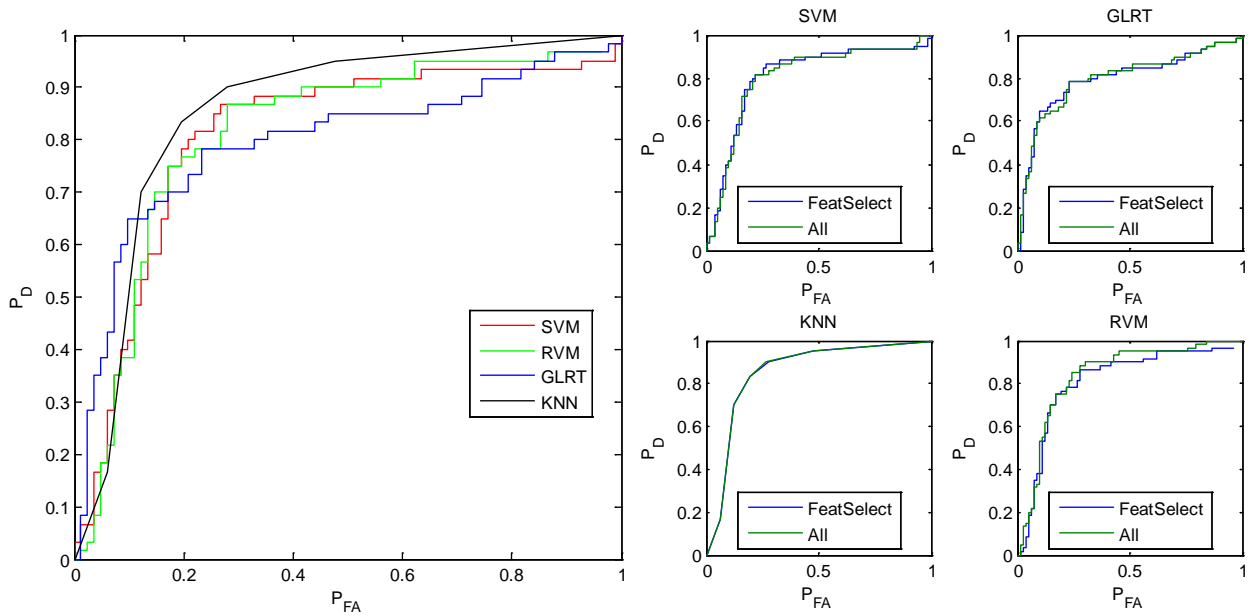


Figure 6-12 ROC curves for NRL Mag array data at YPG for different classifiers and features selection methodologies using features of anomalies with fit errors less than 31% . The targets of interest were large sized ordnance items (105mm, 155mm).

Table 6-4 Best set of features for each of the classifiers with different TOI using the NRL EM61 and Mag array data and the cooperative inversion approach at YPG.

Classifier	TOI All Ordnance Features	TOI Small Ordnance Features	TOI Medium Ordnance Features	TOI Large Ordnance Features
GLRT	1Beta2/1Beta3, 2Beta2/2Beta3	1Beta2, 1Beta3, 2Beta3, 3Beta1, 1Beta2/1Beta3	2Beta3, 1Beta1/1Beta2, 1Beta2/1Beta3	1Beta1, 1Beta2/1Beta3, 1Beta sum, 2Beta1/2Beta2, 3Beta1/3Beta2
SVM	1Beta2/1Beta3, 2Beta1, 2Beta sum	2Beta3, 3Beta1, 1Beta1/1Beta2, 1Beta2/1Beta3, 1Beta sum	2Beta2, 2Beta3, 3Beta1, 1Beta2/1Beta3, 3Beta sum	1Beta2, 1Beta3, 1Beta2/1Beta3, 1Beta sum
RVM	2Beta1/2Beta2, 1Beta2/1Beta3,	1Beta2, 2Beta3, 1Beta sum	2Beta2, 1Beta1/1Beta2, 1Beta2/1Beta3, 2Beta sum	1Beta1, 1Beta2/1Beta3, 1Beta sum
KNN	1Beta2/1Beta3, 1Beta1/1Beta2, 1Beta3, 1Beta sum, 3Beta1, 1Beta1, 2Beta2/2Beta3, 3Beta3, 1Beta2, 3Beta2	1Beta1, 1Beta3, 2Beta3, 2Beta sum	2Beta1, 2Beta3, 1Beta1/1Beta2, 1Beta2/1Beta3, 2Beta2/2Beta3	1Beta2, 1Beta3
All features	XBeta1, XBeta2, XBeta3, XBeta1/XBeta2, XBeta2/XBeta3, XBeta sum where "X" is 1,2 or 3 representing the first, second and third time gate			

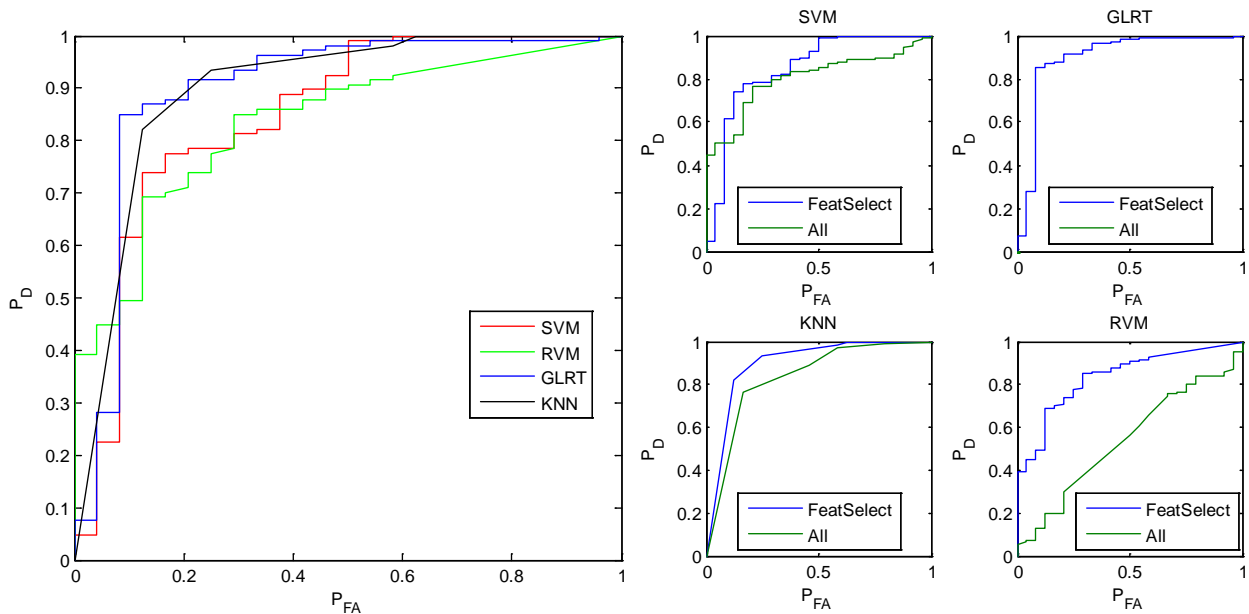


Figure 6-13 ROC curves for NRL array data using the cooperative Mag/EM approach at YPG for different classifiers and features selection methodologies using features of anomalies with fit errors less than 31% . The targets of interest were all ordnance ranging from 20mm to 155mm.

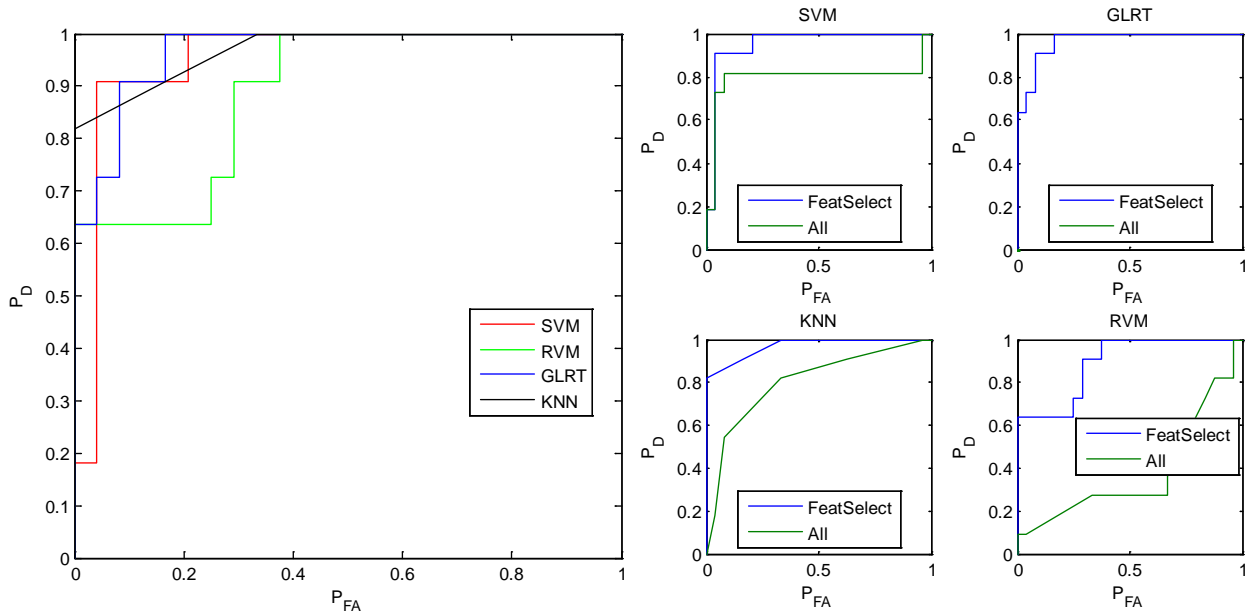


Figure 6-14 ROC curves for NRL array data using the cooperative Mag/EM approach at YPG for different classifiers and features selection methodologies using features of anomalies with fit errors less than 31% . The targets of interest were small sized ordnance items (20mm, 40mm, M42, BDU-28, BDU-26).

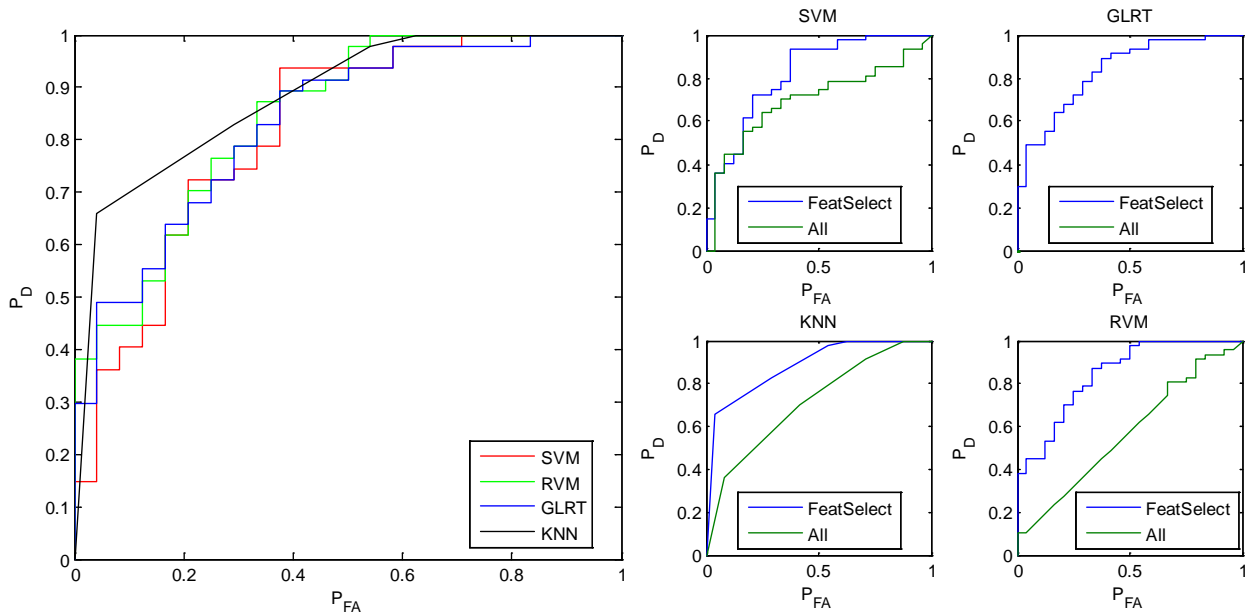


Figure 6-15 ROC curves for NRL array data using the cooperative Mag/EM approach at YPG for different classifiers and features selection methodologies using features of anomalies with fit errors less than 31% . The targets of interest were medium sized ordnance items (57mm, MK118, 60mm, 81mm, 2.75in).

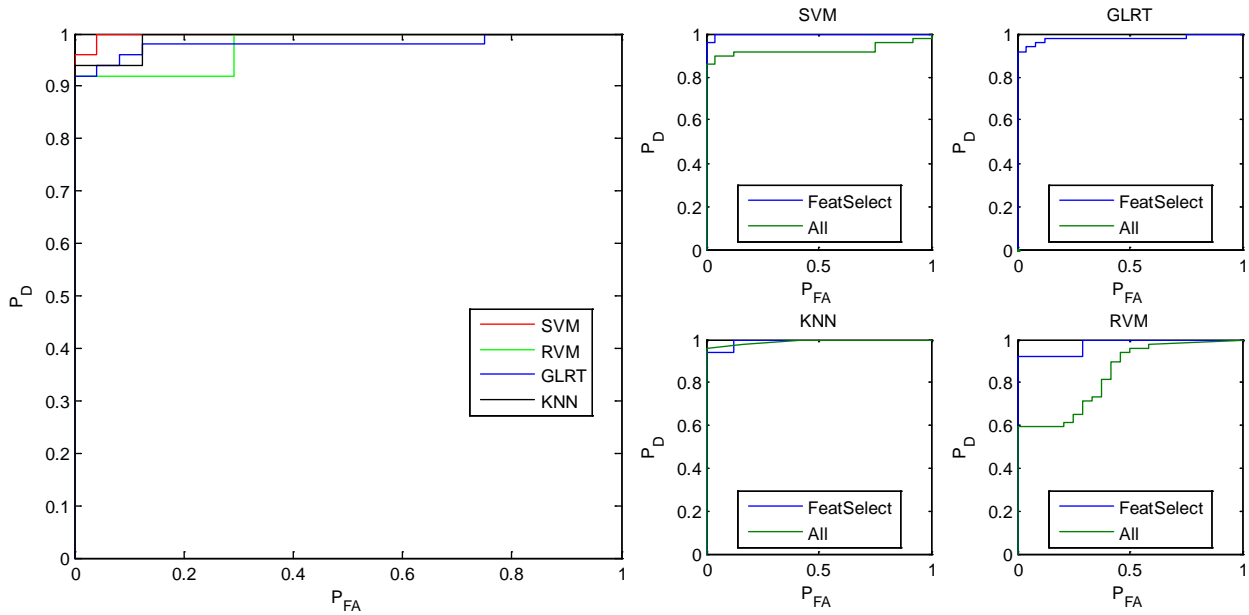


Figure 6-16 ROC curves for NRL array data using the cooperative Mag/EM approach at YPG for different classifiers and features selection methodologies using features of anomalies with fit errors less than 31% . The targets of interest were large sized ordnance items (105mm, 155mm).

Table 6-5 Best set of features for each of the classifiers with different TOI using the WES EM63 data and the POB model at YPG.

Classifier	TOI All Features	TOI Small Ordnance Features	TOI Medium Ordnance Features	TOI Large Ordnance Features
GLRT	B1	B2, B2/K2, K sum	B1, B2, K2, K1, B sum	B2, K2, B sum, K1/K2, K sum
SVM	B1, B2, K2	K2, K1/K2	B1, B2, K1, K2	B1, B2/K2
RVM	B1, B2, K1, K2	B1, K2, K sum	B1, B2, K sum	B1, B2, K2, B sum, K sum
KNN	B1, B2, K2, K1	B1, K2, K1, B sum	B1, B2, K2, K1	B1, K2, B2/K2
All features	B1, B2, K1, K2, B1/B2, B sum, K1/K2, K sum, B2/K2			

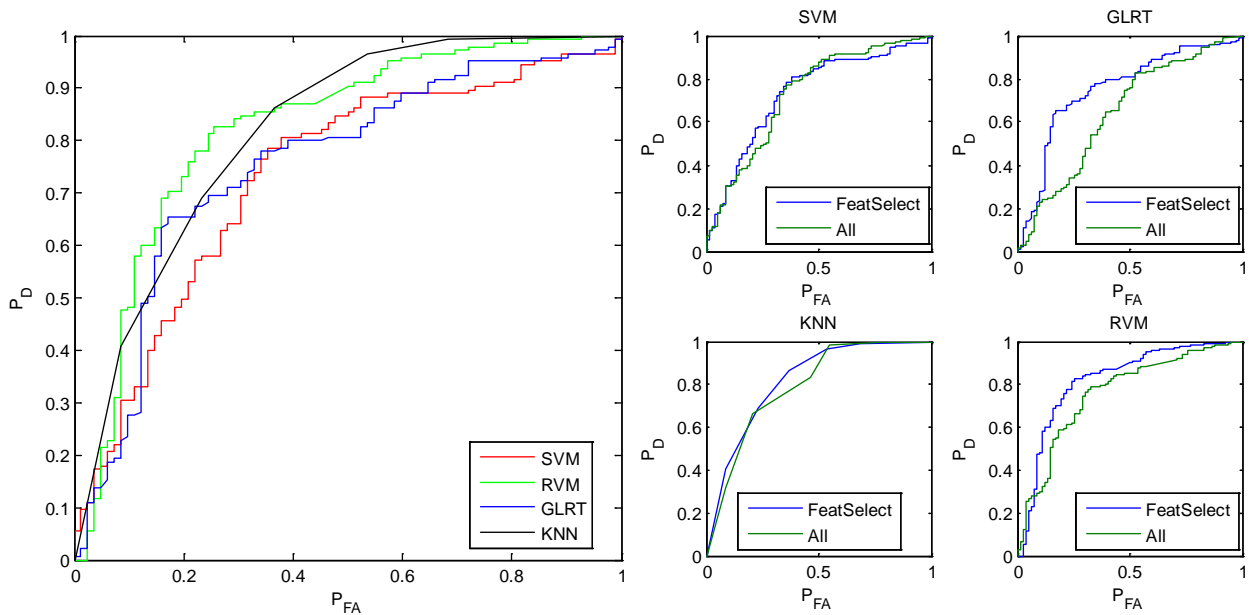


Figure 6-17 ROC curves for WES EM63 data using the POB model at YPG for different classifiers and features selection methodologies using features of anomalies with fit errors less than 31% . The targets of interest were all ordnance ranging from 20mm to 155mm.

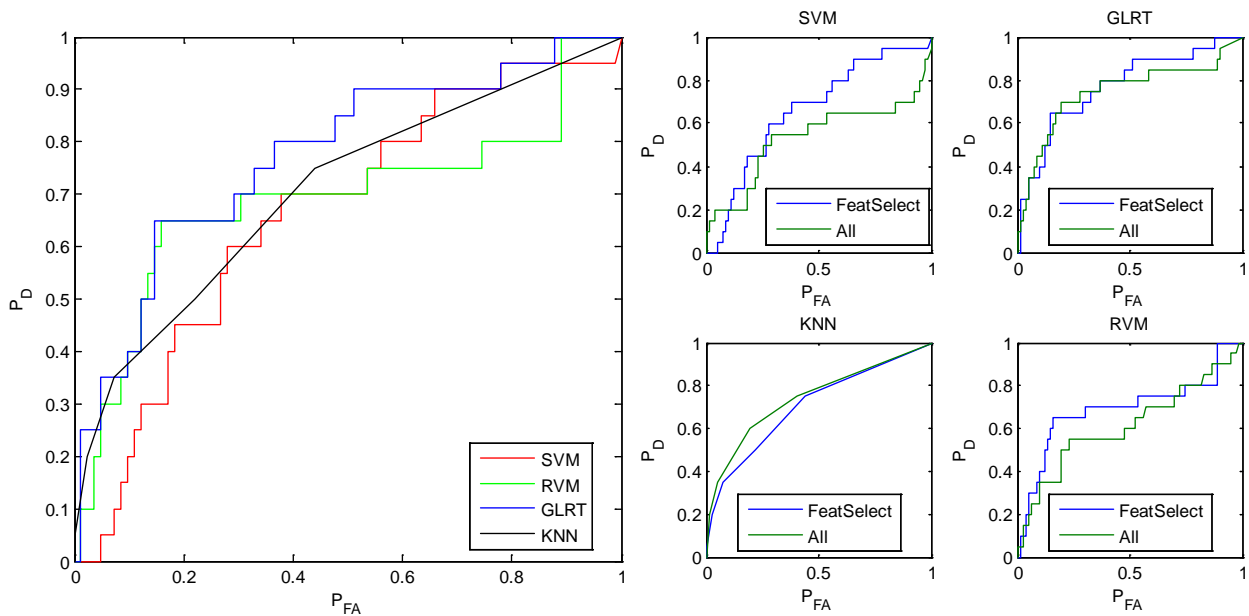


Figure 6-18 ROC curves for WES EM63 data using the POB model at YPG for different classifiers and features selection methodologies using features of anomalies with fit errors less than 31% . The targets of interest were small sized ordnance items (20mm, 40mm, M42, BDU-28, BDU-26).

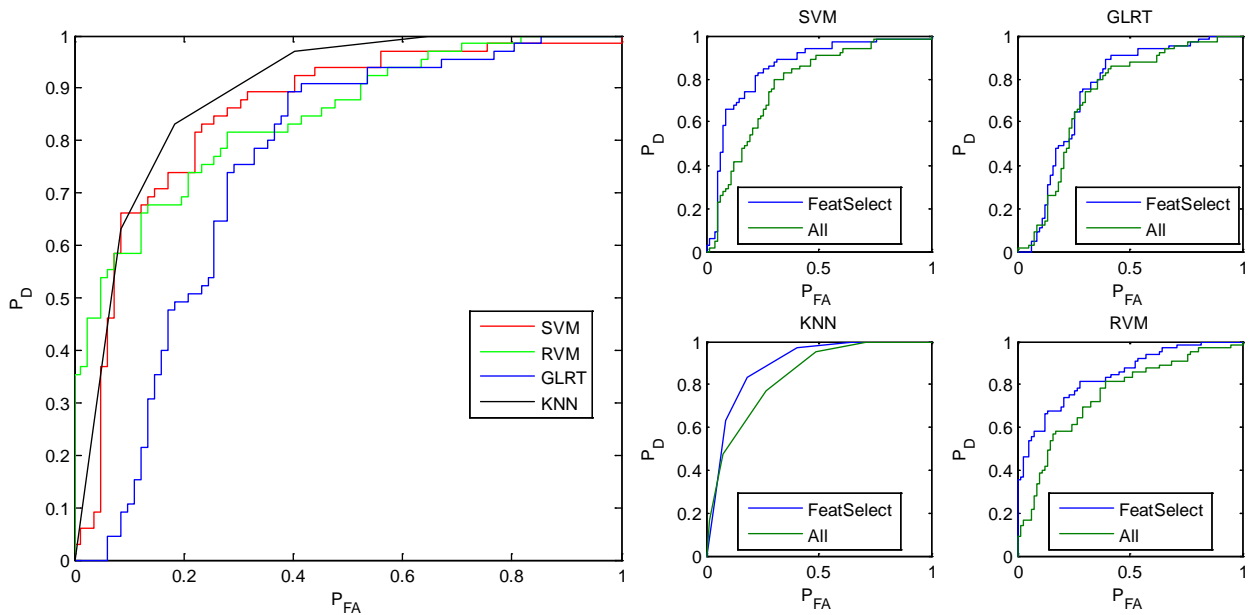


Figure 6-19 ROC curves for WES EM63 data using the POB model at YPG for different classifiers and features selection methodologies using features of anomalies with fit errors less than 31% . The targets of interest were medium sized ordnance items (57mm, MK118, 60mm, 81mm, 2.75in).

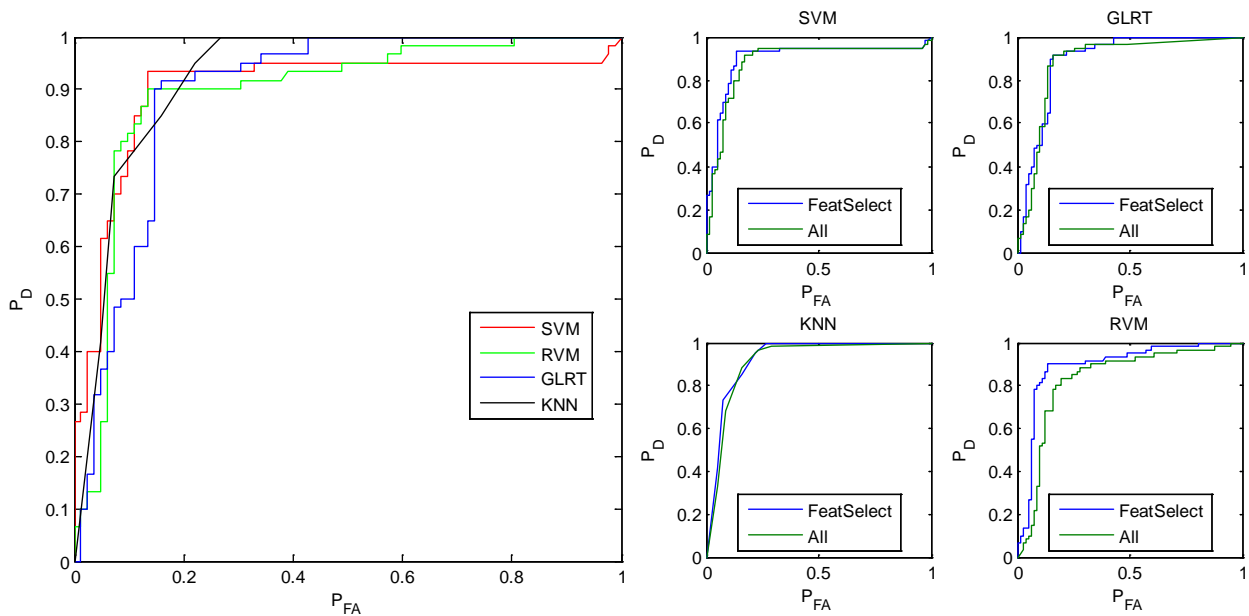


Figure 6-20 ROC curves for WES EM63 using the POB model at YPG for different classifiers and features selection methodologies using features of anomalies with fit errors less than 31% . The targets of interest were large sized ordnance items (105mm, 155mm).

Table 6-6 Best set of features for each of the classifiers with different TOI using the WES EM63 data and the SEM model at YPG.

Classifier	TOI All Features	TOI Small Ordnance Features	TOI Medium Ordnance Features	TOI Large Ordnance Features
GLRT	W2	M1	W2	W2, M sum
SVM	W1, M1/M2, W sum	M1, W2, M1/M2	M1, W1, W2	W2, M1/M2, W sum
RVM	W2, M1/M2, M sum	M1, M1/M2	M1, W sum	M2, W2, M sum
KNN	M1, M2, W2, W1/W2, W sum	M1, W2, M1/M2, W sum	M1, W2, W1/W2	M1, M2, W2, M sum, W1/W2
All features	M1, M2, W1, W2, M1/M2, M sum, W1/W2, W sum			

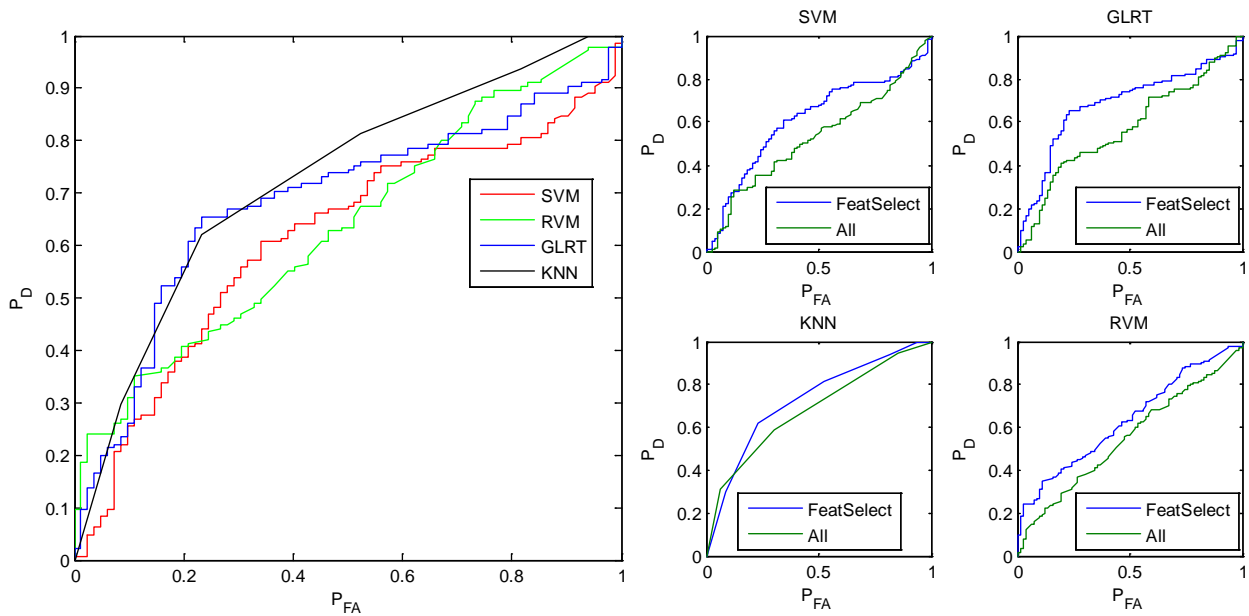


Figure 6-21 ROC curves for WES EM63 data using the SEM model at YPG for different classifiers and features selection methodologies using features of anomalies with fit errors less than 31% . The targets of interest were all ordnance ranging from 20mm to 155mm.

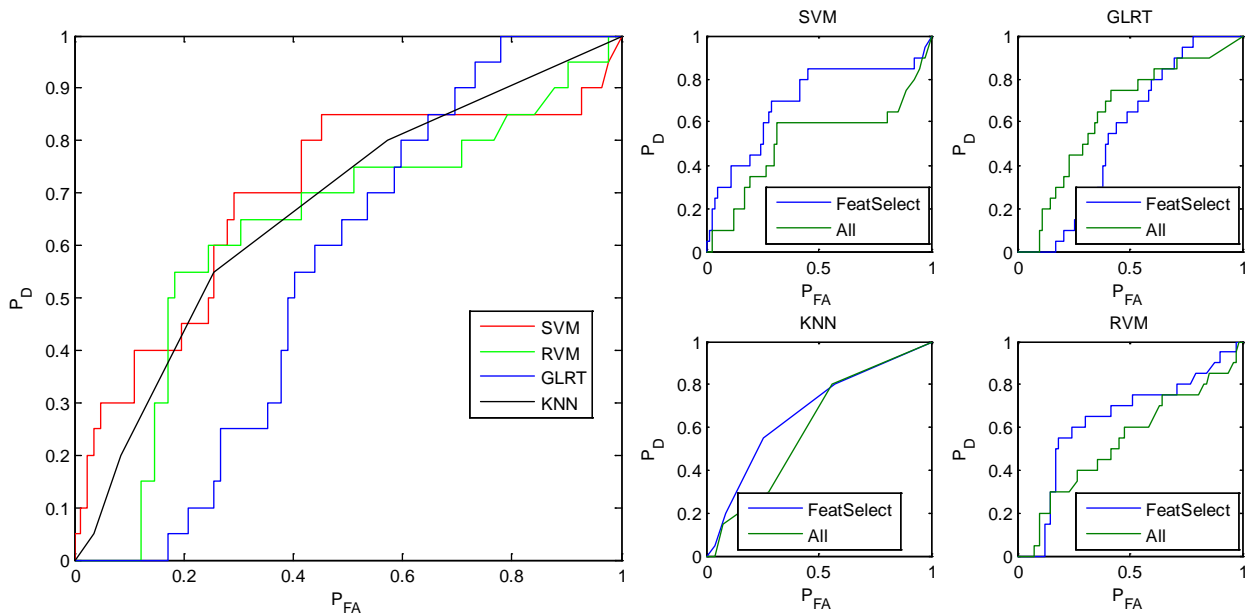


Figure 6-22 ROC curves for WES EM63 data using the SEM model at YPG for different classifiers and features selection methodologies using features of anomalies with fit errors less than 31% . The targets of interest were small sized ordnance items (20mm, 40mm, M42, BDU-28, BDU-26).

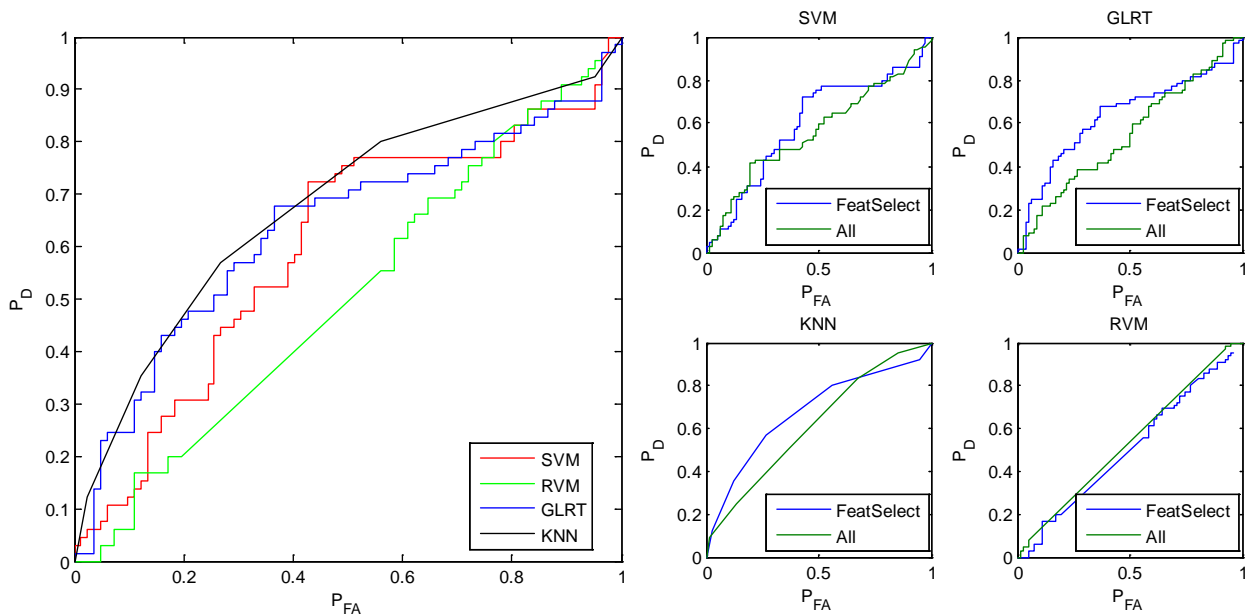


Figure 6-23 ROC curves for WES EM63 data using the SEM model at YPG for different classifiers and features selection methodologies using features of anomalies with fit errors less than 31% . The targets of interest were medium sized ordnance items (57mm, MK118, 60mm, 81mm, 2.75in).

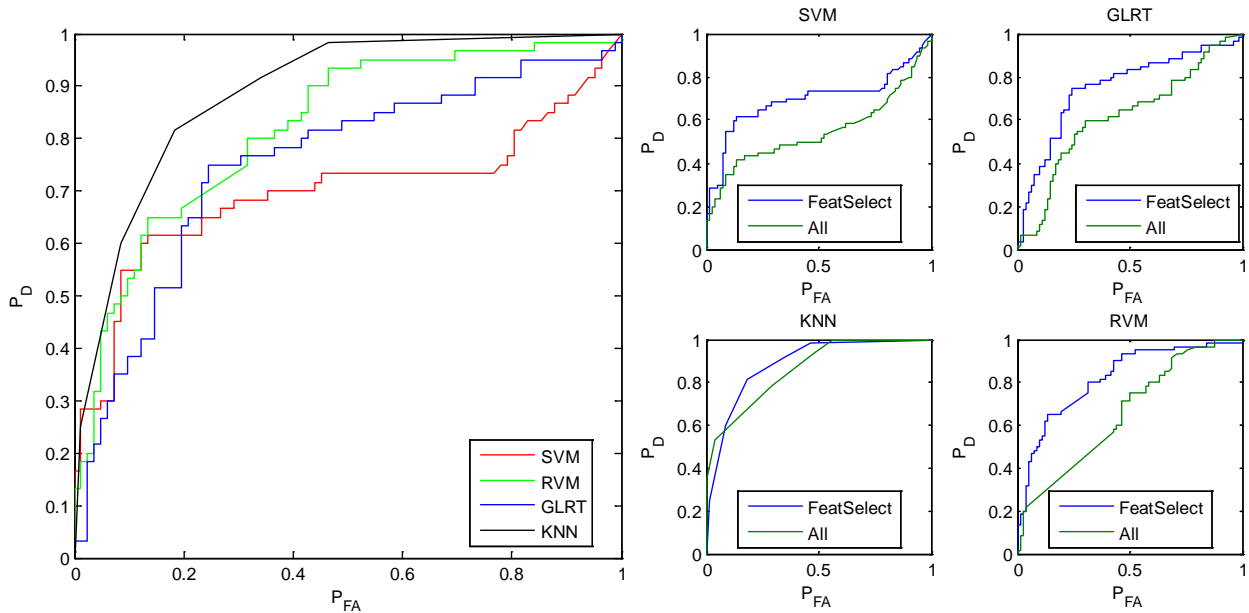


Figure 6-24 ROC curves for WES EM63 data using the SEM model at YPG for different classifiers and features selection methodologies using features of anomalies with fit errors less than 31% . The targets of interest were large sized ordnance items (105mm, 155mm).

Table 6-7 Best set of features for each of the classifiers with different TOI using the NRL GEM-3 array and the ellipsoidal scale model at YPG.

Classifier	TOI All Features	Ordnance	TOI Small Features	Ordnance	TOI Medium Features	Ordnance	TOI Large Features	Ordnance
GLRT	A, A/B, B/C		A, A/B, B/C, ABC sum		B, B/C		C, Scale, A/B, B/C, ABC sum	
SVM	B/C		B, A/B		A, C, B/C, ABC sum		A, A/B, B/C, ABC sum	
RVM	A, C, MU		B, MU, B/C, ABC sum		B, MU, A/B		A, C, ABC sum	
KNN	B, C, MU, Scale, A/B		B, A/B, B/C		A, C		A, MU, Scale, A/B, B/C	
All features	A, B, C, MU, Scale, A/B, B/C, ABC sum							

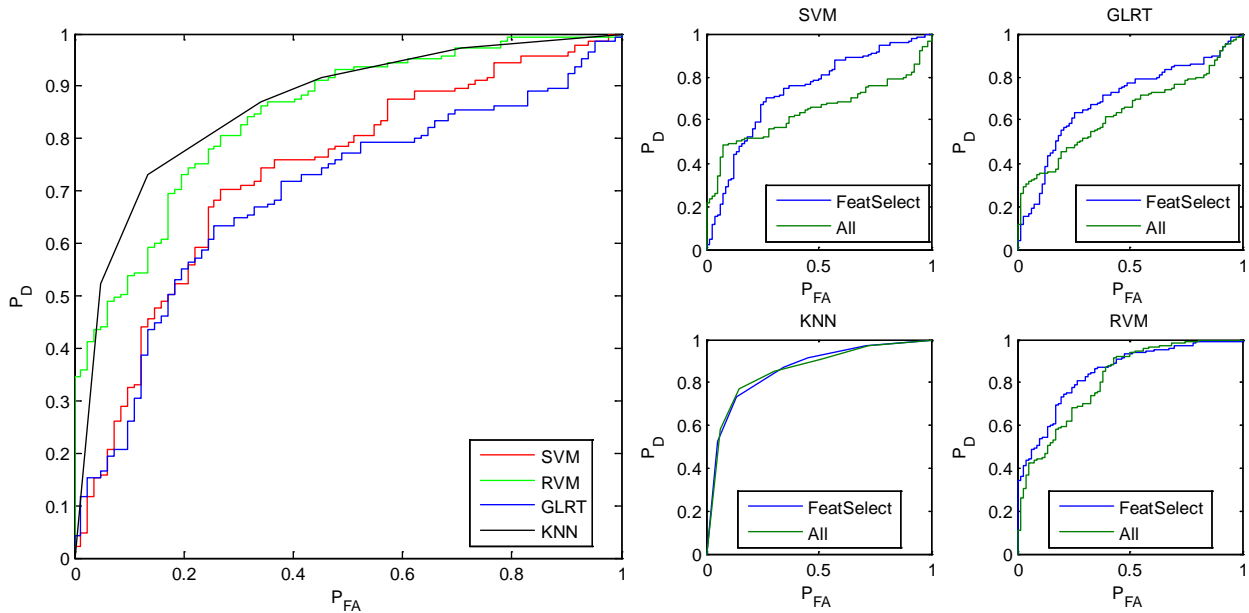


Figure 6-25 ROC curves for NRL GEM-3 array data using the ellipsoidal scale model at YPG for different classifiers and features selection methodologies using features of anomalies with fit errors less than 31% . The targets of interest were all ordnance ranging from 20mm to 155mm.

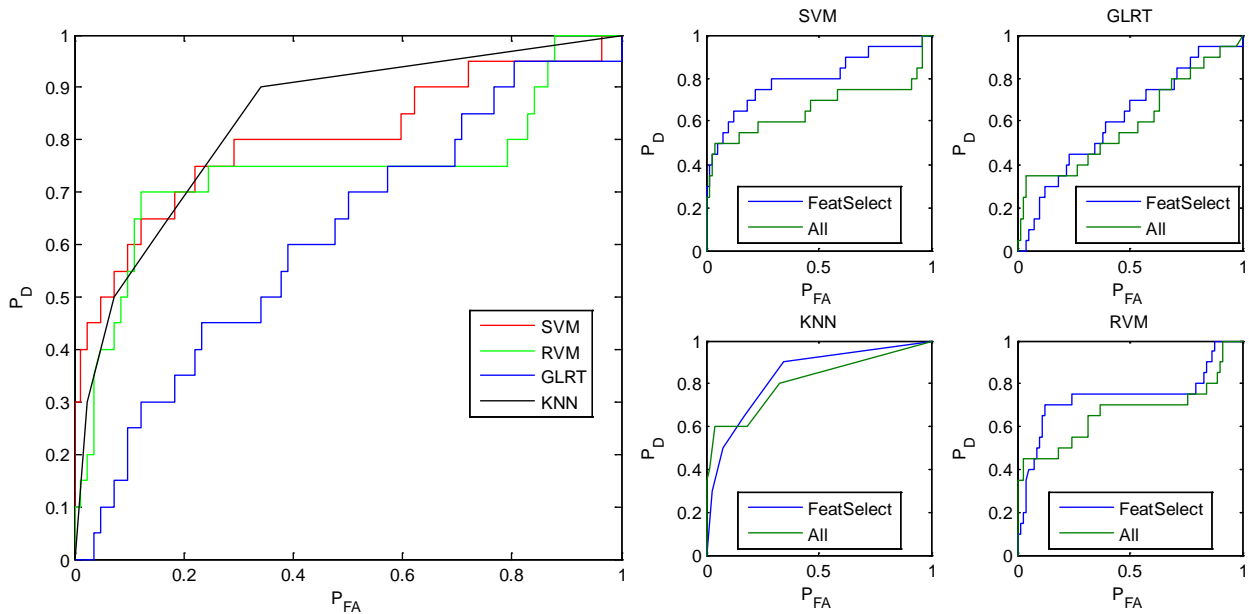


Figure 6-26 ROC curves for NRL GEM-3 array data using the ellipsoidal scale model at YPG for different classifiers and features selection methodologies using features of anomalies with fit errors less than 31% . The targets of interest were small sized ordnance items (20mm, 40mm, M42, BDU-28, BDU-26).

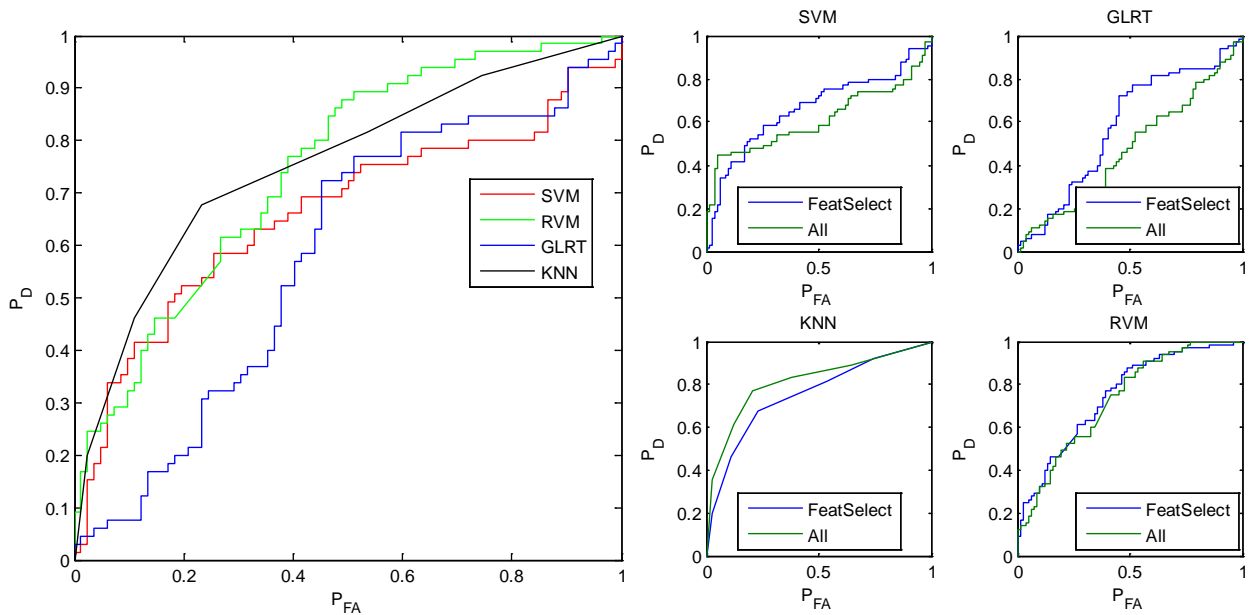


Figure 6-27 ROC curves for NRL GEM-3 array data using the ellipsoidal scale model at YPG for different classifiers and features selection methodologies using features of anomalies with fit errors less than 31% . The targets of interest were medium sized ordnance items (57mm, MK118, 60mm, 81mm, 2.75in).

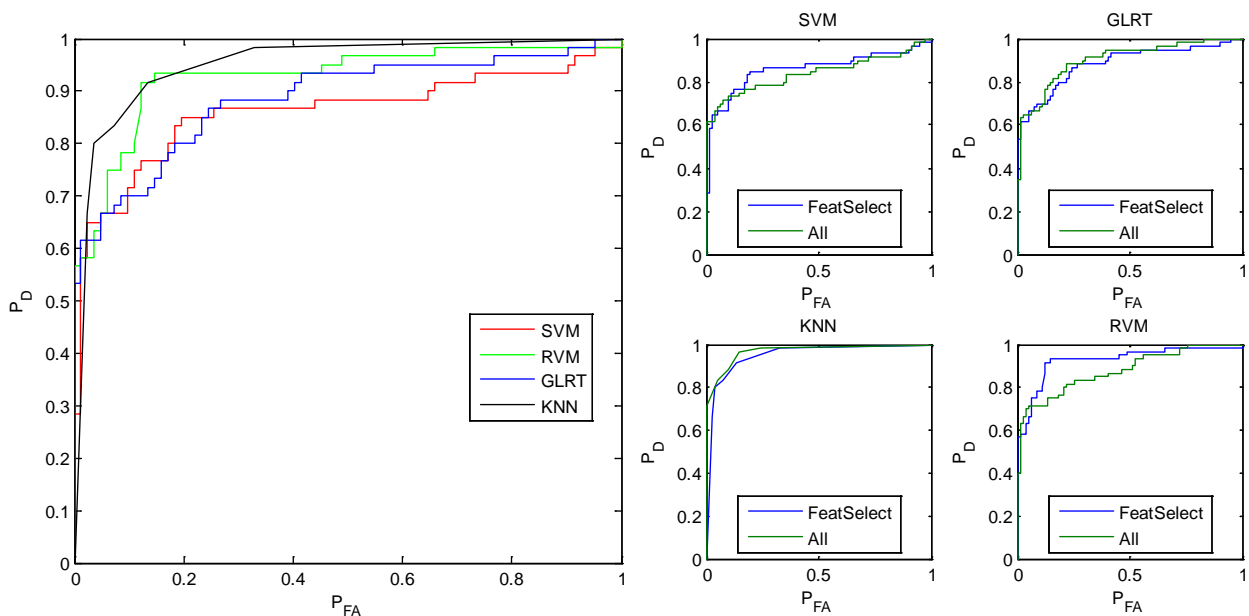


Figure 6-28 ROC curves for NRL GEM-3 array data using the ellipsoidal scale model at YPG for different classifiers and features selection methodologies using features of anomalies with fit errors less than 31% . The targets of interest were large sized ordnance items (105mm, 155mm).

Table 6-8 Best set of features for each of the classifiers with different TOI using the NRL GEM-3 array data and the ellipsoidal tau model at YPG.

Classifier	TOI All Features	TOI Small Ordnance Features	TOI Medium Ordnance Features	TOI Large Ordnance Features
GLRT	B, A/B, B/C, Tau sum	Tau1, Tau2, B/C, ABC sum, Tau1/Tau2	C, Tau3	A, A/B, B/C, ABC sum, Tau sum
SVM	Tau3, A/B, B/C, Tau1/Tau2, Tau2/Tau3	B, Tau2, B/C, ABC sum	C, Tau3, B/C, ABC sum, Tau1/Tau2	C, Tau1, B/C, Tau1/Tau2
RVM	Tau1, Tau2, B/c	A, C, Tau2, Tau2/Tau3	A, B, C, B/C	C, Tau1/Tau2
KNN	B, Tau3, B/C, Tau sum	A, B, C, ABC sum, Tau1/Tau2	B, C, Tau1, ABC sum	C, Tau1, Tau2, B/C, Tau1/Tau2
All features	A, B, C, Tau1, Tau2, Tau3, A/B, B/C, ABC sum, Tau1/Tau2, Tau2/Tau3, Tau sum			

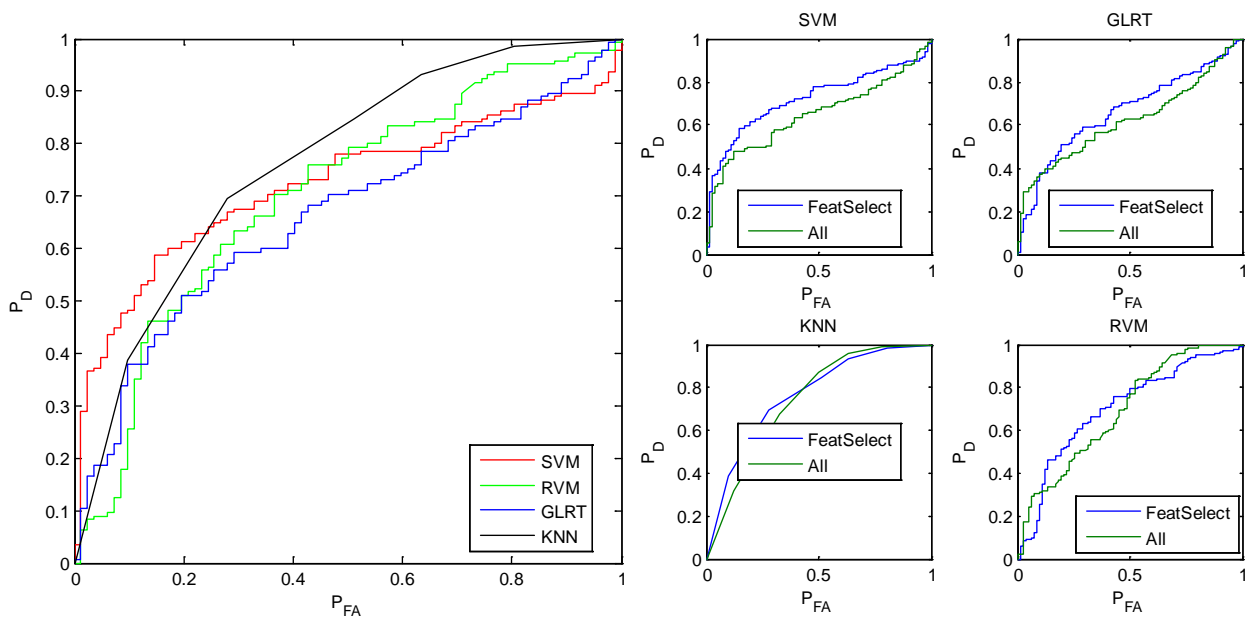


Figure 6-29 ROC curves for NRL GEM-3 array data using the ellipsoidal tau model at YPG for different classifiers and features selection methodologies using features of anomalies with fit errors less than 31% . The targets of interest were all ordnance ranging from 20mm to 155mm.

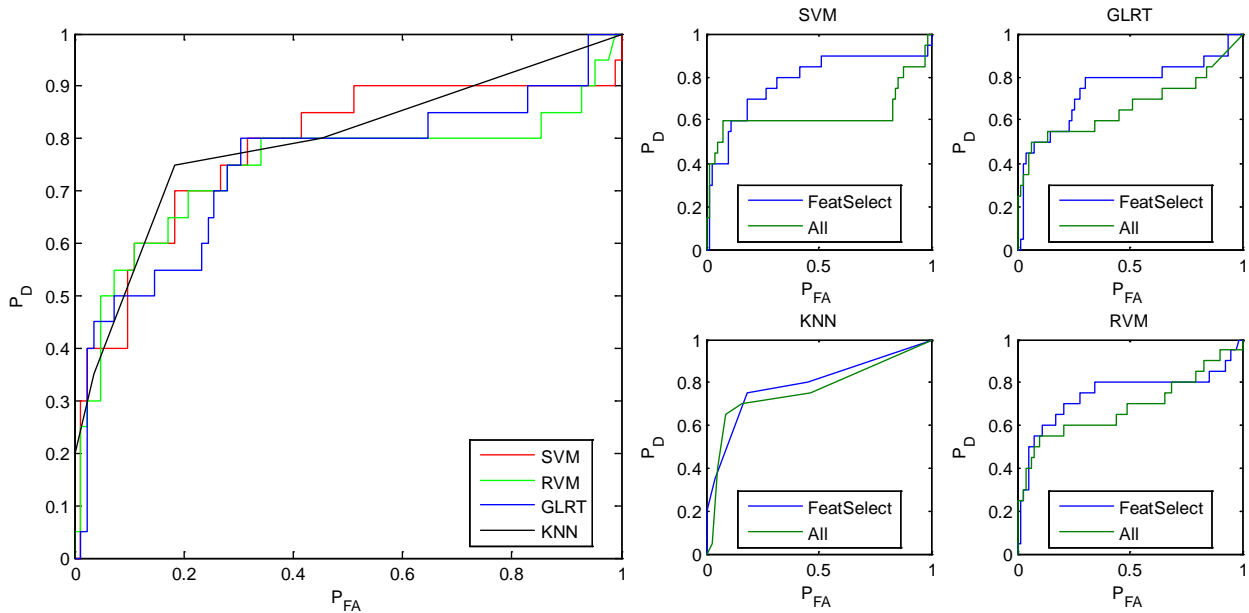


Figure 6-30 ROC curves for NRL GEM-3 array data using the ellipsoidal tau model at YPG for different classifiers and features selection methodologies using features of anomalies with fit errors less than 31% . The targets of interest were small sized ordnance items (20mm, 40mm, M42, BDU-28, BDU-26).

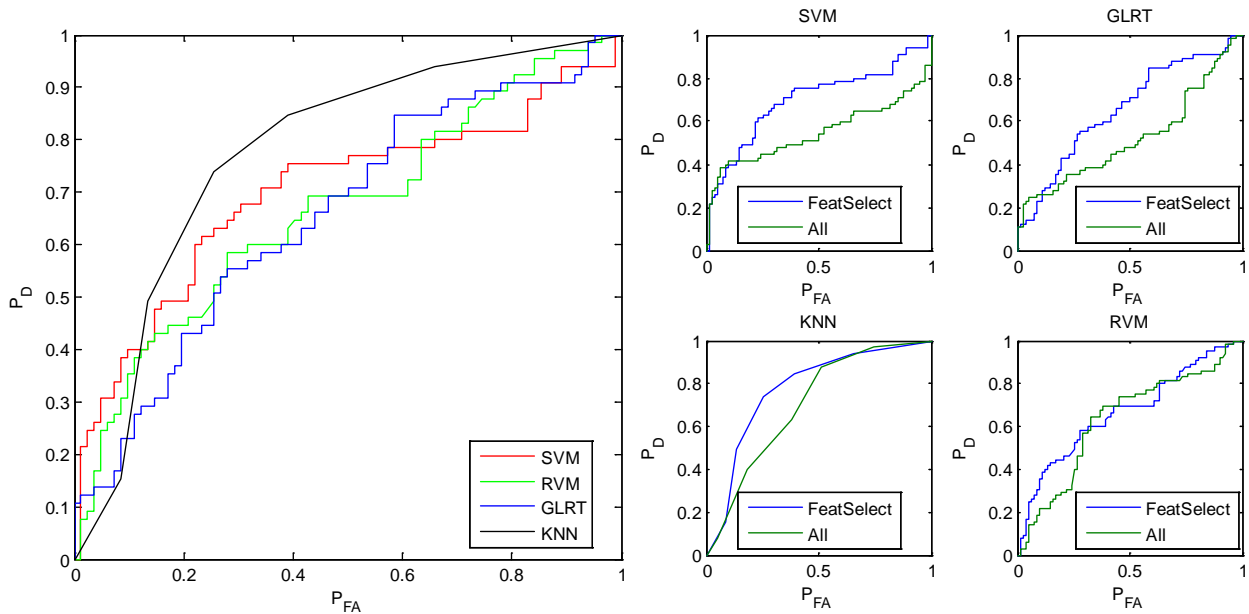


Figure 6-31 ROC curves for NRL GEM-3 array data using the ellipsoidal tau model at YPG for different classifiers and features selection methodologies using features of anomalies with fit errors less than 31% . The targets of interest were medium sized ordnance items (57mm, MK118, 60mm, 81mm, 2.75in).

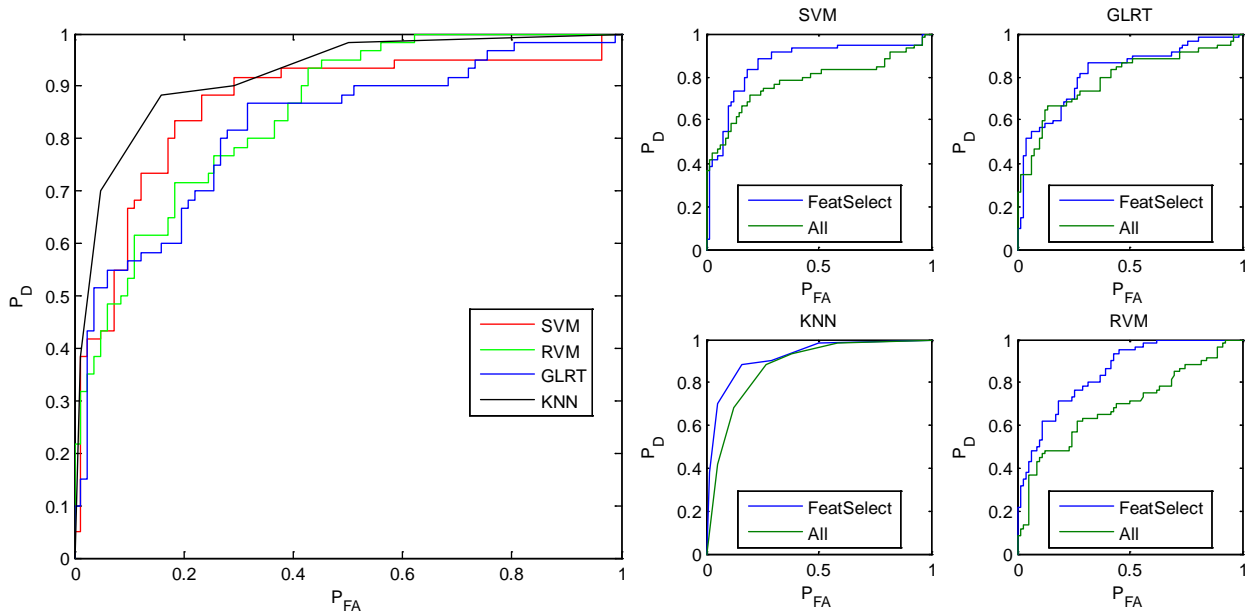


Figure 6-32 ROC curves for NRL GEM-3 array data using the ellipsoidal tau model at YPG for different classifiers and features selection methodologies using features of anomalies with fit errors less than 31% . The targets of interest were large sized ordnance items (105mm, 155mm).

Table 6-9 Best set of features for each of the classifiers with different TOI using the NRL GEM-3 array data and the empirical model at YPG.

Classifier	TOI All Features	TOI Small Ordnance Features	TOI Medium Ordnance Features	TOI Large Ordnance Features
GLRT	S2, S1	amp2, a3, b2, b2/b3, S2, S1, a sum	S2, S1	S2, t3, S3, a3, S sum, b3
SVM	b2, S sum, a3, S1, a sum	amp2, b3, S2, S1, amp1	b2/b3, b2, b3, amp2, S2, S1, S sum, a2	amp sum, S1, S sum
RVM	S sum, b2, S1, S2, S3	S sum, S1, S2	b2, S2/S3, t2	amp sum, S2, S3, amp3, t3
KNN	S2, b3, S1, S3, t3, b1/b2, S1/S2	amp sum, t3, S2, b3, t sum	S2, S1, t2/t3, b1, a1, S1/S2, S3, amp3, S2/S3	amp sum, S2/S3, b3, b sum, amp3, t1/t2, amp2, S2, a2, t3
All features	amp1, amp2, amp3, b1, b2, b3, t1, t2, t3, a1, a2, a3, S1, S2, S3, amp1/amp2, amp2/amp3, amp sum, b1/b2, b2/b3, b sum, t1/t2, t2/t3, t sum, a1/a2, a2/a3, a sum, S1/S2, S2/S3, S sum			

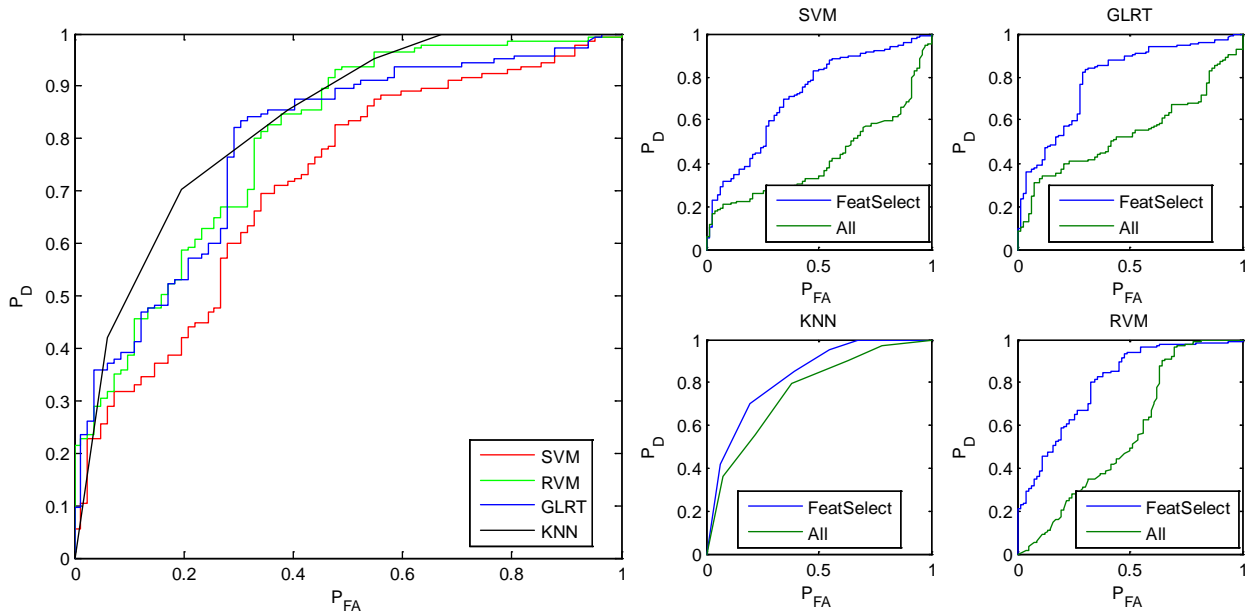


Figure 6-33 ROC curves for NRL GEM-3 array data using the empirical model at YPG for different classifiers and features selection methodologies using features of anomalies with fit errors less than 31% . The targets of interest were all ordnance ranging from 20mm to 155mm.

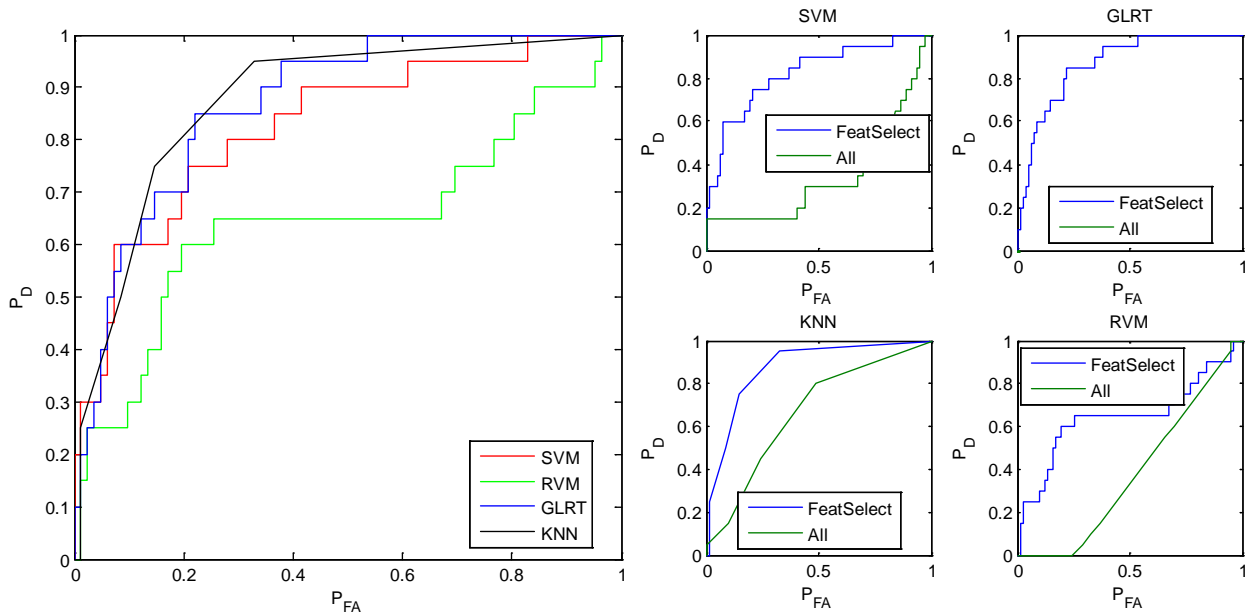


Figure 6-34 ROC curves for NRL GEM-3 array data using the empirical model at YPG for different classifiers and features selection methodologies using features of anomalies with fit errors less than 31% . The targets of interest were small sized ordnance items (20mm, 40mm, M42, BDU-28, BDU-26).

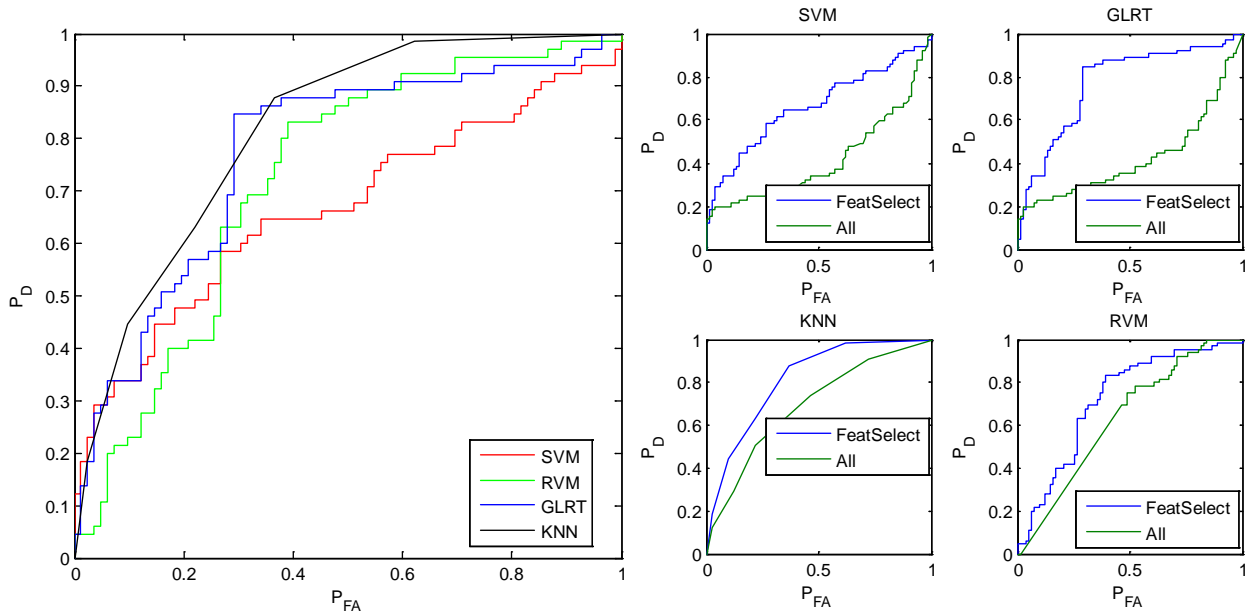


Figure 6-35 ROC curves for NRL GEM-3 array data using the empirical model at YPG for different classifiers and features selection methodologies using features of anomalies with fit errors less than 31% . The targets of interest were medium sized ordnance items (57mm, MK118, 60mm, 81mm, 2.75in).

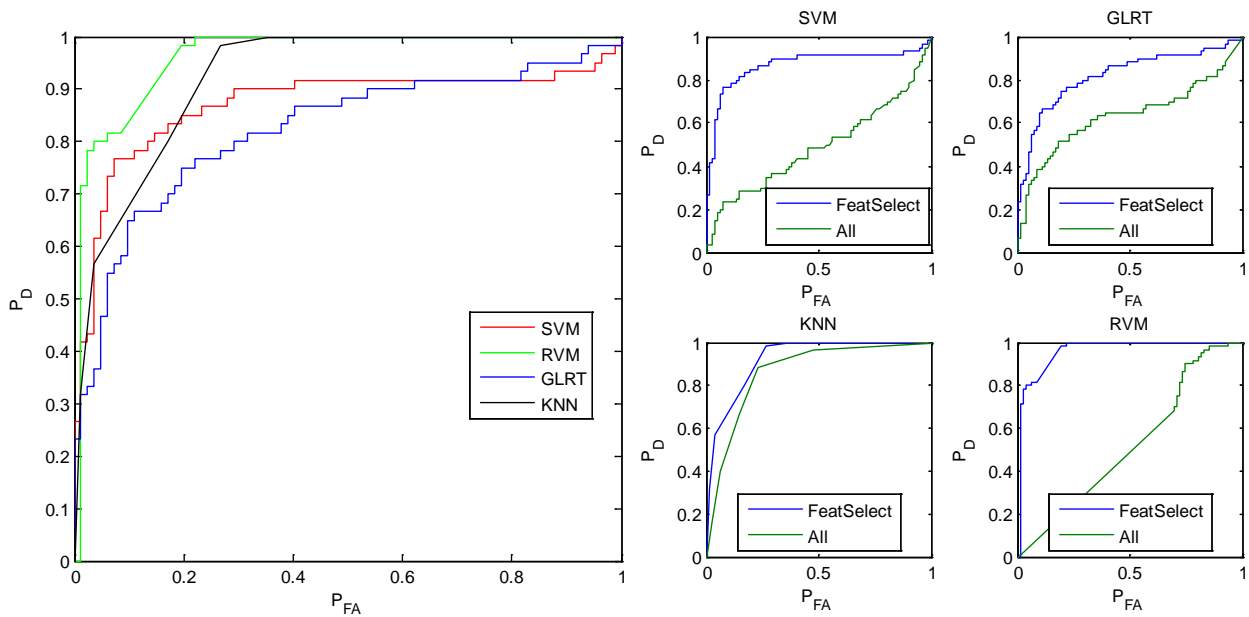


Figure 6-36 ROC curves for NRL GEM-3 array data using the empirical model at YPG for different classifiers and features selection methodologies using features of anomalies with fit errors less than 31% . The targets of interest were large sized ordnance items (105mm, 155mm).

Table 6-10 Best set of features for each of the classifiers with different TOI using the NRL GEM-3 array data and the loop model at YPG.

Classifier	TOI All Ordnance Features	TOI Small Ordnance Features	TOI Medium Ordnance Features	TOI Large Ordnance Features
GLRT	270i2/270i3, 1230q1/1230q2, 570i3, 270q1, CohB13, 2610i2/2610i3, 2610q1/2610q2, 90q1/90q2, 570i2/570i3, 150i2	5430q1/5430q2, 570i2/570i2, S1, CohB13, 90i1, 2610q1/2610q2, 570i2, 11430q sum, 150q1/150q2, MagB2, 150i1, MagB3, 2610i2/2610i3	90i2/90i3, 270i2/270i3, 150q2/150q3, 570i2/570i3, 1230q2, 570q sum, 1230q2/1230q3, 90q sum, 570i1/570i2, 5430i3, 150i sum, S1, 5430q1, 1230i2/1230i3, 90q3, 570q1/570q2, 270i sum, 5430i sum, 2610i2, 90i2	1230q sum, 90i2/90i3, MagB2, 150i1/150i2, CohB12/CohB23, 570q1/570q2, 1230q3, 20010i1, 20010i2/20010i3, 90q sum, 1230i1/1230i2, 2610i2/2610i3, 2610q2/2610q3, 570i2/570i3, 270i1/270i2, 270i2/270i3
SVM	150i2/150i3, 1230q1/1230q2, 1230q2/1230q3	150i1, 270i2/270i3, 270i2, 90i1, S2, 150i1/150i2, CohB23, 270q1/270q2	570i2/570i3, 150i2, 90i2, 150i1, 90i sum	90i2/90i3, 20010i sum, 2610i2/2610i3, CohB13, 20010i2/20010i3, 90q1/90q2, 11430q3, 11430q1, MagB3, 150q sum, 570q2/570q3
RVM	CohB12, 570i sum, 570q1, 1230q sum, 270q sum, 90i1, 570q3, 150q sum, 5430q3, 270i3, S sum, allq3 sum, 11430q3, 90i sum, allq1 sum, 90i1/90i2, 90q1, 5430q2, 150i sum	11430i1, 2610q1, 1230i1, MagB2, 570q sum, 5430i1/5430i2, 150q sum, 11430q2, 5430i1, 570q2, 570q2/570q3, allq2 sum, 1230q1, S1	CohB12, 1230i sum, 270i1, 570q1, 150q3	11430i sum, 150i2, 1230i1, 270i sum, 90i sum, CohB23, 270i1, S2, MagB1, 570i2, 570q1
KNN	2610i2, CohB12, 570i3, 270q1, 150i1/150i2, 2610q2, 90i2, 1230i1, 150q1	5430i1, 570q2/570q3, 5430i2, 1230i1, 2610q2, 5430q3, 5430q2/5430q3, CohB12/CohB23, 2610q1, 570i sum	270i1/270i2, 1230i1, 90q sum, CohB12, 270i1, 90i sum, 2610q sum, 150i3, 90i2, 90q1, 90i1	90q sum, 150i1, S3, 270i1
All features	Xi1, Xi2, Xi3, Xq1, Xq2, Xq3, CohB12, CohB23, CohB13, MagB1, MagB2, MagB3, S1, S2, S3, S1/S2, S2/S3, S sum, CohB12/CohB23, CohB12_B23 sum, Xi1/Xi2, Xi2/Xi3, Xi sum, Xq1/Xq2, Xq2/Xq3, Xq sum, Allq sum where "X" is 90, 150, 270, 570, 1230, 2610, 5430, 11430 or 20010Hz			

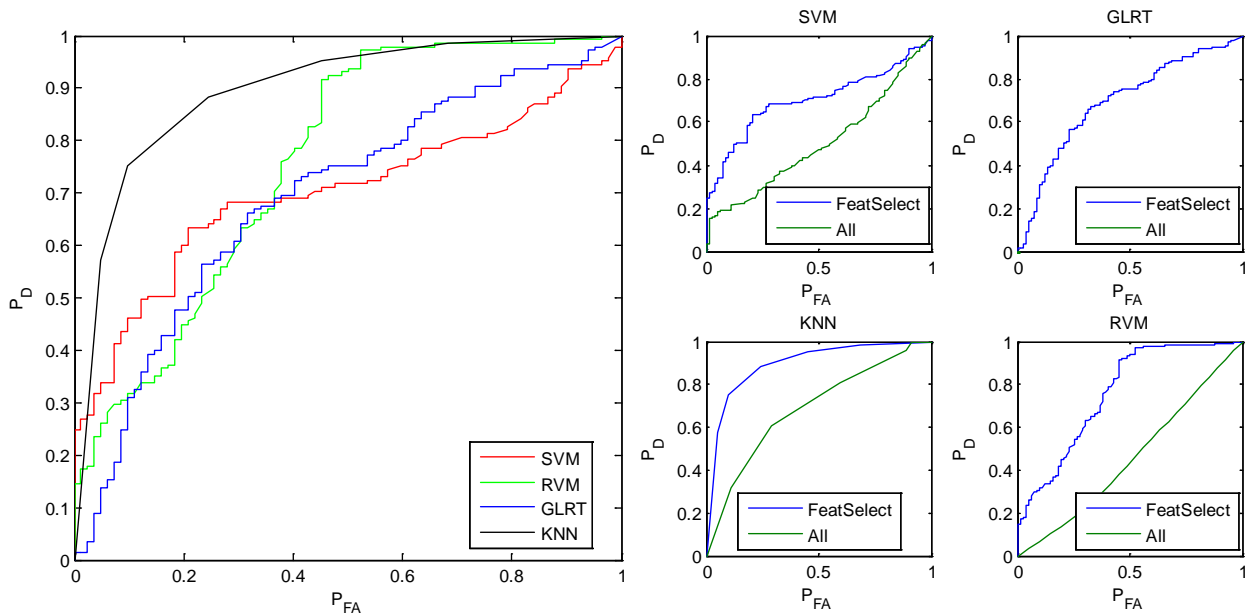


Figure 6-37 ROC curves for NRL GEM-3 array data using the loop model at YPG for different classifiers and features selection methodologies using features of anomalies with fit errors less than 31% . The targets of interest were all ordnance ranging from 20mm to 155mm.

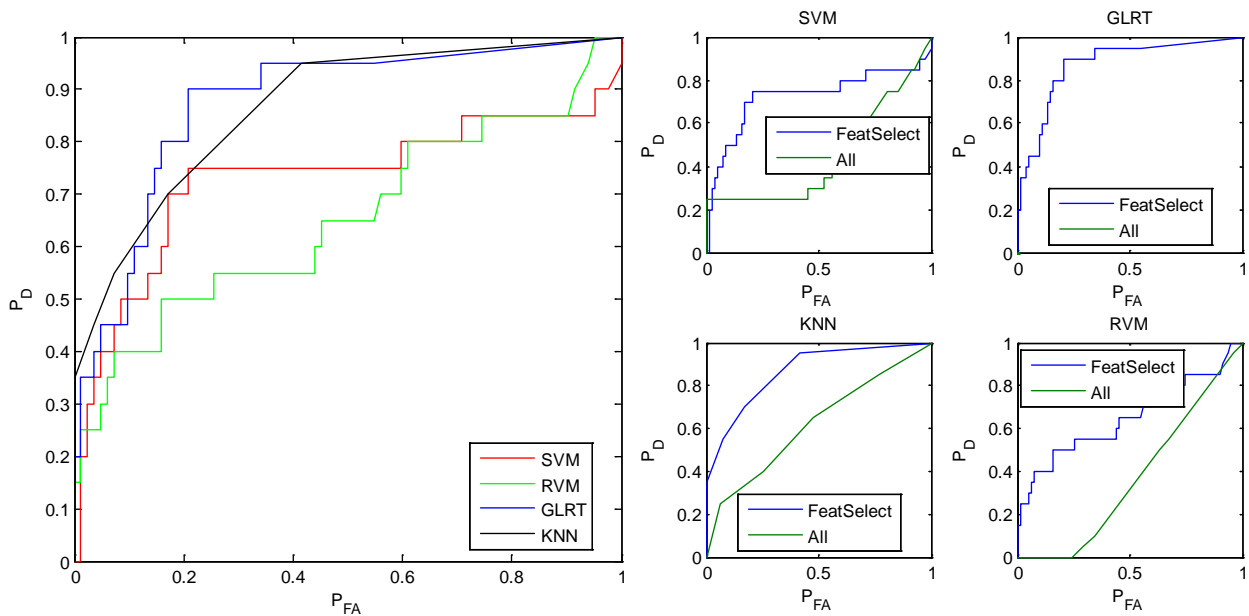


Figure 6-38 ROC curves for NRL GEM-3 array data using the loop model at YPG for different classifiers and features selection methodologies using features of anomalies with fit errors less than 31% . The targets of interest were small sized ordnance items (20mm, 40mm, M42, BDU-28, BDU-26).

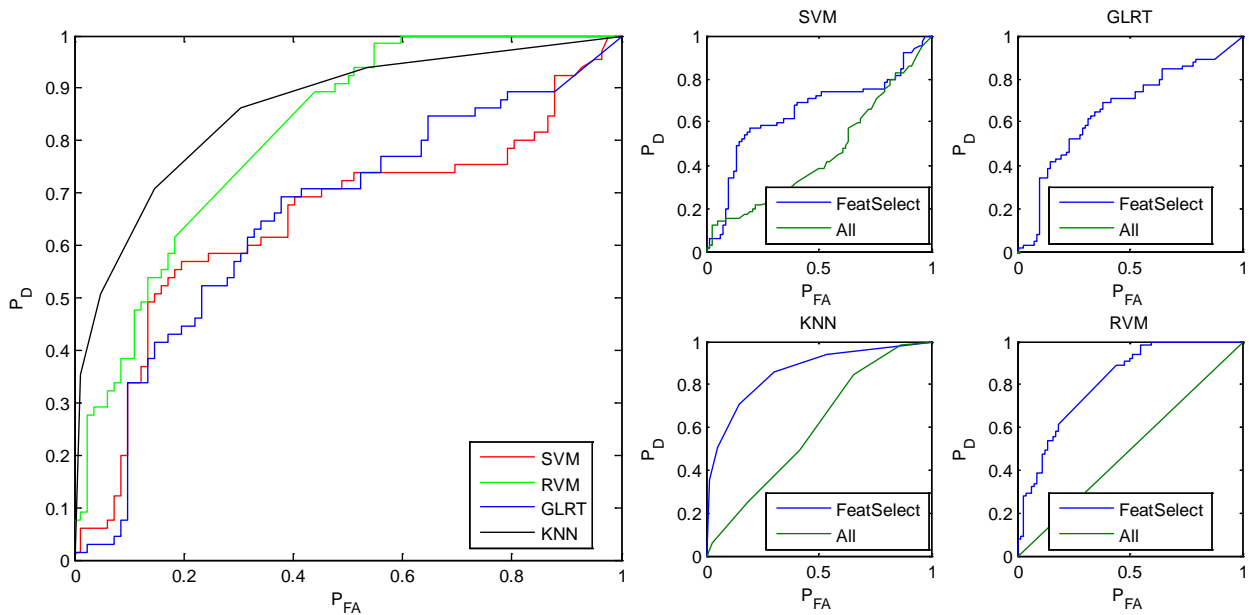


Figure 6-39 ROC curves for NRL GEM-3 array data using the loop model at YPG for different classifiers and features selection methodologies using features of anomalies with fit errors less than 31% . The targets of interest were medium sized ordnance items (57mm, MK118, 60mm, 81mm, 2.75in).

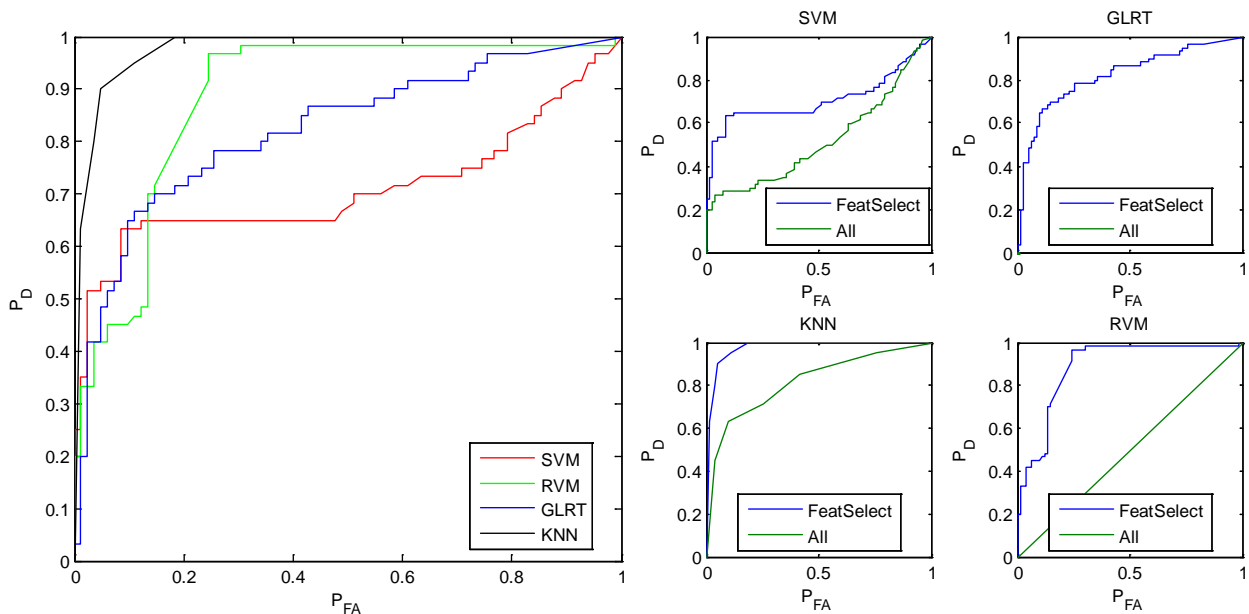


Figure 6-40 ROC curves for NRL GEM-3 array data using the loop model at YPG for different classifiers and features selection methodologies using features of anomalies with fit errors less than 31% . The targets of interest were large sized ordnance items (105mm, 155mm).